NON-MUSCLE MYOSIN II AND CYTOPLASMIC DYNEIN REGULATE CYTOSKELETON TRANSLOCATION DURING AXONAL ELONGATION

By

Douglas H. Roossien Jr.

A DISSERTATION

Submitted to
Michigan State University
in partial fulfillment of the requirements
for the degree of

Cell and Molecular Biology – Doctor of Philosophy

2014

ABSTRACT

NON-MUSCLE MYOSIN II
AND CYTOPLASMIC DYNEIN REGULATE CYTOSKELETON
TRANSLOCATION DURING AXONAL ELONGATION

By

Douglas H. Roossien Jr.

Neurons are complex cellular machines that utilize a dynamic cytoskeleton to elaborate long axonal processes. During embryonic development, these long processes eventually terminate and form a synapse with a prescribed target. Elongation is driven in part by a unique structure called the growth cone at the tip of the axon. A recently developed biophysical model for axonal elongation has proposed that forces cause the growth cone to translocate in bulk, while stretching the axon. This is followed by intercalated mass addition along the length of the axon to prevent thinning. As a result of axonal stretching, the cytoskeleton undergoes *en masse* translocation. While this has been observed in cultured neurons from a variety of different species, whether this occurs *in vivo* is unknown. In addition, the molecular force generating mechanisms in the axon that regulate axonal stretching and cytoskeleton translocation have not been characterized.

Here, we use mitochondria docked to the cytoskeleton as fiduciary markers for bulk cytoskeletal movements. We use this technique in cultured *Drosophila* neurons to show that cytoskeleton translocation is conserved between vertebrates and invertebrates. Then we track the movement of docked mitochondria in the aCC motoneuron in stage 16 *Drosophila* embryos to show that the cytoskeleton translocates during axonal elongation. This suggests that axons grow by stretching *in vivo*.

Non-muscle myosin II is a well-known force generating motor found in neurons. To characterize how myosin II contributes to axonal stretching and cytoskeleton translocation, we used the pharmacological agent blebbistatin to disrupt myosin II function in chick sensory neurons and genetic reduction of myosin II heavy chain in primary *Drosophila* neurons. We found an antagonistic relationship between myosin II in the growth cone and along the axon: myosin II in the growth cone promotes growth cone translocation, while myosin II along the axon restrains it by preventing axonal stretching.

Cytoplasmic dynein is a microtubule motor previously implicated in axonal elongation. To test if dynein contributes to cytoskeleton translocation, we used microinjection of function-blocking antibodies and the pharmacological dynein inhibitor Ciliobrevin D to disrupt dynein function and found that elongation decreases due to a reduction in cytoskeleton translocation. We also found an increase in axonal tension upon dynein disruption, suggesting that dynein pushes microtubules embedded in the cytoskeletal meshwork forward. Altogether these results lead to a model for axonal elongation in which the cytoskeleton can be pulled forward by myosin II in the growth cone or pushed forward by dynein along the length of the axon, while myosin II along the length of the axon restrains growth cone advance by preventing axonal stretching. This offers the axon a convenient mechanism to regulate the rate of elongation and has the potential to illuminate new strategies for augmenting axonal regeneration following nerve damage.

ACKNOWLEDGMENTS

First and foremost I would like to thank my mentor, Dr. Kyle E. Miller, for the superb training I have received under his guidance. His resourcefulness, ingenuity, and persistence have taught me to design, perform, and analyze experiments of deep insight. He has encouraged me to not only think critically about data and ideas presented in the literature, but to be the toughest critic of my own work. He has been a terrific mentor and a great friend, all the while providing me the opportunity to pursue my passions in his laboratory. It is truly an experience I will always cherish.

I would like to acknowledge and thank Phillip Lamoureux, the research assistant in Dr. Miller's laboratory. He has shared wisdom of the type only attainable over an enduring and highly successful career in the laboratory. Our discussions have surely improved the way I approach and carry out experiments, and our partnership during my time here has contributed to my success in immeasurable ways. I have also had the privilege of working with a handful of skilled and enthusiastic undergraduate students in Dr. Miller's laboratory as well. Specifically, Andrew George, Erica Melkonian, Javier Howard, and Arielle Pietron.

I would also like to thank the Cell and Molecular Biology Program at Michigan State University for recruiting me and providing a great opportunity to pursue my graduate education. In particular Dr. Sue Conrad and Dr. Kathy Meek have created a collegial atmosphere that encourages interdisciplinary interaction and cooperation. Becky Mansel has also been integral to my success here, as there was never a question she could not answer or a problem she could not solve. Being a part of the Cell and Molecular Biology program has truly been an honor. In

addition I would like to thank my committee, Dr. Kathy Gallo, Dr. Mary Rheuben, Dr. Alex Shingleton, and Dr. Hongbing Wang, for their guidance during my graduate training.

My parents have always encouraged me to pursue my interests, and for that I am eternally grateful. Most importantly, I would like to thank and acknowledge my wife Lisa Roossien. Her patience and understanding have provided me unmatched support during my graduate education. Her love, respect, and encouragement are a constant source of inspiration, without which I would not be successful.

TABLE OF CONTENTS

LIST OF TABLES

LIST OF FIGURES

KEY TO ABBREVIATIONS

αDIC – anti-dynein intermediate chain antibody

BDM – 2,3-butanedione-2-monoxine

C-domain – central domain

CilD – ciliobrevin D

ConA – concanavalin A

DECM – *Drosophila* extracellular matrix proteins

DIC – dynein intermediate chain

EB1 – end binding protein 1

EB3 – end binding protein 3

F-actin – filamentous actin

FAK – focal adhesion kinase

G-actin – globular actin

GFP – green fluorescent protein

hAEL – hours after egg lay

HiLn – high laminin

IgG – immunoglobulin G

LoLnPO – low laminin with poly-ornithine

MBS – myosin binding subunit

MLCK – myosin light chain kinase

MLCP – myosin light chain phosphatase

NMII – non-muscle myosin II

P-domain – peripheral domain

PEC – Protrusion, Engorgement, and Consolidation

PO – poly-ornithine

RLC – regulatory light chain

ROCK – Rho-associated protein kinase

SAI – Stretch and Intercalation

T-zone – transition zone

CHAPTER 1:

Review of Current Literature

1.1 Introduction

During development, neurons send out long cellular processes called axons that navigate through a complex array of environments and eventually form synapses with prescribed targets. Even after reaching its synaptic target, the axon must be able to stretch in response to the increasing body size of the animal in order to maintain proper connections. This results in axons that can be up to a meter long in humans and 30 meters long in aquatic mammals (Smith, 2009). How individual cells accomplish such an impressive feat has been the subject of intense research for over a century.

In the late 1800's, Ramon Y Cajal described the nervous system as a contiguous network of connected individual neurons. In addition, he identified the growth cone: the most distal structure of the axon, which he predicted to be required for axonal elongation (Ramon Y Cajal, 1890). Indeed, almost a century later it was shown that axons with severed growth cones fail to elongate until a new growth cone is formed (Shaw and Bray, 1977; Wessells et al., 1978). Growth cones are responsible for integrating signals initiated by extracellular guidance molecules into decisions about which direction to grow or not to grow. This includes decisions to continue elongating per se.

Many guidance cues signal downstream to the growth cone cytoskeleton (Dickson, 2002), which is organized into three distinct domains (Figure 1.1) (Bridgman and Dailey, 1989; Forscher and Smith, 1988; Lewis and Bridgman, 1992). The peripheral domain or P-domain is rich in actin filaments arranged in either thick actin bundles that protrude outward to form filopodia or in a meshwork in the lamellipodia veil. The central domain or C-domain is dense in microtubules and other membranous organelles such as mitochondria, endoplasmic reticulum, and endosomes. The area in which microtubules interact with actin filaments between the P- and

C-domains is called the transition zone or T-zone. The T-zone contains a unique actin structure called actin arcs, which are short bundles of actin filaments. These actin arcs circumscribe the C-domain and keeps microtubules contained (Schaefer et al., 2002).

The growth cone and axonal cytoskeleton are closely associated with motor proteins. Non-muscle myosin II (NMII), for instance is enriched in the T-zone (Bridgman and Dailey, 1989; Rochlin et al., 1995) where it generates contractile forces that assist in maintaining growth cone structure and regulate axonal elongation. A variety of other motor proteins, such as additional myosin family members, kinesins, and cytoplasmic dynein, are found throughout the growth cone as well. These motors exert forces on the axonal cytoskeleton in response to external stimuli to affect axonal elongation, such that the growth cone can be viewed as a biological engine (Lowery and Van Vactor, 2009).

The standard model for axonal elongation is called the Protrusion, Engorgement, and Consolidation hypothesis (PEC) and proposes that as the actin-rich P-domain advances, it leaves behind an empty corridor between the P- and C-domain (Figure 1.2A). This allows for the deposition of new material by cytoskeleton polymerization and fast transport, which gives the appearance that the growth cone is being engorged with new material. The final step is a consolidation step which converts the engorged C-domain into new axon. This is analogous to building a railroad, where pieces of track are laid down in succession until the destination is reached. An alternative model for axonal elongation has recently emerged called Stretch and Intercalation (SAI) (Suter and Miller, 2011). This model is based on the idea that forces generated in the axon and growth cone cause the axon to stretch, much like a piece of silly-putty (Figure 1.2B). This model differs from the PEC model in three significant ways: 1 – The C-domain advances as one coherent unit according to SAI, whereas the growth cone is constantly

being assembled with PEC growth. 2 – Axonal stretching causes the cytoskeleton to be in motion. 3 – Motor proteins generate forces to deform the axon in addition to transporting material.

As the observations leading to the SAI hypothesis have been garnered from *in vitro* experiments, whether this mode of outgrowth is physiologically relevant or an artifact of culture conditions is unknown. In addition, the identity and mechanisms of molecular motors that regulate axonal stretching have not been elucidated. These general questions are addressed in this dissertation. A review of relevant literature is presented in this chapter, which is separated into three sections. The first section will discuss the structure and regulation of the microtubule cytoskeleton and the microtubule motor dynein. The second will likewise discuss the actin cytoskeleton and non-muscle myosin II (NMII). In the third section, how these individual components cooperate to drive axonal elongation will be discussed from a historical and critical perspective. Chapters 2-4 each individually address the specific aims outlined below, while Chapter 5 provides a brief discussion of future research directions.

Aim 1) How do axons elongate *in vivo*?

We turn to the model system *Drosophila melanogaster* to address this question. First, embryonic neurons were harvested and grown in culture for the purposes of making direct comparisons of cytoskeletal meshwork translocation between *Drosophila* and vertebrate neurons. We follow this with live time-lapse imaging of developing *Drosophila* embryos to ask if translocation occurs *in vivo*.

Aim 2) How does non-muscle myosin II influence cytoskeletal meshwork translocation?

We use both genetic reduction of myosin II heavy chain in *Drosophila* neurons and the pharmacological inhibitor blebbistatin in chick sensory neurons to ask how non-muscle myosin II disruption affects axonal elongation and cytoskeletal meshwork translocation. We pair this analysis with a biophysical characterization of axonal force generation and mathematical modeling of adhesion strength and axonal viscosity to develop a model for non-muscle myosin II function during axonal elongation.

Aim 3) Does cytoplasmic dynein generate forces required for cytoskeletal meshwork translocation?

For this aim, we use microinjection of function-blocking antibodies targeted to dynein intermediate chain and the pharmacological inhibitor Ciliobrevin D to ask if dynein disruption slows elongation by interfering with cytoskeletal meshwork translocation. In addition, we perform direct measurements of axonal forces to determine the net force contribution dynein makes in the axon.

1.2 The axonal microtubule cytoskeleton

Microtubules have long been recognized as a critical component for axonal growth and stability. Indeed, when the microtubule disrupting drug colchicine was added to neurons in culture, axons retracted and were prevented from resuming growth (Daniels, 1972; Yamada et al., 1971). Microtubules along the axon act as structural support and as tracks for cellular transport. According to PEC, polymerization and / or deposition of microtubules at the distal axon tip is an integral part of the engorgement step (Dent and Gertler, 2003; Lowery and Van Vactor, 2009; Stiess and Bradke, 2011). It is therefore important to understand their biochemical properties and how the microtubule bundle in the axon is formed.

1.2.1 Microtubule dynamics

Microtubules are protein polymers formed from tubulin heterodimers made up of globular α- and β-tubulin subunits. While both of these subunits are bound to GTP nucleotides, only the β-tubulin subunit can hydrolyze the GTP into GDP; α-tubulin always remains bound to GTP (Alberts et al., 2008). Tubulin heterodimers polymerize in a polarized fashion through noncovalent interactions in linear filaments called protofilaments (Desai and Mitchison, 1997). Protofilaments polymerize alongside one another to form a hollow microtubule typically consisting of 13 protofilaments (Desai and Mitchison, 1997).

Tubulin heterodimers align in a “head-to-tail” fashion (Amos and Klug, 1974; Bergen and Borisy, 1980) such that each protofilament contains alternating α- and β-tubulin subunits, giving rise to a polarized microtubule structure with α-tubulin exposed at one end (the minus end) and β-tubulin at the other (the plus end) (Fan et al., 1996; Hirose et al., 1995; Mitchison, 1993). The rate limiting step of microtubule polymerization is the nucleation of microtubule

subunits into a seed, which creates sites for subsequent cooperative binding of tubulin monomer (Hill and Kirschner, 1982). In the cell, centrosomes act as stable sites for the nucleation of new microtubules (Mitchison and Kirschner, 1984b) by providing γ-tubulin ring complexes which closely mimic β-tubulin binding sites but are much more stable (Joshi et al., 1992; Oakley and Oakley, 1989).

Once bound in the microtubule lattice, the β-tubulin subunit hydrolyzes GTP into GDP. However, the hydrolysis reaction lags behind the rate of new GTP-bound subunit addition, which creates a "GTP cap" (Carlier and Pantaloni, 1981). The off rate of GTP-bound subunits is much lower than GDP-bound monomers, resulting in a higher polymerization rate at the plus end compared to the minus end (Allen and Borisy, 1974; Carlier et al., 1984; Dentler et al., 1974; Margolis and Wilson, 1978; Summers and Kirschner, 1979). If the pool of free tubulin heterodimer is depleted, however, the rate of GTP hydrolysis becomes greater than the rate of new subunit addition. GDP-bound tubulin subunits at the plus end become exposed at the tip, which then rapidly dissociate from the microtubule lattice and cause extensive depolymerization of the microtubule (Carlier and Pantaloni, 1981; Mitchison and Kirschner, 1984a; Weisenberg et al., 1976). This event is called "catastrophe" and can be reversed by a "rescue" event in which depolymerization is halted and polymerization resumes (Desai and Mitchison, 1997; Mitchison and Kirschner, 1984a). The details of rescue events are less clear, but in neurons rescue is promoted by microtubule associated proteins (Drechsel et al., 1992; Pryer et al., 1992; Trinczek et al., 1995). This ability of microtubules to alternate between states of polymerization and depolymerization is termed dynamic instability and allows the cell tight regulation of microtubule remodeling. Microtubules in the axon operate under these same fundamental principles, though the axon has adapted them in various ways.

1.2.2 Establishment of axonal microtubules

The microtubule cytoskeleton is an integral structural component underlying axonal morphology (Yamada et al., 1970). Axonal microtubules can reach lengths of at least 100 μm (Bray and Bunge, 1981) and are oriented with their plus ends facing distally, or toward the growth cone (Heidemann et al., 1981). This polarized orientation is unique to the axon and is an early step in establishing which neurite becomes the axon while the rest, with a mixed microtubule polarity (Baas et al., 1988), become dendrites (Stiess and Bradke, 2011). Microtubules along the length of the axon overlap and are highly cross linked such that the microtubule cytoskeleton is a mechanical continuum that stretches the entire length of the axon, despite being longer than the individual microtubules that comprise it (Hirokawa, 1982).

How does the axon establish polar orientation of microtubules in the axon? Immunostaining for the microtubule nucleation protein γ-tubulin revealed it is only found in the pericentriolar region of the cell body and not along the axon (Baas and Joshi, 1992; Miller and Joshi, 1996), suggesting that all microtubules are nucleated in cell body. Nucleation is followed by a brief bout of polymerization, after which the short microtubule is severed from the centrosome by katanin and transported down the axon by the microtubule motor dynein (Ahmad et al., 1998; Ahmad et al., 2006; Baas and Ahmad, 1992; Baas et al., 2005). The transport of short microtubules, ~10 μm in length, is rapid but intermittent (Wang and Brown, 2002) and is thus termed Stop-and-Go transport. By limiting nucleation to the cell body followed by transport in this fashion the axon is supplied with microtubules with the plus ends facing distally.

To compensate for the lack of nucleation sites in the axon shaft, microtubules become stabilized at their minus end (Nicklas et al., 1989; White et al., 1987). This prevents wholesale depolymerization and provides the axon with stable sites for new polymerization. Indeed, by

using tyrosinated tubulin as a marker for young microtubule and detyrosinated tubulin for old microtubule, it was found that individual microtubules are detyrosinated near the minus end and tyrosinated near the plus end (Baas and Black, 1990). Tubulin is transported down the axon in soluble form (Ma et al., 2004; Miller and Joshi, 1996) by kinesin (Terada et al., 2000) to supply the axon with heterodimers for incorporation into these pre-existing stable microtubules.

While microtubule polymerization occurs throughout the axon, (Keith, 1987; Lim et al., 1990; Lim et al., 1989; Okabe and Hirokawa, 1988; Okabe and Hirokawa, 1990; Okabe and Hirokawa, 1992; Okabe and Hirokawa, 1993), it is enriched in the proximal region near the cell body and the distal region near the growth cone. Staining for tyrosinated tubulin shows the microtubule bundle contains an increase in young microtubules near the cell body and in the distal axon, while the central axon contains an enrichment of detyrosinated / stable microtubules (Brown et al., 1993). More recently, these observations were confirmed by tracking EB3/1-GFP comets (Kollins et al., 2009; Stepanova et al., 2003), a method for tracking the plus ends of polymerizing microtubules (Akhmanova and Steinmetz, 2008). Microtubule dynamics in the axon are spatially and temporally regulated in the axon by signaling networks (Conde and Caceres, 2009). While the full details of regulation are beyond the scope of this review, how microtubule dynamics contribute to axonal elongation will be discussed in a later section.

1.2.3 Dynein: a microtubule motor protein

Motor proteins are a class of specialized enzymes that transform the chemical energy stored in ATP molecules to mechanical energy. There are three superfamilies of motor proteins (kinesins, myosins, and dyneins), each of which are further subdivided into over 100 different types of motor proteins in humans (Vale, 2003). Though they vary in function, they are all

closely associated with cytoskeletal filaments. In particular, the dynein superfamily is an ATPase associated with microtubules, on which it can walk toward the minus end (Paschal et al., 1987; Paschal and Vallee, 1987; Sale and Satir, 1977). Dynein is divided into three classes. Axonemal dynein is found between microtubule doublets in cilia and flagella and powers sliding during motility. Cytoplasmic dynein contains two classes, one of which drives transport along microtubules in cilia and flagella (referred to as class 2 or IFT dynein) and another found throughout the remainder of the cell with a variety of functions (class 1) (Vale, 2003). Cytoplasmic dynein 1 will herein be referred to as dynein as the other two classes will not be discussed further.

Research on the structure and mechanism of dynein function has lagged behind that of the kinesin and myosin motor superfamilies because of its large size and the large number of closely associated regulatory proteins. Recent advances in solving dynein crystal structures, however, has begun to reveal the mechanochemical mechanism of this large 500+ kDa enzyme that was previously inferred from functional studies. The motor head of dynein is made up of six ATPase domains arranged in a ring (Neuwald et al., 1999). Across this lies a linker domain that changes shape based on the status of ATP binding (Burgess et al., 2003; Imamula et al., 2007; Kon et al., 2005; Kon et al., 2012; Roberts et al., 2009). This linker domain is contiguous with a tail domain, which interacts with a wide variety of regulatory proteins and cargo. A coiled-coil stalk domain emanates from out of the motor head ring and contains a microtubule binding domain (MTBD) at its tip (Gee et al., 1997). When ATP binds to the motor head, the linker domain rotates like a hinge (Roberts et al., 2012) and the MTBD detaches from the microtubule (Porter and Johnson, 1983). ATP hydrolysis then occurs causing the MTBD to bind in a new position further along the microtubule toward the minus end (Carter et al., 2008), which in turn

induces ADP + P_i release (Holzbaur and Johnson, 1989). This last step in the cycle causes the linker domain to straighten and pull its attached cargo forward as the 'power stroke' step (Kikkawa, 2013; Kon et al., 2005) and the mechanochemical cycle can begin again.

How dynein achieves long distance processivity is still unclear, though several lines of evidence suggest dimerization of two heavy chains is responsible for ensuring the motors do not dissociate from the microtubule (Reck-Peterson et al., 2006). The proposed mechanism for dimer function is that stepping of the two dynein heavy chains is uncoordinated and that the presence of the linker between the two increases the probability each will take forward steps as opposed to backward, such that the net result is forward movement of the dimer in 8 nm increments (DeWitt et al., 2012; Qiu et al., 2012; Reck-Peterson et al., 2006). This does not, however, account for the observation that individual heavy chains can processively take 8 nm steps under high load (Mallik et al., 2004), the mechanism of which remains controversial.

Unlike the kinesin and myosin superfamilies, each of which have evolved a large number of subfamilies and isoforms designed to perform specific functions in the cell, the dynein superfamily contains relatively few types (Vale, 2003). Instead, the cell utilizes accessory proteins to adapt the dynein motor complex to numerous cellular functions. These include non-catalytic subunits of the dynein holoenzyme itself; two dynein light chains, a light intermediate chain, and an intermediate chain (DIC). These non-catalytic subunits mostly regulate binding to additional regulatory proteins and cargo (Roberts et al., 2013). Dynactin is a regulatory protein required for long distance dynein-driven transport of materials in living cells (Gill et al., 1991; Schroer and Sheetz, 1991). It is the most commonly studied dynein regulator and is required for almost all known functions of dynein *in vivo* (Schroer, 2004).

Dynactin itself is a large multi-protein complex. The major subunit, p150^{Glued}, binds to DIC to maintain an intact dynein-dynactin complex (Karki and Holzbaur, 1995; Vaughan and Vallee, 1995). It can also bind microtubules at its N-terminus (Vaughan et al., 2002; Waterman-Storer et al., 1995). This interaction may keep dynein tethered to the microtubule to increase processivity (King and Schroer, 2000). In addition to direct microtubule binding, p150^{Glued} can interact with the microtubule +TIP proteins EB1 and CLIP-170 (Valetti et al., 1999; Vaughan et al., 1999; Vaughan et al., 2002). Though the precise mechanism is not yet understood, the interactions between dynactin and CLIP-170 target dynein specifically to the plus ends of microtubules, where it can remain in position until cargo binds for transport toward the minus end (Vaughan et al., 2002). Alternatively, the plus end complex can be targeted to the cell cortex along with dynein via Num1 (Markus et al., 2009) or IQGAP1 (Fukata et al., 2002). Dynactin thus augments dynein function by both increasing the processivity of the motor and regulating its localization.

The most well-known function of dynein is for cellular transport. *In vitro*, purified dynein bound to coverslips can move microtubules and can transport plastic beads across microtubules when in solution (Euteneuer et al., 1988; Lye et al., 1987; Paschal et al., 1987); later it was confirmed in living cells and axons that dynein moves membranous vesicles toward microtubule minus ends (Schnapp and Reese, 1989; Schroer et al., 1989). Various membranous organelles, such as mitochondria (Pilling et al., 2006), endosomes (Aniento et al., 1993; Driskell et al., 2007), and Golgi (Corthesy-Theulaz et al., 1992), can bind to dynein and are thus transported throughout the cell. Because microtubules in the axon are oriented with their minus ends facing the cell body, dynein drives axonal transport of membrane organelles in the retrograde direction (Pilling et al., 2006; Schnapp and Reese, 1989; Yi et al., 2011). Dynein also transports short

microtubules in the axon via Stop-and-Go transport, though in the anterograde direction (Ahmad et al., 1998; Ahmad et al., 2006). This is proposed to occur because the dynein motor domain is bound to a short microtubule while the cargo-binding domain is anchored to a structure with more resistance (Baas et al., 2006; Pfister, 1999). As dynein walks toward the minus end, the microtubule moves forward. Thus, dynein plays a critical role in the transport of a variety of different types of cargo in the axon and in non-neuronal cells. In all of these cases, the mechanochemical cycle brings the motor head closer to the minus end of the microtubule regardless of whether the microtubule or motor head is stationary.

Other cellular functions have recently been ascribed to dynein in addition to cellular transport, all of which rely on dynein force generation. During mitosis, dynein is required for proper mitotic spindle assembly and alignment (Goshima et al., 2005; Nguyen-Ngoc et al., 2007; O'Connell and Wang, 2000; Rusan et al., 2002), capture and alignment of chromosomes (Schmidt et al., 2005), and separation of the centrosomes (Gonczy et al., 1999). Dynein at the actin-rich cortex is presumed to drive a majority of these mitotic functions. By using cortical actin as an anchor, the tendency of the motor to try to walk toward the minus end moves the microtubule in the plus end direction (Hendricks et al., 2012; Mazel et al., 2013). There is also a growing body of evidence in large cells, such as Zebrafish and *Xenopus* zygotes, that dynein is anchored in the cytoplasm to exert forces on large microtubule arrays (Kimura and Onami, 2005; Wuhr et al., 2010).

Most studies on dynein function in axons have focused on transport, be it Stop-and-Go transport of microtubules or retrograde transport of organelles. There have been, however, a few notable observations made of dynein function in the context of axonal elongation. Overexpression or injection of the dynactin subunit dynamitin disrupts dynein function by

dissociating the dynein-dynactin complex (Echeverri et al., 1996; Wittmann and Hyman, 1999). When injected into weakly adhered neurons, the axons lose their ability to resist retraction forces generated by NMII (Ahmad et al., 2000). Depletion of dynein heavy chain by siRNA makes axons more sensitive to retraction induced by nitric oxide and disrupts growth cone turning (Myers et al., 2006). The rate of elongation is drastically reduced with both of these means of dynein disruption as well (Ahmad et al., 2000; Myers et al., 2006). In neurons grown on poly-amine substrates and then treated with soluble laminin, which increases the rate of elongation (Lein et al., 1992), there is a dramatic relocalization of dynein to the leading edge of the growth cone that correlates with increases in growth (Grabham et al., 2007). It therefore seems as though dynein may be making a significant contribution to axonal elongation in addition to driving axonal transport.

In both non-neuronal cells and neurons, dynein converts chemical energy stored in ATP to generate mechanical forces to perform a variety of different tasks. The central theme to all of these cellular functions is that dynein forces cause the movement of large objects through the cell, be they membrane organelles, individual or networks of microtubules, or chromosomes. If and how dynein forces affect the cross linked microtubule cytoskeleton along the axon is an intriguing question, and investigating this could reveal new mechanisms for axonal stretching during elongation.

1.3 Actin and growth cone motility

Cell migration is a multi-step cycle involving protrusion of the plasma membrane at the leading edge, substrate adhesion formation and turnover, and cytoskeleton contraction at the rear of the cell to move the cell body forward (Lauffenburger and Horwitz, 1996; Ridley et al., 2003). All of these steps involve the actin cytoskeleton and myosin. The Rho-family GTPases RhoA, Rac1, and Cdc42 are master regulators of cell motility in that they all regulate actin dynamics and myosin activity. In general, Rac1 and Cdc42 induce formation of the two main protrusive structures lamellipodia and filopodia, respectively, whereas RhoA regulates adhesion and stress fiber formation (Nobes and Hall, 1995). The main components of the actin machinery relevant to axonal elongation are discussed in the following section. Although there is significant overlap in the structure and function of proteins involved in non-neuronal cell and growth cone motility (Pak et al., 2008), important differences will be noted.

1.3.1 Actin dynamics

Actin is another of three classes of protein polymer found in cells that comprise the cytoskeleton. Actin filaments are singular bi-helical filaments (F-actin) made up of spontaneously polymerizing globular actin subunits (G-actin). This makes them less stiff than microtubules, but has the advantage of adding a degree of pliability (Isambert et al., 1995). G-actin monomers are bound to ATP and, like microtubules, polymerize in a head-to-tail fashion more favorably at the plus end of the actin filament, also called the barbed end. ATP hydrolysis occurs stochastically after polymerization and there is a subsequent delay in P_i release from the monomer such that filaments can have three distinct regions based on the state of adenine nucleotide bound to G-actin: ATP near the actively growing barbed end, ADP-P_i just proximal to

this region, followed by an ADP region that spans all the way to the pointed end (Blanchoin and Pollard, 2002; Carlier and Pantaloni, 1986; Carlier et al., 1988).

Actin polymerization is a function of the local concentration of G-actin, giving rise to a 'critical concentration' at which polymerization occurs at concentrations above and depolymerization below (Pollard, 1986). A notable property of F-actin is that the critical concentration at the barbed end is much lower than at the pointed end. Thus, at G-actin concentrations between these two critical concentrations, actin filaments grow at one end and shrink at the other, a process called treadmilling that can be visualized directly in living cells with fluorescently labeled actin (Fujiwara et al., 2002). During F-actin treadmilling, the net location of the filament advances even though the individual monomers are stationary relative to the substrate (Theriot and Mitchison, 1991). However, as the cell maintains a G-actin concentration well above the critical concentration, it utilizes a host of actin binding proteins to regulate actin polymerization and treadmilling (Pollard and Borisy, 2003).

1.3.2 Actin-based protrusive structures

An integral process in growth cone motility and cell migration is protrusion of the leading edge of the plasma membrane, which is predominantly driven by two main structures. First, the lamellipodia, which appear as thin sheets devoid of organelles and microtubules. In the lamellipodia, F-actin filaments are arranged in a branched network (Hoglund et al., 1980) meeting at 70° angles (Karlsson et al., 1984; Rinnerthaler et al., 1991) with their barbed ends facing the leading edge of the plasma membrane (Begg et al., 1978; Isenberg et al., 1978; Small et al., 1978). The second are the filopodia, finger-like structures comprised of a bundle of actin filaments oriented with their plus ends facing the distal tip (Bridgman and Dailey, 1989; Tosney

and Wessells, 1983). According to the Brownian ratchet model, F-actin filaments randomly vibrate and bend, which create gaps between the tip of the filament and the plasma membrane into which new G-actin subunits can be added. Pushing is created on the plasma membrane when the filament returns to its relaxed, fully extended state (Mogilner and Oster, 1996; Oster and Perelson, 1987; Peskin et al., 1993). This occurs in both the filopodia and lamellipodia to drive membrane protrusion.

Protrusion at the leading edge of lamellipodia does not occur by the pushing of individual actin filaments, but by a branched network of connected filaments. Arp2/3 protein facilitates branching (Amann and Pollard, 2001; Blanchoin et al., 2000; Pantaloni et al., 2000) by binding to the sides of F-actin and mimicking a barbed end subunit (Robinson et al., 2001). This nucleates a new filament that grows at a 70° angle to the original (Mullins et al., 1998). The branched network of actin filaments creates a high density of ~100 filaments per micron that acts as a "nanomachine" to drive plasma membrane protrusion (Abraham et al., 1999). This forms the basis for the dendritic nucleation model for cell motility (Pollard and Borisy, 2003), which is based on the premise that a highly branched network of short actin filaments can create a stronger pushing force against the plasma membrane than long individual actin filaments.

According to the dendritic nucleation model, actin dynamics are regulated in addition to branching by a host of actin binding proteins to regulate lamellipodial protrusion. Capping proteins such as CapZ and gelsolin bind to the barbed ends to prevent polymerization in unwanted directions (Cooper and Schafer, 2000; Sun et al., 1999). Further back from the plasma membrane, disassembly of actin filaments is facilitated by a highly conserved family of actin binding proteins called the ADF/cofilins (Bamburg et al., 1999). ADF/cofilin binds to actin subunits and causes them to dissociate from the filament (Nishida, 1985; Nishida et al., 1984a;

Nishida et al., 1984b). After dissociation, the nucleotide exchange factor profilin binds the actin monomer (Mockrin and Korn, 1980; Vinson et al., 1998). The actin-profilin complex binds ATP with higher affinity than ADP, so nucleotide exchange is facilitated rapidly (Rosenblatt et al., 1995; Vinson et al., 1998). In this manner, actin is continuously recycled and polymerization can occur at the plasma membrane whenever needed.

Whether the dendritic nucleation model is directly applicable to growth cones is a matter of debate. An early observation of actin filament structure in the growth cone using EM techniques found that there is a significant population of actin filaments in the growth cone P-domain oriented with their pointed ends facing the plasma membrane and that they meet at random angles (Lewis and Bridgman, 1992). Likewise, Arp2/3 was not found at high levels in growth cone lamellipodia in immunolocalization studies and Arp2/3 inhibition did not alter growth cone morphology in hippocampal neurons (Strasser et al., 2004). In these growth cones, actin filaments were sparse and longer than in non-neuronal lamellipodia. In contrast, direct comparison of actin networks in veils during protrusion and retraction showed protruding veils have actin networks with geometry predicted by the dendritic nucleation model and contain Arp2/3. Retracting veils contained fewer but longer filaments (Mongiu et al., 2007), which resembled those found previously in hippocampal neurons (Strasser et al., 2004). As this is still an area of active research, it will be interesting to see what further insights into actin dynamics in the lamellipodia are gained.

The second major actin-based protrusive structure in growth cones and motile cells are the dynamic, finger-like filopodia. As in the lamellipodia, F-actin filaments that comprise actin bundles are oriented with their barbed ends facing the plasma membrane (Lewis and Bridgman, 1992). There are two proposed mechanisms for how actin bundles destined to become filopodia

are formed (Mellor, 2010). In the first, actin filaments in the lamellipodia become bundled via N-WASP (Miki et al., 1998). Alternatively, formin proteins nucleate a new bundle at the plasma membrane (Peng et al., 2003). While both of these are regulated the Rho-family GTPase Cdc42 (Nobes and Hall, 1995), they differ in whether or not the filopodia actin bundle is formed from pre-existing or newly nucleated filaments. Once the filopodium is formed, filamin proteins stabilize the bundle (Ohta et al., 1999). At the tips of filopodia, the capping proteins CapZ (Heiss and Cooper, 1991) and adducin (Matsuoka et al., 1998) prevent extension and are antagonized by Ena/VASP proteins (Bear et al., 2002; Lanier et al., 1999). As in the dendritic nucleation model, the combined polymerization of the actin bundle pushes the plasma membrane forward creating protrusion.

Filopodia are highly dynamic structures that elongate, retract, and become absorbed many times faster than the rate of growth cone advance (Sheetz et al., 1992). Actin bundles in the filopodia undergo constant retrograde movement (Sheetz et al., 1992). Interestingly, the rate of backward motion remains constant regardless of whether the filopodium is shrinking, elongating, or maintaining a constant length (Mallavarapu and Mitchison, 1999). This suggests that net filopodia length is determined by the balance of rearward motion and actin assembly at the filopodia tip, with assembly being the tunable factor (Mallavarapu and Mitchison, 1999). The erratic initiation and retraction of growth cone filopodia has led to the belief that the major role of filopodia in axonal growth is to survey the extracellular environment and form attachment points that lead to traction force during guidance (Dennerll et al., 1989; Heidemann et al., 1990; Lin and Forscher, 1993). Indeed, when grasshopper embryos are bathed with the actin disrupting drug cytochalasin B, growth cones lose their filopodia and fail to turn at guidepost cells (Bentley and Toroian-Raymond, 1986). In this and other ways, discussed throughout the remainder of this

review, actin-based protrusive structures are essential for axonal elongation and guidance during development of the nervous system.

1.3.3 Non-muscle myosin II

In close association with the actin cytoskeleton are members of the myosin motor protein superfamily (Krendel and Mooseker, 2005). Myosin was originally identified as a component in the sarcomeres of muscle cells that form linear cross-bridge structures that together with actin filaments generate contractile forces. It was later uncovered as one member of a much larger superfamily of motor proteins found in all non-muscle cells (Pollard and Korn, 1973; Richards and Cavalier-Smith, 2005).

Of these, non-muscle myosin II (NMII) is fundamental to growth cone and cell motility. Indeed, knockout of NMII in the slime mold dictyostelium drastically reduces cell locomotion (Doolittle et al., 1995; Jay et al., 1995; Wessels et al., 1988). NMII molecules are found as homodimers of two heavy chains bound non-covalently through tight interactions in long coiled-coil C-terminal domains, which form a flexible rod-like structure (Craig and Woodhead, 2006). The alternating positive and negative charges on these rods create a strong interaction between NMII proteins, allowing for the formation of bipolar myosin filaments (Ikebe et al., 2001; Nakasawa et al., 2005). These myosin filaments are thick clusters of myosin motors with a tightly packed C-terminal rod backbone and N-terminal motor domains exposed to the cytoplasm at both ends (Craig and Woodhead, 2006). Myosin filaments align with F-actin and cause actin filament sliding.

Like dynein, NMII utilizes chemical energy stored in ATP to generate force. At the N-terminus is the globular motor domain that contains the enzymatic Mg^{2+}-ATPase domain

required for force generation (Dominguez et al., 1998; Rayment et al., 1993b). A tremendous amount of structural and kinetic data over the last several decades has led to a detailed description of the mechanism and cycle of actomyosin contraction in skeletal muscle, smooth muscle and non-muscle cells (Alberts et al., 2008; Rayment et al., 1993a). In general, when the N-terminal myosin II head binds ATP, it releases from the actin filament which subsequently induces ATP hydrolysis. ADP + P_i remain bound to the head, but hydrolysis causes a conformational change in the head that causes it to move ~ 5 nm relative to the actin filament in the barbed end direction (Spudich, 2001). A weak binding interaction with the new site on the actin filament causes P_i release, which strengthens the interaction with the actin filament (Wessels et al., 1988). At this point, the power stroke occurs as the head returns to its original conformation and releases ADP. The open nucleotide cleft is available to bind ATP and repeat the cycle (Rayment et al., 1993b). In this cycle, an individual NMII molecule can generate 3-4 pN of force (Finer et al., 1994).

In *Drosophila*, the myosin heavy chain is encoded by one gene, named *zipper* (Mansfield et al., 1996). In mammalian cells, however, NMII heavy chains can be found in three isoforms, NMIIA, B, and C each encoded by separate genes (Odronitz and Kollmar, 2007). The heavy chains never form heterodimers as evidenced by the failure of isoform-specific antibodies to pull down alternate isoforms (Golomb et al., 2004). The different isoforms have different biophysical characteristics. For example, NMIIA has a higher rate of ATP hydrolysis and can move individual actin filaments at a three-fold higher rate than NMIIB (Kelley et al., 1996), whereas NMIIB is bound to actin in a force-generating state for a longer period of time (duty ratio) (Kovacs et al., 2003; Wang et al., 2003). This means NMIIB is better suited to exert tension on actin networks for longer periods in a more energy efficient fashion.

Both NMIIA and B isoforms are found in rat sympathetic neurons isolated from superior cervical ganglia, though their distribution is slightly different. The highest concentration of NMIIB is normally found in the T-zone where it co-localizes with actin arc structures, whereas NMIIA is found mostly in the C-domain (Rochlin et al., 1995). In rat neurons from dorsal root ganglia NMIIB was found to be located closer to the leading edge in the growth cone P-domain (Miller et al., 1992), though whether the differences in localization were due to differences in cell-types, fixation methods, or growth substrate is unknown. Along the axon, NMIIA can be found closely associated with the cell cortex (Rochlin et al., 1995), which also contains a dense actin meshwork. Owing to the lack of pharmacological inhibitors for specific NMII isoforms and the limitations of genetic knockouts, separating the functions of the different isoforms in the axon and growth cone remains a challenge.

NMII activity is regulated by phosphorylation, most of which occurs on its regulatory light chain (RLC) (Vicente-Manzanares et al., 2009). Structural evidence suggests that when RLC is not phosphorylated, NMII forms a compact loop via head-to-tail interactions that prevents bipolar filament assembly (Burgess et al., 2007; Wendt et al., 2001). Phosphorylation of RLC relieves this compaction and results in the unfolded NMII protein motor available to form filaments and generate force (Jung et al., 2008; Scholey et al., 1980; Smolensky et al., 2005). In addition, phosphorylation of RLC directly alters the conformation of the motor heads resulting in increased ATPase activity (Wendt et al., 2001).

Phosphorylation of the RLC is regulated by a complex network of kinases and phosphatases, of which there is significant overlap with those that regulate actin dynamics such as Rho-family GTPases. The simplest signaling axis that results in RLC phosphorylation is the Ca^{2+}-calmodulin activation of myosin light chain kinase (MLCK) (Kamm and Stull, 1985;

Moussavi et al., 1993). Deactivation of NMII is achieved by myosin light chain phosphatase (MLCP), a protein containing three subunits: a catalytic type 1 protein phosphatase, myosin phosphatase target subunit (MYPT1 / MBS) required for substrate binding, and a small subunit of unknown function named M20 (Hartshorne et al., 2004). Rho-associated protein kinase (ROCK), a downstream effector of RhoA (Ishizaki et al., 1996; Matsui et al., 1996), can activate NMII by direct phosphorylation of the regulatory light chain and indirectly by inhibiting MLCP (Amano et al., 1996; Kimura et al., 1996).

While phosphorylation of the RLC by MLCK and ROCK occurs at the same serine, one particular study showed that ROCK phosphorylates the RLC near the center of the cell while MLCK does so near the periphery (Totsukawa et al., 2000). This suggests that the two kinases cooperate in spatially regulating NMII activity as opposed to wholly overlapping in function. Likewise, NMII-driven retraction of the growth cone C-domain is activated by ROCK, while retrograde actin flow in the P-domain is insensitive to ROCK phosphorylation (Zhang et al., 2003). While the complete network of proteins that regulates NMII in the axon has yet to be revealed, its importance in axonal elongation is underscored by the fact that ROCK inhibition has been considered a potential candidate for augmenting axon regeneration following nerve damage (Borisoff et al., 2003; Tonges et al., 2011).

1.3.4 Adhesions

For cells to move, they must interact with their external environment. Focal adhesions are considered to be the main link between the inside of motile cells and their extracellular environment. Over 50 different molecules have been identified in the complexes themselves (Zamir and Geiger, 2001). While many of these have additional effectors whose physical

interaction with the complex has not been found (Zamir and Geiger, 2001), there are several notable proteins that are integral to the formation and maturation of focal adhesions in most contexts.

Focal adhesion initiation occurs when integrin receptors, transmembrane proteins that are the direct physical link between the extracellular matrix / substrate and the cytoplasm (Liu et al., 2000), cluster locally while actively engaging extracellular ligands (Miyamoto et al., 1995). These nascent focal adhesions are also referred to as focal complexes or as point contacts in growth cones (Gomez et al., 1996). Integrin clustering can occur stochastically based on location and concentration of extracellular ligand or be induced directly by intracellular Rac signaling (Nobes and Hall, 1995; Rottner et al., 1999). Clustering occurs near the leading edge under the lamellipodia of migrating cells (Kiosses et al., 2001) and growth cones (Gomez et al., 1996; Woo and Gomez, 2006). Two talin molecules bind during early focal adhesion initiation, which directly connect integrin to actin filaments (Brown et al., 2002; Nayal et al., 2004; Smith and McCann, 2007; Tanentzapf et al., 2006). These tripartite talin-based connections are sufficient to create weak links between the extracellular matrix and cortical actin measured biophysically as ‘slip-bonds’ (Jiang et al., 2003).

Focal complexes or point contacts can be transient, providing anchorage for traction forces at the leading edge of fast migrating cells (Beningo et al., 2001), or they can mature and become stable. Maturation of dynamic focal adhesions into stable complexes involves an increase in size and strength, an increase in the proteins recruited to the complex, and initiation of additional signaling mechanisms. This depends on RhoA activity, and is independent of Rac1 (Chrzanowska-Wodnicka and Burridge, 1996). NMII activity can also induce complex maturation (Bershadsky et al., 1996; Chrzanowska-Wodnicka and Burridge, 1996; Even-Ram et

al., 2007). Large, stable adhesions are generally found at a higher density in slowly moving or non-motile cells compared to rapidly moving cells such as fish keratocytes (Geiger et al., 2001).

The proper formation and turnover of adhesions is essential for proper axon outgrowth (Gomez et al., 1996; Woo and Gomez, 2006). Point contacts in the growth cone contain most of the same critical proteins as in non-neuronal cells including integrins, paxillin, vinculin, and FAK along with RhoA (Renaudin et al., 1999). Small point contacts form in both lamellipodia and filopodia, where they remain stationary relative to the substrate as the leading edge advances (Gomez et al., 1996; Woo and Gomez, 2006). Adding soluble laminin to cultured *Xenpous* spinal cord neurons causes an increase in the number of point contacts immediately followed by an increase in the rate of elongation (Woo and Gomez, 2006). There seems to be a need for transient sites for the growth cone to use for traction as seen in non-neuronal cells (Balaban et al., 2001). As the importance of forces in axonal elongation is becoming more apparent (Suter and Miller, 2011), understanding how neurons use focal adhesions to the stationary extracellular environment during force transduction is an increasing priority.

1.4 Biophysical models for axonal elongation

So far, the emphasis of this review has been on the major cytoskeletal structures found in axons. However, these systems do not act alone; it takes a coordinated effort of both the actin and microtubule cytoskeletons for proper wiring of the nervous system during development (Rodriguez et al., 2003). Neurons can extend axons without a proper functioning actin cytoskeleton *in vivo*, but they are unable to integrate guidance cues needed for proper targeting (Bentley and Toroian-Raymond, 1986). There is also evidence for a mechanical continuum between actin in the P-domain and microtubules in the C-domain required for coordinated growth cone advance (Suter et al., 1998). Although much progress has been made in identifying the proteins involved in axonal elongation, learning how they are integrated as a whole on a biophysical level remains a challenge.

1.4.1 Models for axonal elongation: a historical perspective

The question of how axons elongate dates back to the earliest descriptions of the nervous system by Ramon Y Cajal over a century ago (Ramon Y Cajal, 1890). As such, understanding current models of axonal elongation requires a historical discussion of how they were developed. Early efforts focused on how the axon was supplied with material. In 1948, Weiss and Hiscoe published a series of experiments in which strings were tied around nerve fibers to constrict axonal diameter. They observed the formation of a bulge just proximal to the constriction site (Weiss and Hiscoe, 1948). When the constriction was removed, the bulge slowly dissipated as it moved forward toward the growth cone. This suggested that material was being synthesized in the cell body and transported in bulk to the distal axon during outgrowth. In a series of papers throughout the 1960's, Sidney Ochs and colleagues injected radiolabeled amino acids into

mammalian spinal cords and followed their transport in nerve fibers over time. They repeatedly found coherent peaks of radioactivity that moved along the axon at different rates (Kidwai and Ochs, 1969; Ochs et al., 1962; Ochs and Johnson, 1969; Ochs et al., 1967). Thus, the hypothesis put forth by Weiss and Hiscoe stating that material was synthesized in the cell body and pushed forward like an "axonal pump" remained popular for several decades (Weiss and Hiscoe, 1948).

In 1970, however, Dennis Bray attached particles to elongating axons and found them to be stationary near the cell body. From this he concluded that the internal axonal framework was stationary (Bray, 1970), and it followed that axons were assembled at the distal tip. This idea was challenged by a study using a similar radioisotope approach as Ochs' group to show that the majority of the slow component of axonal transport was made up of tubulin and intermediate filaments (Hoffman and Lasek, 1975). This formed the basis for what was termed the Structural Hypothesis, which posited that the cytoskeleton was assembled in the cell body and transported into the axon as one coherent unit in a mechanism similar to the "axonal pump", thus driving axonal elongation (Hoffman and Lasek, 1975; Lasek, 1982). These two opposing ideas began a contentious debate over whether the axonal cytoskeleton is in motion or stationary.

Around this same time, Goldberg and Burmeister (1986) used video-enhanced differential interference contrast microscopy to record large *Aplysia* growth cones cultured on poly-lysine. Their observations led to the development of the Protrusion, Engorgement, and Consolidation model (PEC) for axonal elongation. According to this model, growth begins by protrusion of the leading edge plasma membrane, after which the growth cone becomes engorged by microtubules and organelles via fast axonal transport (Figure 1.2A). The final step is a consolidation step which converts the engorged C-domain into the new axon (Goldberg and Burmeister, 1986). Concurrently, Dennis Bray's group reported that local application of drugs

that interfere with microtubule polymerization to the growth cone blocked elongation, while application to the axon near the cell body did not (Bamburg et al., 1986). Together, the PEC and "tip-growth" models suggested that the growth cone was the critical site for axon assembly and not the cell body.

While the PEC model opposed the Structural Hypothesis by presuming a stationary cytoskeletal meshwork, it did not directly test this. In an attempt to disprove the Structural Hypothesis, subsequent experiments were designed to ask whether or not microtubules were transported out of the cell body in assembled form. As such, marks were made on the microtubule bundle near the cell body using photobleaching and photoactivation of fluorescently labeled tubulin. When tracked over time, the marks were consistently stationary both *in vitro* (Lim et al., 1990; Okabe and Hirokawa, 1988; Okabe and Hirokawa, 1990; Okabe and Hirokawa, 1992; Okabe and Hirokawa, 1993) and *in vivo* (Sabry et al., 1995; Sabry et al., 1991). The Structural Hypothesis was therefore abandoned in favor of models of axonal elongation that featured a stationary cytoskeletal framework, such as PEC.

There were, however, a few notable cases in which the photobleached marks were made on microtubule bundles near the growth cone in cultured *Xenopus* neurons. These marks, in contrast to those made near the cell body, were not stationary and instead moved forward as the growth cone advanced (Okabe and Hirokawa, 1990; Okabe and Hirokawa, 1992; Reinsch et al., 1991). Instead of investigating whether this represented relevant differences in *en masse* microtubule translocation between the proximal and distal axon, these observations were thought to simply be an oddity of *Xenopus* axons that were stretching as they grew (Chang et al., 1998; Okabe and Hirokawa, 1992; Wang and Brown, 2002).

While photobleaching approaches can give insight on bulk movements of the microtubule bundle, the rapid turnover of microtubules makes the observations limited to a brief period of time (Chang et al., 1998). Fluorescent speckle microscopy, a technique used to image individual microtubules and actin filaments (Waterman-Storer et al., 1998), requires high levels of illumination that can impair axonal elongation. In addition, imaging must be done at high magnification to achieve the resolution required to resolve the fluorescent speckles, which is not useful for comparing movements at different positions in a single axon. To circumvent these technical issues, Miller and Sheetz (2006) developed the use of docked mitochondria as fiduciary markers for the axonal cytoskeletal meshwork. Mitochondria are large organelles that can be easily visualized in low light conditions using fluorescent dyes. Mitochondria stably dock to the cytoskeleton at regular intervals along the axon, where they can remain in position for several hours at a time (Chada and Hollenbeck, 2004; Hirokawa, 1982; Miller and Sheetz, 2004; Morris and Hollenbeck, 1993; Saxton and Hollenbeck, 2012). This allows for a systematic analysis of cytoskeleton translocation throughout the entire length of the axon over long time scales on which significant elongation occurs.

By tracking docked mitochondria in elongating chick sensory neurons, Miller and Sheetz reported two notable findings: (1) mitochondria in the growth cone C-domain advanced in tandem with the growth cone and (2) while docked mitochondria near the cell body were stationary, there was a velocity gradient of motion that increased distally toward the growth cone (Miller and Sheetz, 2006). This pattern of movement indicated that the growth cone was advancing in bulk and that axons were being stretched during elongation. Importantly, this suggested that perhaps axonal stretching is a more relevant process than had been considered before and not an oddity of cultured *Xenopus* neurons.

Additional reports on the bulk movement of microtubules and axonal stretching began to emerge, supporting the idea that axonal stretching is a physiologically relevant process. Rat neurons, for instance, also grow by stretching (Lamoureux et al., 2010). Fluorescent speckle microscopy of microtubules in the growth cone showed they were being pulled forward in bulk together with the C-domain in *Aplysia* neurons (Lee and Suter, 2008; Schaefer et al., 2008). Together these observations led to the development of the Stretch and Intercalation model for axonal elongation (SAI) (Suter and Miller, 2011), wherein forces generated by the growth cone cause it to advance in bulk, which in turn stretches the axon. This is paired with mass addition along the length of the axon to prevent thinning (Lamoureux et al., 2010). Though this model is still being developed, there is mounting evidence that the cytoskeleton is in motion in the distal axon and growth cone.

With the hindsight that there is a velocity gradient of cytoskeleton movement along the axon, previous observations of bulk movement near the growth cone become significant. For instance, the forward movement of material near the growth cone was observed in rat neurons in 1970, where particles attached at the neck of the growth cone (where the growth cone adjoins with the axon) advanced as the growth cone advanced (Bray, 1970). Particles attached to the same axons near the cell body were stationary. Together with the docked mitochondria observations, this demonstrates that axonal stretching does not contradict the conclusions drawn from experiments on axonal transport that found the proximal cytoskeleton to be stationary. Therefore, the current question is not if axons stretch, but how.

1.4.2 Retrograde actin flow

One of the most striking phenomena of growth cones is the retrograde flow of actin in the P-domain. In a seminal study on the structure of large *Aplysia* growth cones, Forscher and Smith (1988) found that actin filaments in the lamellipodia moved from the leading edge of the P-domain centripetally toward the C-domain, where they were disassembled for recycling at the leading edge. As there is an inverse relationship between the rate of retrograde flow and the rate of growth cone advance (Lin and Forscher, 1995), investigating how retrograde flow affects growth cone motility has been at the forefront of the field of neuronal cell biology.

When the actin disrupting drug cytochalasin B is added to *Aplysia* growth cones, microtubules surge forward and engorge what was originally the P-domain (Forscher and Smith, 1988; Lin and Forscher, 1993). This has led to the popular view that retrograde actin flow is a barrier to axonal elongation by restricting microtubule advance. Depending on the school of thought, microtubules advance by polymerization (Hur et al., 2012; Stiess and Bradke, 2011), transport (Baas et al., 2006; Myers et al., 2006), or both (Dent and Gertler, 2003). In *Aplysia* growth cones, microtubules can polymerize into the P-domain using F-actin bundles as a guide, to which they become coupled in the process (Schaefer et al., 2002). This causes the microtubules to be simultaneously swept backwards by retrograde flow, which compresses the microtubule until it ultimately buckles and breaks (Schaefer et al., 2002). The fragmented microtubule is cleared from the P-domain while the plus end of the original microtubule is now located in the C-domain. Thus, retrograde actin flow prevents microtubule advance.

Microtubules can also enter the P-domain independently of F-actin bundles, which appear to do so by translocation (Burnette et al., 2007; Lee and Suter, 2008). This could be occurring as the end result of Stop-and-Go transport of individual microtubules (Ahmad et al., 2006; Baas et

al., 2006; Myers et al., 2006), or alternatively could be driven by substrate coupling. To explain the latter, actin filaments moving by retrograde flow can be coupled to the extracellular substrate, which reduces flow rate and acts as an anchor so barbed end polymerization can push the plasma membrane forward (Lin and Forscher, 1995; Mitchison and Kirschner, 1988; Suter et al., 1998). At the same time, coupling to the substrate causes the C-domain to be pulled forward in bulk, suggesting there is a mechanical continuum between actin in the P-domain and microtubules in the C-domain (Suter et al., 1998; Suter and Forscher, 2000; Suter and Miller, 2011). This is seen quite clearly when beads coated with cell adhesion molecules are bound to a growth cone, allowed to couple actin in the P-domain, and restrained from being transport backwards (Suter et al., 1998). The molecular basis for the forces required to pull the C-domain forward is still in question.

NMII is well-positioned to play a role in substrate-mediated elongation. When NMII is disrupted, traction force generated in the growth cone is reduced by 80% (Bridgman et al., 2001; Koch et al., 2012). These traction forces have been proposed to generate tension during actin-substrate coupling to pull microtubules from the C-domain forward (Lee and Suter, 2008; Suter and Miller, 2011). The bundle of microtubules in the C-domain advance in a manner similar to that of docked mitochondria in the growth cone (Lamoureux et al., 2010; Miller and Sheetz, 2006). It is quite possible, therefore, that NMII is a driving force for bulk growth cone advance and axonal stretching (Suter and Miller, 2011).

Another well-accepted function of NMII in the growth cone is to drive retrograde actin flow. When NMII function is disrupted in *Aplysia* growth cones by microinjection of inactivated myosin heads or treatment with 2,3-butanedione-2-monoxine (BDM), retrograde flow is greatly attenuated (Lin et al., 1996). Confirming this, blebbistatin, a pharmacological inhibitor with a

much higher specificity for NMII isoforms compared to BDM (Straight et al., 2003), also slows retrograde flow (Medeiros et al., 2006). Growing neurons from NMIIB null mice has hinted that this isoform specifically drives retrograde flow (Brown and Bridgman, 2003).

If NMII is generating traction force to pull the growth cone forward, one would expect that disruption of NMII would decrease the rate of elongation as traction force would be reduced. Conversely, if retrograde flow is a barrier to elongation then by definition so is NMII. In this case, NMII disruption would be predicted to increase the rate of elongation. Somewhat paradoxically, both of these have been reported. Though the exact reason for these disparate reports is unknown, the type of culture substrate has a profound effect: disruption of NMII increases the rate of elongation on poly-amines or on the non-permissive substrate chondroitin sulfate proteoglycan (Hur et al., 2011; Ketschek et al., 2007; Turney and Bridgman, 2005; Yu et al., 2012), whereas it decreases it on laminin (Bridgman et al., 2001; Ketschek et al., 2007; Tullio et al., 2001; Turney and Bridgman, 2005). In order to get a clear understanding of NMII and retrograde actin flow function during axonal elongation, considerations must be made for the other cellular processes that are altered when NMII and actin are disrupted (such as regulating focal adhesion dynamics). An additional caveat worth mentioning is that the majority of studies on how retrograde flow clears microtubules from the P-domain were conducted in *Aplysia* growth cones that were intentionally prevented from elongating by the use of highly adherent substrates (Burnette et al., 2007; Medeiros et al., 2006; Schaefer et al., 2002). Whether the same cytoskeletal interactions occur in stationary and rapidly advancing growth cones is unknown.

1.4.3 Microtubule dynamics in the growth cone

Microtubule dynamics are an important component of elongating axons. Local reduction of microtubule polymerization in the growth cone causes them to retract (Bamburg et al., 1986). Axonal elongation also decreases when neurons are treated with the polymerization promoting drug taxol (Letourneau et al., 1987; Rochlin et al., 1996) even though the total mass of microtubule polymer increases (Rochlin et al., 1996). This suggests that it is the disruption of microtubule dynamic instability and not just polymerization that is blocking elongation. As such, the ability to rapidly reorganize the microtubule cytoskeleton in the growth cone may be required for axonal elongation.

Dynamic microtubules in the growth cone are needed to respond properly to guidance cues. Several studies have shown that the microtubule array in the growth cone undergoes constant rearrangement, with a trend for reorientation in the direction of turning (Lin and Forscher, 1993; Sabry et al., 1991; Tanaka et al., 1995; Tanaka and Sabry, 1995; Tanaka and Kirschner, 1991). Dampening microtubule dynamics reduces a growth cone's ability to turn away from inhibitory substrate borders (Challacombe et al., 1997) or repulsive guidance cues (Zhou et al., 2002). The hypothesis is that dynamic microtubules explore the P-domain in order to "sense" the extracellular environment and integrate this information into the proper turning and / or growth response (Dent et al., 1999; Dent and Gertler, 2003). In this context, one can imagine that continuous establishment and turnover of microtubules in the growth cone allows for a rapid response to extracellular cues.

Presumably, the reorganization of microtubules can occur more rapidly with young, dynamic microtubules as opposed to older, more stable ones. This would explain why the growth cone and distal axon feature a dynamic population of microtubules as opposed to the more stable

ones found along the length (Baas and Black, 1990; Kollins et al., 2009; Lim et al., 1989). Likewise, detyrosinated tubulin, a marker for old microtubules (Brown et al., 1993), is not found in the P-domain of turning growth cones (Challacombe et al., 1996). The retrograde flow of actin likely prevents microtubules from becoming stabilized in the growth cone by clearing them from the P-domain and supplying plus ends for polymerization (Schaefer et al., 2002).

Growth cone turning does, however, require more than just microtubule dynamics. While growth cones turn away from gradients of microtubule destabilizing drugs and toward gradients of taxol, both are blocked by toxin B (Buck and Zheng, 2002), an inhibitor of the Rho family GTPases (Just et al., 1995). The implication is that altering microtubule dynamics can lead to changes in other cellular processes such as NMII force generation. Indeed, microtubule depolymerization initiates a Rho signaling cascade that activates NMII in non-neuronal cells (Kolodney and Elson, 1995; Liu et al., 1998). Therefore, there is a direct link between microtubule depolymerization and force generation. Separating these two experimentally is a current challenge, but doing so will yield insight into the independent contributions microtubule dynamics and forces make to axonal elongation.

1.4.4 The role of forces in axonal elongation

A relationship between forces and axonal elongation has been acknowledged since it was shown that tension externally applied to an axon is sufficient to induce axonal growth (Bray, 1984). The ability of neurons to sustain persistent stretching is remarkable. Individual axons in large aquatic mammals can reach up to 30 m, mostly due to stretching after synapse formation (Smith, 2009). The use of specialized two-platform culture chambers has demonstrated that axons can stretch at rates up to 8 mm/day while increasing in diameter and maintaining their

electrophysiological capacity (Pfister et al., 2006; Pfister et al., 2004). While this “towed growth” mechanism is required to maintain synaptic connections as the developing animal grows in size, how this translates to growth cone-mediated elongation is unclear.

Our current understanding of forces in the axon is quite rudimentary. A classic study using force-calibrated towing needles demonstrated the growth cone can generate force to pull on its substrate (Lamoureux et al., 1989). Mathematical modeling suggests that force generated at the growth cone can cause the axon to stretch, but that stretching is a function of the complex relationship between forces, strength of adhesion to the substrate and viscosity of the axon (O'Toole et al., 2008). Forces generated along the axon that promote the telescoping of microtubules might also contribute to axonal stretching. While NMII forces are clearly important for elongation, they seem to perform multiple, sometimes opposing, functions. They can cause axonal retraction (Ahmad et al., 2000; Gallo, 2006), prevent microtubule advance (Hur et al., 2012; Stiess and Bradke, 2011; Vallee et al., 2009), or could be pulling material forward (Suter and Miller, 2011). Microtubule polymerization activates signaling pathways that alter force generation (Buck and Zheng, 2002). While the individual components of force generation in axons are beginning to be identified, assembling them into a coherent biophysical description of the axon is a current challenge.

As the significance of axonal stretching and bulk movement during elongation has become apparent, understanding how this occurs is a priority. A large amount of force is required to move the growth cone and cytoskeletal meshwork in bulk (Suter and Miller, 2011). Therefore, in order to develop comprehensive models for elongation, we must understand how forces are generated and regulated. In doing so, the hope is to aid in the refinement of clinical strategies to repair axons following nerve damage.

APPENDIX

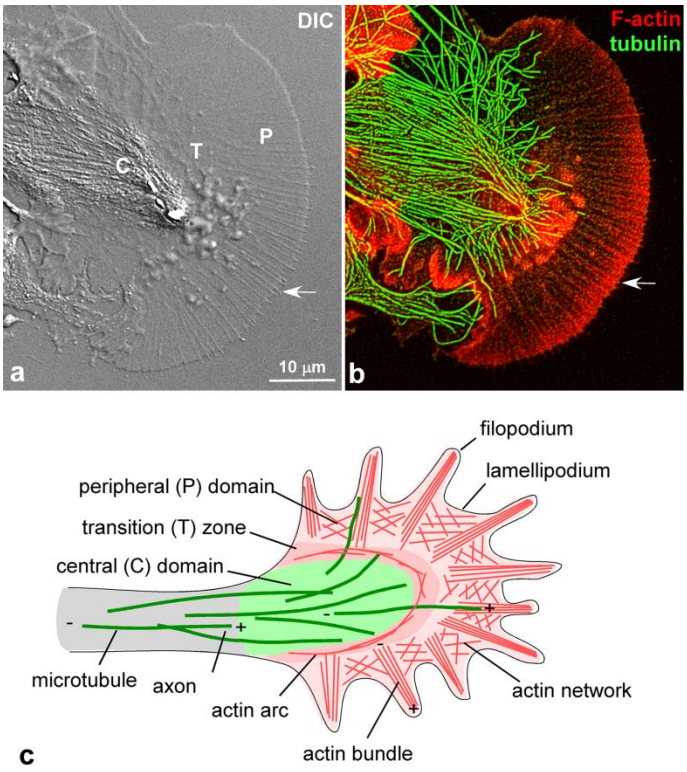

Figure 1.1. Cytoskeleton organization in neuronal growth cones. (**a**) Differential interference contrast image of an *Aplysia* growth cone grown on poly-lysine substrate. (**b**) Corresponding fluorescent image showing individual actin filaments labeled with fluorescently tagged phalloidin and microtubules labeled by tubulin immunofluorescence. (**c**) Schematic representation of the various growth cone domains, which can also be identified in (a) and (b). This figure was adapted from Suter and Miller, "The Emerging Role of Forces in Axonal Elongation" Progress in Neurobiology, © Elsevier, 2011.

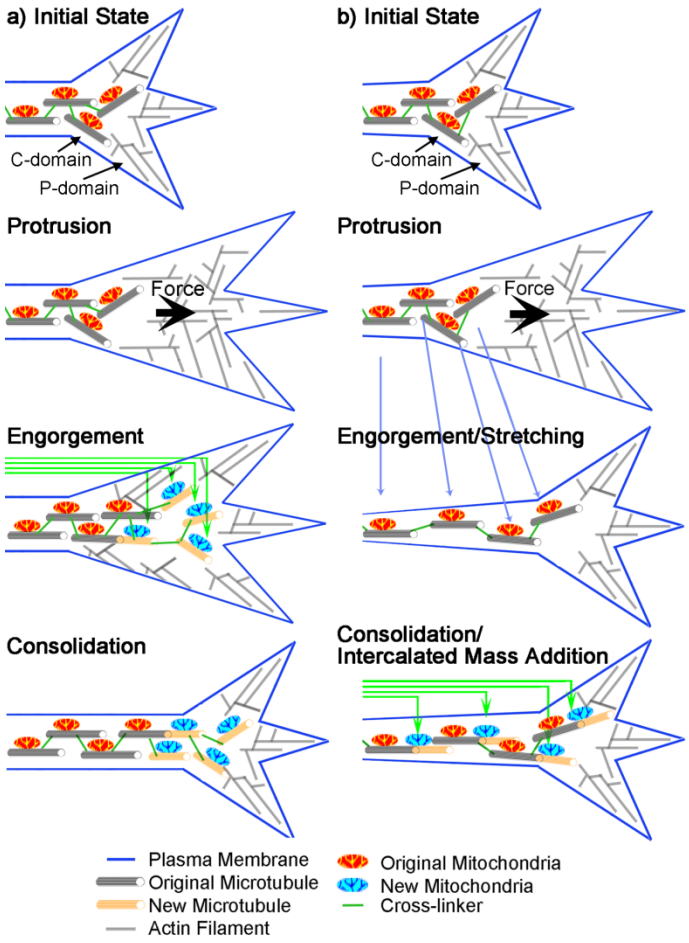

Figure 1.2. Two models of axonal elongation. (**a**) The Protrusion, Engorgement and Consolidation model. The actin cytoskeleton protrudes forward through polymerization at the leading edge of the cell. Forces generated at the interface of the C and P domains clear a corridor for the assembly of microtubules. Engorgement occurs as microtubule polymerization and the delivery of organelles by fast transport adds new material at the tip of the C-domain. Consolidation occurs as microtubules in the neck of the growth cone are bundled and actin filaments are disassembled. (**b**) The Stretch and Intercalated Growth model. Protrusion occurs by assembly as in the previous model, but Engorgement differs in that forces generated in the growth cone pull the C-domain and the rest of the axon forward and stretch the axon. Consolidation occurs as pulling forces bundle the microtubules and new mass is added along the length of the axon in an intercalated fashion to prevent thinning (green arrows). In this model, the growth cone is not assembled at the leading edge and disassembled at the neck; instead the entire growth cone advances as a coherent unit. Figure reproduced from Suter and Miller, "The Emerging Role of Forces in Axonal Elongation" Progress in Neurobiology, © Elsevier, 2011.

REFERENCES

REFERENCES

Abraham, V.C., V. Krishnamurthi, D.L. Taylor, and F. Lanni. 1999. The actin-based nanomachine at the leading edge of migrating cells. *Biophysical journal*. 77:1721-1732.

Ahmad, F.J., C.J. Echeverri, R.B. Vallee, and P.W. Baas. 1998. Cytoplasmic dynein and dynactin are required for the transport of microtubules into the axon. *The Journal of cell biology*. 140:391-401.

Ahmad, F.J., Y. He, K.A. Myers, T.P. Hasaka, F. Francis, M.M. Black, and P.W. Baas. 2006. Effects of dynactin disruption and dynein depletion on axonal microtubules. *Traffic (Copenhagen, Denmark)*. 7:524-537.

Ahmad, F.J., J. Hughey, T. Wittmann, A. Hyman, M. Greaser, and P.W. Baas. 2000. Motor proteins regulate force interactions between microtubules and microfilaments in the axon. *Nature cell biology*. 2:276-280.

Akhmanova, A., and M.O. Steinmetz. 2008. Tracking the ends: a dynamic protein network controls the fate of microtubule tips. *Nature reviews. Molecular cell biology*. 9:309-322.

Alberts, B., A. Johnson, J. Lewis, M. Raff, K. Roberts, and P. Walter. 2008. Molecular Biology of the Cell. Garland Science, New York, NY.

Allen, C., and G.G. Borisy. 1974. Structural polarity and directional growth of microtubules of Chlamydomonas flagella. *J Mol Biol*. 90:381-402.

Amann, K.J., and T.D. Pollard. 2001. Direct real-time observation of actin filament branching mediated by Arp2/3 complex using total internal reflection fluorescence microscopy. *Proceedings of the National Academy of Sciences of the United States of America*. 98:15009-15013.

Amano, M., M. Ito, K. Kimura, Y. Fukata, K. Chihara, T. Nakano, Y. Matsuura, and K. Kaibuchi. 1996. Phosphorylation and activation of myosin by Rho-associated kinase (Rho-kinase). *The Journal of biological chemistry*. 271:20246-20249.

Amos, L., and A. Klug. 1974. Arrangement of subunits in flagellar microtubules. *Journal of cell science*. 14:523-549.

Aniento, F., N. Emans, G. Griffiths, and J. Gruenberg. 1993. Cytoplasmic dynein-dependent vesicular transport from early to late endosomes. *The Journal of cell biology*. 123:1373-1387.

Baas, P.W., and F.J. Ahmad. 1992. The plus ends of stable microtubules are the exclusive nucleating structures for microtubules in the axon. *The Journal of cell biology*. 116:1231-1241.

Baas, P.W., and M.M. Black. 1990. Individual microtubules in the axon consist of domains that differ in both composition and stability. *The Journal of cell biology*. 111:495-509.

Baas, P.W., J.S. Deitch, M.M. Black, and G.A. Banker. 1988. Polarity orientation of microtubules in hippocampal neurons: uniformity in the axon and nonuniformity in the dendrite. *Proceedings of the National Academy of Sciences of the United States of America*. 85:8335-8339.

Baas, P.W., and H.C. Joshi. 1992. Gamma-tubulin distribution in the neuron: implications for the origins of neuritic microtubules. *The Journal of cell biology*. 119:171-178.

Baas, P.W., A. Karabay, and L. Qiang. 2005. Microtubules cut and run. *Trends Cell Biol*. 15:518-524.

Baas, P.W., C. Vidya Nadar, and K.A. Myers. 2006. Axonal transport of microtubules: the long and short of it. *Traffic (Copenhagen, Denmark)*. 7:490-498.

Balaban, N.Q., U.S. Schwarz, D. Riveline, P. Goichberg, G. Tzur, I. Sabanay, D. Mahalu, S. Safran, A. Bershadsky, L. Addadi, and B. Geiger. 2001. Force and focal adhesion assembly: a close relationship studied using elastic micropatterned substrates. *Nature cell biology*. 3:466-472.

Bamburg, J.R., D. Bray, and K. Chapman. 1986. Assembly of microtubules at the tip of growing axons. *Nature*. 321:788-790.

Bamburg, J.R., A. McGough, and S. Ono. 1999. Putting a new twist on actin: ADF/cofilins modulate actin dynamics. *Trends Cell Biol*. 9:364-370.

Bear, J.E., T.M. Svitkina, M. Krause, D.A. Schafer, J.J. Loureiro, G.A. Strasser, I.V. Maly, O.Y. Chaga, J.A. Cooper, G.G. Borisy, and F.B. Gertler. 2002. Antagonism between

Ena/VASP proteins and actin filament capping regulates fibroblast motility. *Cell*. 109:509-521.

Begg, D.A., R. Rodewald, and L.I. Rebhun. 1978. The visualization of actin filament polarity in thin sections. Evidence for the uniform polarity of membrane-associated filaments. *The Journal of cell biology*. 79:846-852.

Beningo, K.A., M. Dembo, I. Kaverina, J.V. Small, and Y.L. Wang. 2001. Nascent focal adhesions are responsible for the generation of strong propulsive forces in migrating fibroblasts. *The Journal of cell biology*. 153:881-888.

Bentley, D., and A. Toroian-Raymond. 1986. Disoriented pathfinding by pioneer neurone growth cones deprived of filopodia by cytochalasin treatment. *Nature*. 323:712-715.

Bergen, L.G., and G.G. Borisy. 1980. Head-to-tail polymerization of microtubules in vitro. Electron microscope analysis of seeded assembly. *The Journal of cell biology*. 84:141-150.

Bershadsky, A., A. Chausovsky, E. Becker, A. Lyubimova, and B. Geiger. 1996. Involvement of microtubules in the control of adhesion-dependent signal transduction. *Current biology : CB*. 6:1279-1289.

Blanchoin, L., K.J. Amann, H.N. Higgs, J.B. Marchand, D.A. Kaiser, and T.D. Pollard. 2000. Direct observation of dendritic actin filament networks nucleated by Arp2/3 complex and WASP/Scar proteins. *Nature*. 404:1007-1011.

Blanchoin, L., and T.D. Pollard. 2002. Hydrolysis of ATP by polymerized actin depends on the bound divalent cation but not profilin. *Biochemistry*. 41:597-602.

Borisoff, J.F., C.C. Chan, G.W. Hiebert, L. Oschipok, G.S. Robertson, R. Zamboni, J.D. Steeves, and W. Tetzlaff. 2003. Suppression of Rho-kinase activity promotes axonal growth on inhibitory CNS substrates. *Mol Cell Neurosci*. 22:405-416.

Bray, D. 1970. Surface movements during the growth of single explanted neurons. *Proceedings of the National Academy of Sciences of the United States of America*. 65:905-910.

Bray, D. 1984. Axonal growth in response to experimentally applied mechanical tension. *Dev Biol*. 102:379-389.

Bray, D., and M.B. Bunge. 1981. Serial analysis of microtubules in cultured rat sensory axons. *J Neurocytol*. 10:589-605.

Bridgman, P.C., and M.E. Dailey. 1989. The organization of myosin and actin in rapid frozen nerve growth cones. *The Journal of cell biology*. 108:95-109.

Bridgman, P.C., S. Dave, C.F. Asnes, A.N. Tullio, and R.S. Adelstein. 2001. Myosin IIB is required for growth cone motility. *J Neurosci*. 21:6159-6169.

Brown, A., Y. Li, T. Slaughter, and M.M. Black. 1993. Composite microtubules of the axon: quantitative analysis of tyrosinated and acetylated tubulin along individual axonal microtubules. *Journal of cell science*. 104 (Pt 2):339-352.

Brown, M.E., and P.C. Bridgman. 2003. Retrograde flow rate is increased in growth cones from myosin IIB knockout mice. *Journal of cell science*. 116:1087-1094.

Brown, N.H., S.L. Gregory, W.L. Rickoll, L.I. Fessler, M. Prout, R.A. White, and J.W. Fristrom. 2002. Talin is essential for integrin function in Drosophila. *Developmental cell*. 3:569-579.

Buck, K.B., and J.Q. Zheng. 2002. Growth cone turning induced by direct local modification of microtubule dynamics. *The Journal of neuroscience : the official journal of the Society for Neuroscience*. 22:9358-9367.

Burgess, S.A., M.L. Walker, H. Sakakibara, P.J. Knight, and K. Oiwa. 2003. Dynein structure and power stroke. *Nature*. 421:715-718.

Burgess, S.A., S. Yu, M.L. Walker, R.J. Hawkins, J.M. Chalovich, and P.J. Knight. 2007. Structures of smooth muscle myosin and heavy meromyosin in the folded, shutdown state. *J Mol Biol*. 372:1165-1178.

Burnette, D.T., A.W. Schaefer, L. Ji, G. Danuser, and P. Forscher. 2007. Filopodial actin bundles are not necessary for microtubule advance into the peripheral domain of Aplysia neuronal growth cones. *Nature cell biology*. 9:1360-1369.

Carlier, M.F., T.L. Hill, and Y. Chen. 1984. Interference of GTP hydrolysis in the mechanism of microtubule assembly: an experimental study. *Proceedings of the National Academy of Sciences of the United States of America*. 81:771-775.

Carlier, M.F., and D. Pantaloni. 1981. Kinetic analysis of guanosine 5'-triphosphate hydrolysis associated with tubulin polymerization. *Biochemistry*. 20:1918-1924.

Carlier, M.F., and D. Pantaloni. 1986. Direct evidence for ADP-Pi-F-actin as the major intermediate in ATP-actin polymerization. Rate of dissociation of Pi from actin filaments. *Biochemistry*. 25:7789-7792.

Carlier, M.F., D. Pantaloni, J.A. Evans, P.K. Lambooy, E.D. Korn, and M.R. Webb. 1988. The hydrolysis of ATP that accompanies actin polymerization is essentially irreversible. *FEBS Lett*. 235:211-214.

Carter, A.P., J.E. Garbarino, E.M. Wilson-Kubalek, W.E. Shipley, C. Cho, R.A. Milligan, R.D. Vale, and I.R. Gibbons. 2008. Structure and functional role of dynein's microtubule-binding domain. *Science (New York, N.Y.* 322:1691-1695.

Chada, S.R., and P.J. Hollenbeck. 2004. Nerve growth factor signaling regulates motility and docking of axonal mitochondria. *Current biology : CB*. 14:1272-1276.

Challacombe, J.F., D.M. Snow, and P.C. Letourneau. 1996. Actin filament bundles are required for microtubule reorientation during growth cone turning to avoid an inhibitory guidance cue. *Journal of cell science*. 109 (Pt 8):2031-2040.

Challacombe, J.F., D.M. Snow, and P.C. Letourneau. 1997. Dynamic microtubule ends are required for growth cone turning to avoid an inhibitory guidance cue. *The Journal of neuroscience : the official journal of the Society for Neuroscience*. 17:3085-3095.

Chang, S., V.I. Rodionov, G.G. Borisy, and S.V. Popov. 1998. Transport and turnover of microtubules in frog neurons depend on the pattern of axonal growth. *The Journal of neuroscience : the official journal of the Society for Neuroscience*. 18:821-829.

Chrzanowska-Wodnicka, M., and K. Burridge. 1996. Rho-stimulated contractility drives the formation of stress fibers and focal adhesions. *The Journal of cell biology*. 133:1403-1415.

Conde, C., and A. Caceres. 2009. Microtubule assembly, organization and dynamics in axons and dendrites. *Nature reviews. Neuroscience*. 10:319-332.

Cooper, J.A., and D.A. Schafer. 2000. Control of actin assembly and disassembly at filament ends. *Current opinion in cell biology*. 12:97-103.

Corthesy-Theulaz, I., A. Pauloin, and S.R. Pfeffer. 1992. Cytoplasmic dynein participates in the centrosomal localization of the Golgi complex. *The Journal of cell biology*. 118:1333-1345.

Craig, R., and J.L. Woodhead. 2006. Structure and function of myosin filaments. *Curr Opin Struct Biol*. 16:204-212.

Daniels, M.P. 1972. Colchicine inhibition of nerve fiber formation in vitro. *The Journal of cell biology*. 53:164-176.

Dennerll, T.J., P. Lamoureux, R.E. Buxbaum, and S.R. Heidemann. 1989. The cytomechanics of axonal elongation and retraction. *The Journal of cell biology*. 109:3073-3083.

Dent, E.W., J.L. Callaway, G. Szebenyi, P.W. Baas, and K. Kalil. 1999. Reorganization and movement of microtubules in axonal growth cones and developing interstitial branches. *The Journal of neuroscience : the official journal of the Society for Neuroscience*. 19:8894-8908.

Dent, E.W., and F.B. Gertler. 2003. Cytoskeletal dynamics and transport in growth cone motility and axon guidance. *Neuron*. 40:209-227.

Dentler, W.L., S. Granett, G.B. Witman, and J.L. Rosenbaum. 1974. Directionality of brain microtubule assembly in vitro. *Proceedings of the National Academy of Sciences of the United States of America*. 71:1710-1714.

Desai, A., and T.J. Mitchison. 1997. Microtubule polymerization dynamics. *Annual review of cell and developmental biology*. 13:83-117.

DeWitt, M.A., A.Y. Chang, P.A. Combs, and A. Yildiz. 2012. Cytoplasmic dynein moves through uncoordinated stepping of the AAA+ ring domains. *Science (New York, N.Y.* 335:221-225.

Dickson, B.J. 2002. Molecular mechanisms of axon guidance. *Science (New York, N.Y.* 298:1959-1964.

Dominguez, R., Y. Freyzon, K.M. Trybus, and C. Cohen. 1998. Crystal structure of a vertebrate smooth muscle myosin motor domain and its complex with the essential light chain: visualization of the pre-power stroke state. *Cell*. 94:559-571.

Doolittle, K.W., I. Reddy, and J.G. McNally. 1995. 3D analysis of cell movement during normal and myosin-II-null cell morphogenesis in dictyostelium. *Developmental biology*. 167:118-129.

Drechsel, D.N., A.A. Hyman, M.H. Cobb, and M.W. Kirschner. 1992. Modulation of the dynamic instability of tubulin assembly by the microtubule-associated protein tau. *Mol Biol Cell*. 3:1141-1154.

Driskell, O.J., A. Mironov, V.J. Allan, and P.G. Woodman. 2007. Dynein is required for receptor sorting and the morphogenesis of early endosomes. *Nature cell biology*. 9:113-120.

Echeverri, C.J., B.M. Paschal, K.T. Vaughan, and R.B. Vallee. 1996. Molecular characterization of the 50-kD subunit of dynactin reveals function for the complex in chromosome alignment and spindle organization during mitosis. *The Journal of cell biology*. 132:617-633.

Euteneuer, U., M.P. Koonce, K.K. Pfister, and M. Schliwa. 1988. An ATPase with properties expected for the organelle motor of the giant amoeba, Reticulomyxa. *Nature*. 332:176-178.

Even-Ram, S., A.D. Doyle, M.A. Conti, K. Matsumoto, R.S. Adelstein, and K.M. Yamada. 2007. Myosin IIA regulates cell motility and actomyosin-microtubule crosstalk. *Nature cell biology*. 9:299-309.

Fan, J., A.D. Griffiths, A. Lockhart, R.A. Cross, and L.A. Amos. 1996. Microtubule minus ends can be labelled with a phage display antibody specific to alpha-tubulin. *J Mol Biol*. 259:325-330.

Finer, J.T., R.M. Simmons, and J.A. Spudich. 1994. Single myosin molecule mechanics: piconewton forces and nanometre steps. *Nature*. 368:113-119.

Forscher, P., and S.J. Smith. 1988. Actions of cytochalasins on the organization of actin filaments and microtubules in a neuronal growth cone. *The Journal of cell biology*. 107:1505-1516.

Fujiwara, I., S. Takahashi, H. Tadakuma, T. Funatsu, and S. Ishiwata. 2002. Microscopic analysis of polymerization dynamics with individual actin filaments. *Nature cell biology*. 4:666-673.

Fukata, M., T. Watanabe, J. Noritake, M. Nakagawa, M. Yamaga, S. Kuroda, Y. Matsuura, A. Iwamatsu, F. Perez, and K. Kaibuchi. 2002. Rac1 and Cdc42 capture microtubules through IQGAP1 and CLIP-170. *Cell*. 109:873-885.

Gallo, G. 2006. RhoA-kinase coordinates F-actin organization and myosin II activity during semaphorin-3A-induced axon retraction. *Journal of cell science*. 119:3413-3423.

Gee, M.A., J.E. Heuser, and R.B. Vallee. 1997. An extended microtubule-binding structure within the dynein motor domain. *Nature*. 390:636-639.

Geiger, B., A. Bershadsky, R. Pankov, and K.M. Yamada. 2001. Transmembrane crosstalk between the extracellular matrix--cytoskeleton crosstalk. *Nature reviews. Molecular cell biology*. 2:793-805.

Gill, S.R., T.A. Schroer, I. Szilak, E.R. Steuer, M.P. Sheetz, and D.W. Cleveland. 1991. Dynactin, a conserved, ubiquitously expressed component of an activator of vesicle motility mediated by cytoplasmic dynein. *The Journal of cell biology*. 115:1639-1650.

Goldberg, D.J., and D.W. Burmeister. 1986. Stages in axon formation: observations of growth of Aplysia axons in culture using video-enhanced contrast-differential interference contrast microscopy. *The Journal of cell biology*. 103:1921-1931.

Golomb, E., X. Ma, S.S. Jana, Y.A. Preston, S. Kawamoto, N.G. Shoham, E. Goldin, M.A. Conti, J.R. Sellers, and R.S. Adelstein. 2004. Identification and characterization of nonmuscle myosin II-C, a new member of the myosin II family. *The Journal of biological chemistry*. 279:2800-2808.

Gomez, T.M., F.K. Roche, and P.C. Letourneau. 1996. Chick sensory neuronal growth cones distinguish fibronectin from laminin by making substratum contacts that resemble focal contacts. *Journal of neurobiology*. 29:18-34.

Gonczy, P., S. Pichler, M. Kirkham, and A.A. Hyman. 1999. Cytoplasmic dynein is required for distinct aspects of MTOC positioning, including centrosome separation, in the one cell stage Caenorhabditis elegans embryo. *The Journal of cell biology*. 147:135-150.

Goshima, G., F. Nedelec, and R.D. Vale. 2005. Mechanisms for focusing mitotic spindle poles by minus end-directed motor proteins. *The Journal of cell biology*. 171:229-240.

Grabham, P.W., G.E. Seale, M. Bennecib, D.J. Goldberg, and R.B. Vallee. 2007. Cytoplasmic dynein and LIS1 are required for microtubule advance during growth cone remodeling and fast axonal outgrowth. *The Journal of neuroscience : the official journal of the Society for Neuroscience*. 27:5823-5834.

Hartshorne, D.J., M. Ito, and F. Erdodi. 2004. Role of protein phosphatase type 1 in contractile functions: myosin phosphatase. *The Journal of biological chemistry*. 279:37211-37214.

Heidemann, S.R., P. Lamoureux, and R.E. Buxbaum. 1990. Growth cone behavior and production of traction force. *The Journal of cell biology*. 111:1949-1957.

Heidemann, S.R., J.M. Landers, and M.A. Hamborg. 1981. Polarity orientation of axonal microtubules. *The Journal of cell biology*. 91:661-665.

Heiss, S.G., and J.A. Cooper. 1991. Regulation of CapZ, an actin capping protein of chicken muscle, by anionic phospholipids. *Biochemistry*. 30:8753-8758.

Hendricks, A.G., J.E. Lazarus, E. Perlson, M.K. Gardner, D.J. Odde, Y.E. Goldman, and E.L. Holzbaur. 2012. Dynein tethers and stabilizes dynamic microtubule plus ends. *Current biology : CB*. 22:632-637.

Hill, T.L., and M.W. Kirschner. 1982. Bioenergetics and kinetics of microtubule and actin filament assembly-disassembly. *Int Rev Cytol*. 78:1-125.

Hirokawa, N. 1982. Cross-linker system between neurofilaments, microtubules, and membranous organelles in frog axons revealed by the quick-freeze, deep-etching method. *The Journal of cell biology*. 94:129-142.

Hirose, K., J. Fan, and L.A. Amos. 1995. Re-examination of the polarity of microtubules and sheets decorated with kinesin motor domain. *J Mol Biol*. 251:329-333.

Hoffman, P.N., and R.J. Lasek. 1975. The slow component of axonal transport. Identification of major structural polypeptides of the axon and their generality among mammalian neurons. *The Journal of cell biology*. 66:351-366.

Hoglund, A.S., R. Karlsson, E. Arro, B.A. Fredriksson, and U. Lindberg. 1980. Visualization of the peripheral weave of microfilaments in glia cells. *J Muscle Res Cell Motil*. 1:127-146.

Holzbaur, E.L., and K.A. Johnson. 1989. Microtubules accelerate ADP release by dynein. *Biochemistry*. 28:7010-7016.

Hur, E.M., Saijilafu, and F.Q. Zhou. 2012. Growing the growth cone: remodeling the cytoskeleton to promote axon regeneration. *Trends in neurosciences*. 35:164-174.

Hur, E.M., I.H. Yang, D.H. Kim, J. Byun, Saijilafu, W.L. Xu, P.R. Nicovich, R. Cheong, A. Levchenko, N. Thakor, and F.Q. Zhou. 2011. Engineering neuronal growth cones to promote axon regeneration over inhibitory molecules. *Proceedings of the National Academy of Sciences of the United States of America*. 108:5057-5062.

Ikebe, M., S. Komatsu, J.L. Woodhead, K. Mabuchi, R. Ikebe, J. Saito, R. Craig, and M. Higashihara. 2001. The tip of the coiled-coil rod determines the filament formation of smooth muscle and nonmuscle myosin. *The Journal of biological chemistry*. 276:30293-30300.

Imamula, K., T. Kon, R. Ohkura, and K. Sutoh. 2007. The coordination of cyclic microtubule association/dissociation and tail swing of cytoplasmic dynein. *Proceedings of the National Academy of Sciences of the United States of America*. 104:16134-16139.

Isambert, H., P. Venier, A.C. Maggs, A. Fattoum, R. Kassab, D. Pantaloni, and M.F. Carlier. 1995. Flexibility of actin filaments derived from thermal fluctuations. Effect of bound nucleotide, phalloidin, and muscle regulatory proteins. *The Journal of biological chemistry*. 270:11437-11444.

Isenberg, G., J.V. Small, and G.W. Kreutzberg. 1978. Correlation between actin polymerization and surface receptor segregation in neuroblastoma cells treated with concanavalin A. *J Neurocytol*. 7:649-661.

Ishizaki, T., M. Maekawa, K. Fujisawa, K. Okawa, A. Iwamatsu, A. Fujita, N. Watanabe, Y. Saito, A. Kakizuka, N. Morii, and S. Narumiya. 1996. The small GTP-binding protein Rho binds to and activates a 160 kDa Ser/Thr protein kinase homologous to myotonic dystrophy kinase. *Embo J*. 15:1885-1893.

Jay, P.Y., P.A. Pham, S.A. Wong, and E.L. Elson. 1995. A mechanical function of myosin II in cell motility. *Journal of cell science*. 108 (Pt 1):387-393.

Jiang, G., G. Giannone, D.R. Critchley, E. Fukumoto, and M.P. Sheetz. 2003. Two-piconewton slip bond between fibronectin and the cytoskeleton depends on talin. *Nature*. 424:334-337.

Joshi, H.C., M.J. Palacios, L. McNamara, and D.W. Cleveland. 1992. Gamma-tubulin is a centrosomal protein required for cell cycle-dependent microtubule nucleation. *Nature*. 356:80-83.

Jung, H.S., S. Komatsu, M. Ikebe, and R. Craig. 2008. Head-head and head-tail interaction: a general mechanism for switching off myosin II activity in cells. *Mol Biol Cell*. 19:3234-3242.

Just, I., J. Selzer, M. Wilm, C. von Eichel-Streiber, M. Mann, and K. Aktories. 1995. Glucosylation of Rho proteins by Clostridium difficile toxin B. *Nature*. 375:500-503.

Kamm, K.E., and J.T. Stull. 1985. The function of myosin and myosin light chain kinase phosphorylation in smooth muscle. *Annu Rev Pharmacol Toxicol*. 25:593-620.

Karki, S., and E.L. Holzbaur. 1995. Affinity chromatography demonstrates a direct binding between cytoplasmic dynein and the dynactin complex. *The Journal of biological chemistry*. 270:28806-28811.

Karlsson, R., I. Lassing, A.S. Hoglund, and U. Lindberg. 1984. The organization of microfilaments in spreading platelets: a comparison with fibroblasts and glial cells. *J Cell Physiol*. 121:96-113.

Keith, C.H. 1987. Slow transport of tubulin in the neurites of differentiated PC12 cells. *Science (New York, N.Y.* 235:337-339.

Kelley, C.A., J.R. Sellers, D.L. Gard, D. Bui, R.S. Adelstein, and I.C. Baines. 1996. Xenopus nonmuscle myosin heavy chain isoforms have different subcellular localizations and enzymatic activities. *The Journal of cell biology*. 134:675-687.

Ketschek, A.R., S.L. Jones, and G. Gallo. 2007. Axon extension in the fast and slow lanes: substratum-dependent engagement of myosin II functions. *Developmental neurobiology*. 67:1305-1320.

Kidwai, A.M., and S. Ochs. 1969. Components of fast and slow phases of axoplasmic flow. *Journal of neurochemistry*. 16:1105-1112.

Kikkawa, M. 2013. Big steps toward understanding dynein. *The Journal of cell biology*. 202:15-23.

Kimura, A., and S. Onami. 2005. Computer simulations and image processing reveal length-dependent pulling force as the primary mechanism for C. elegans male pronuclear migration. *Developmental cell*. 8:765-775.

Kimura, K., M. Ito, M. Amano, K. Chihara, Y. Fukata, M. Nakafuku, B. Yamamori, J. Feng, T. Nakano, K. Okawa, A. Iwamatsu, and K. Kaibuchi. 1996. Regulation of myosin phosphatase by Rho and Rho-associated kinase (Rho-kinase). *Science (New York, N.Y.* 273:245-248.

King, S.J., and T.A. Schroer. 2000. Dynactin increases the processivity of the cytoplasmic dynein motor. *Nature cell biology*. 2:20-24.

Kiosses, W.B., S.J. Shattil, N. Pampori, and M.A. Schwartz. 2001. Rac recruits high-affinity integrin alphavbeta3 to lamellipodia in endothelial cell migration. *Nature cell biology*. 3:316-320.

Koch, D., W.J. Rosoff, J. Jiang, H.M. Geller, and J.S. Urbach. 2012. Strength in the periphery: growth cone biomechanics and substrate rigidity response in peripheral and central nervous system neurons. *Biophysical journal*. 102:452-460.

Kollins, K.M., R.L. Bell, M. Butts, and G.S. Withers. 2009. Dendrites differ from axons in patterns of microtubule stability and polymerization during development. *Neural Dev*. 4:26.

Kolodney, M.S., and E.L. Elson. 1995. Contraction due to microtubule disruption is associated with increased phosphorylation of myosin regulatory light chain. *Proceedings of the National Academy of Sciences of the United States of America*. 92:10252-10256.

Kon, T., T. Mogami, R. Ohkura, M. Nishiura, and K. Sutoh. 2005. ATP hydrolysis cycle-dependent tail motions in cytoplasmic dynein. *Nat Struct Mol Biol*. 12:513-519.

Kon, T., T. Oyama, R. Shimo-Kon, K. Imamula, T. Shima, K. Sutoh, and G. Kurisu. 2012. The 2.8 A crystal structure of the dynein motor domain. *Nature*. 484:345-350.

Kovacs, M., F. Wang, A. Hu, Y. Zhang, and J.R. Sellers. 2003. Functional divergence of human cytoplasmic myosin II: kinetic characterization of the non-muscle IIA isoform. *The Journal of biological chemistry*. 278:38132-38140.

Krendel, M., and M.S. Mooseker. 2005. Myosins: tails (and heads) of functional diversity. *Physiology (Bethesda)*. 20:239-251.

Lamoureux, P., R.E. Buxbaum, and S.R. Heidemann. 1989. Direct evidence that growth cones pull. *Nature*. 340:159-162.

Lamoureux, P., S.R. Heidemann, N.R. Martzke, and K.E. Miller. 2010. Growth and elongation within and along the axon. *Developmental neurobiology*. 70:135-149.

Lanier, L.M., M.A. Gates, W. Witke, A.S. Menzies, A.M. Wehman, J.D. Macklis, D. Kwiatkowski, P. Soriano, and F.B. Gertler. 1999. Mena is required for neurulation and commissure formation. *Neuron*. 22:313-325.

Lasek, R.J. 1982. Translocation of the neuronal cytoskeleton and axonal locomotion. *Philos Trans R Soc Lond B Biol Sci*. 299:313-327.

Lauffenburger, D.A., and A.F. Horwitz. 1996. Cell migration: a physically integrated molecular process. *Cell*. 84:359-369.

Lee, A.C., and D.M. Suter. 2008. Quantitative analysis of microtubule dynamics during adhesion-mediated growth cone guidance. *Developmental neurobiology*. 68:1363-1377.

Lein, P.J., G.A. Banker, and D. Higgins. 1992. Laminin selectively enhances axonal growth and accelerates the development of polarity by hippocampal neurons in culture. *Brain Res Dev Brain Res*. 69:191-197.

Letourneau, P.C., T.A. Shattuck, and A.H. Ressler. 1987. "Pull" and "push" in neurite elongation: observations on the effects of different concentrations of cytochalasin B and taxol. *Cell Motil Cytoskeleton*. 8:193-209.

Lewis, A.K., and P.C. Bridgman. 1992. Nerve growth cone lamellipodia contain two populations of actin filaments that differ in organization and polarity. *The Journal of cell biology*. 119:1219-1243.

Lim, S.S., K.J. Edson, P.C. Letourneau, and G.G. Borisy. 1990. A test of microtubule translocation during neurite elongation. *The Journal of cell biology*. 111:123-130.

Lim, S.S., P.J. Sammak, and G.G. Borisy. 1989. Progressive and spatially differentiated stability of microtubules in developing neuronal cells. *The Journal of cell biology*. 109:253-263.

Lin, C.H., E.M. Espreafico, M.S. Mooseker, and P. Forscher. 1996. Myosin drives retrograde F-actin flow in neuronal growth cones. *Neuron*. 16:769-782.

Lin, C.H., and P. Forscher. 1993. Cytoskeletal remodeling during growth cone-target interactions. *The Journal of cell biology*. 121:1369-1383.

Lin, C.H., and P. Forscher. 1995. Growth cone advance is inversely proportional to retrograde F-actin flow. *Neuron*. 14:763-771.

Liu, B.P., M. Chrzanowska-Wodnicka, and K. Burridge. 1998. Microtubule depolymerization induces stress fibers, focal adhesions, and DNA synthesis via the GTP-binding protein Rho. *Cell Adhes Commun*. 5:249-255.

Liu, S., D.A. Calderwood, and M.H. Ginsberg. 2000. Integrin cytoplasmic domain-binding proteins. *Journal of cell science*. 113 (Pt 20):3563-3571.

Lowery, L.A., and D. Van Vactor. 2009. The trip of the tip: understanding the growth cone machinery. *Nat Rev Mol Cell Biol*. 10:332-343.

Lye, R.J., M.E. Porter, J.M. Scholey, and J.R. McIntosh. 1987. Identification of a microtubule-based cytoplasmic motor in the nematode C. elegans. *Cell*. 51:309-318.

Ma, Y., D. Shakiryanova, I. Vardya, and S.V. Popov. 2004. Quantitative analysis of microtubule transport in growing nerve processes. *Current biology : CB*. 14:725-730.

Mallavarapu, A., and T. Mitchison. 1999. Regulated actin cytoskeleton assembly at filopodium tips controls their extension and retraction. *The Journal of cell biology*. 146:1097-1106.

Mallik, R., B.C. Carter, S.A. Lex, S.J. King, and S.P. Gross. 2004. Cytoplasmic dynein functions as a gear in response to load. *Nature*. 427:649-652.

Mansfield, S.G., D.Y. al-Shirawi, A.S. Ketchum, E.C. Newbern, and D.P. Kiehart. 1996. Molecular organization and alternative splicing in zipper, the gene that encodes the Drosophila non-muscle myosin II heavy chain. *J Mol Biol*. 255:98-109.

Margolis, R.L., and L. Wilson. 1978. Opposite end assembly and disassembly of microtubules at steady state in vitro. *Cell*. 13:1-8.

Markus, S.M., J.J. Punch, and W.L. Lee. 2009. Motor- and tail-dependent targeting of dynein to microtubule plus ends and the cell cortex. *Current biology : CB*. 19:196-205.

Matsui, T., M. Amano, T. Yamamoto, K. Chihara, M. Nakafuku, M. Ito, T. Nakano, K. Okawa, A. Iwamatsu, and K. Kaibuchi. 1996. Rho-associated kinase, a novel serine/threonine kinase, as a putative target for small GTP binding protein Rho. *Embo J*. 15:2208-2216.

Matsuoka, Y., X. Li, and V. Bennett. 1998. Adducin is an in vivo substrate for protein kinase C: phosphorylation in the MARCKS-related domain inhibits activity in promoting spectrin-actin complexes and occurs in many cells, including dendritic spines of neurons. *The Journal of cell biology*. 142:485-497.

Mazel, T., A. Biesemann, M. Krejczy, J. Nowald, O. Muller, and L. Dehmelt. 2013. Direct observation of microtubule pushing by cortical dynein in living cells. *Mol Biol Cell*.

Medeiros, N.A., D.T. Burnette, and P. Forscher. 2006. Myosin II functions in actin-bundle turnover in neuronal growth cones. *Nature cell biology*. 8:215-226.

Mellor, H. 2010. The role of formins in filopodia formation. *Biochim Biophys Acta*. 1803:191-200.

Miki, H., T. Sasaki, Y. Takai, and T. Takenawa. 1998. Induction of filopodium formation by a WASP-related actin-depolymerizing protein N-WASP. *Nature*. 391:93-96.

Miller, K.E., and H.C. Joshi. 1996. Tubulin transport in neurons. *The Journal of cell biology*. 133:1355-1366.

Miller, K.E., and M.P. Sheetz. 2004. Axonal mitochondrial transport and potential are correlated. *Journal of cell science*. 117:2791-2804.

Miller, K.E., and M.P. Sheetz. 2006. Direct evidence for coherent low velocity axonal transport of mitochondria. *The Journal of cell biology*. 173:373-381.

Miller, M., E. Bower, P. Levitt, D. Li, and P.D. Chantler. 1992. Myosin II distribution in neurons is consistent with a role in growth cone motility but not synaptic vesicle mobilization. *Neuron*. 8:25-44.

Mitchison, T., and M. Kirschner. 1984a. Dynamic instability of microtubule growth. *Nature*. 312:237-242.

Mitchison, T., and M. Kirschner. 1984b. Microtubule assembly nucleated by isolated centrosomes. *Nature*. 312:232-237.

Mitchison, T., and M. Kirschner. 1988. Cytoskeletal dynamics and nerve growth. *Neuron*. 1:761-772.

Mitchison, T.J. 1993. Localization of an exchangeable GTP binding site at the plus end of microtubules. *Science (New York, N.Y.* 261:1044-1047.

Miyamoto, S., S.K. Akiyama, and K.M. Yamada. 1995. Synergistic roles for receptor occupancy and aggregation in integrin transmembrane function. *Science (New York, N.Y.* 267:883-885.

Mockrin, S.C., and E.D. Korn. 1980. Acanthamoeba profilin interacts with G-actin to increase the rate of exchange of actin-bound adenosine 5'-triphosphate. *Biochemistry*. 19:5359-5362.

Mogilner, A., and G. Oster. 1996. Cell motility driven by actin polymerization. *Biophysical journal*. 71:3030-3045.

Mongiu, A.K., E.L. Weitzke, O.Y. Chaga, and G.G. Borisy. 2007. Kinetic-structural analysis of neuronal growth cone veil motility. *Journal of cell science*. 120:1113-1125.

Morris, R.L., and P.J. Hollenbeck. 1993. The regulation of bidirectional mitochondrial transport is coordinated with axonal outgrowth. *Journal of cell science*. 104 (Pt 3):917-927.

Moussavi, R.S., C.A. Kelley, and R.S. Adelstein. 1993. Phosphorylation of vertebrate nonmuscle and smooth muscle myosin heavy chains and light chains. *Mol Cell Biochem*. 127-128:219-227.

Mullins, R.D., J.A. Heuser, and T.D. Pollard. 1998. The interaction of Arp2/3 complex with actin: nucleation, high affinity pointed end capping, and formation of branching networks of filaments. *Proceedings of the National Academy of Sciences of the United States of America*. 95:6181-6186.

Myers, K.A., I. Tint, C.V. Nadar, Y. He, M.M. Black, and P.W. Baas. 2006. Antagonistic forces generated by cytoplasmic dynein and myosin-II during growth cone turning and axonal retraction. *Traffic (Copenhagen, Denmark)*. 7:1333-1351.

Nakasawa, T., M. Takahashi, F. Matsuzawa, S. Aikawa, Y. Togashi, T. Saitoh, A. Yamagishi, and M. Yazawa. 2005. Critical regions for assembly of vertebrate nonmuscle myosin II. *Biochemistry*. 44:174-183.

Nayal, A., D.J. Webb, and A.F. Horwitz. 2004. Talin: an emerging focal point of adhesion dynamics. *Current opinion in cell biology*. 16:94-98.

Neuwald, A.F., L. Aravind, J.L. Spouge, and E.V. Koonin. 1999. AAA+: A class of chaperone-like ATPases associated with the assembly, operation, and disassembly of protein complexes. *Genome Res*. 9:27-43.

Nguyen-Ngoc, T., K. Afshar, and P. Gonczy. 2007. Coupling of cortical dynein and G alpha proteins mediates spindle positioning in Caenorhabditis elegans. *Nature cell biology*. 9:1294-1302.

Nicklas, R.B., G.M. Lee, C.L. Rieder, and G. Rupp. 1989. Mechanically cut mitotic spindles: clean cuts and stable microtubules. *Journal of cell science*. 94 (Pt 3):415-423.

Nishida, E. 1985. Opposite effects of cofilin and profilin from porcine brain on rate of exchange of actin-bound adenosine 5'-triphosphate. *Biochemistry*. 24:1160-1164.

Nishida, E., S. Maekawa, E. Muneyuki, and H. Sakai. 1984a. Action of a 19K protein from porcine brain on actin polymerization: a new functional class of actin-binding proteins. *J Biochem*. 95:387-398.

Nishida, E., S. Maekawa, and H. Sakai. 1984b. Cofilin, a protein in porcine brain that binds to actin filaments and inhibits their interactions with myosin and tropomyosin. *Biochemistry*. 23:5307-5313.

Nobes, C.D., and A. Hall. 1995. Rho, rac, and cdc42 GTPases regulate the assembly of multimolecular focal complexes associated with actin stress fibers, lamellipodia, and filopodia. *Cell*. 81:53-62.

O'Connell, C.B., and Y.L. Wang. 2000. Mammalian spindle orientation and position respond to changes in cell shape in a dynein-dependent fashion. *Mol Biol Cell*. 11:1765-1774.

O'Toole, M., P. Lamoureux, and K.E. Miller. 2008. A physical model of axonal elongation: force, viscosity, and adhesions govern the mode of outgrowth. *Biophysical journal*. 94:2610-2620.

Oakley, C.E., and B.R. Oakley. 1989. Identification of gamma-tubulin, a new member of the tubulin superfamily encoded by mipA gene of Aspergillus nidulans. *Nature*. 338:662-664.

Ochs, S., D. Dalrymple, and G. Richards. 1962. Axoplasmic flow in ventral root nerve fibers of the cat. *Experimental neurology*. 5:349-363.

Ochs, S., and J. Johnson. 1969. Fast and slow phases of axoplasmic flow in ventral root nerve fibres. *Journal of neurochemistry*. 16:845-853.

Ochs, S., J. Johnson, and M.H. Ng. 1967. Protein incorporation and axoplasmic flow in motoneuron fibres following intra-cord injection of labelled leucine. *Journal of neurochemistry*. 14:317-331.

Odronitz, F., and M. Kollmar. 2007. Drawing the tree of eukaryotic life based on the analysis of 2,269 manually annotated myosins from 328 species. *Genome Biol*. 8:R196.

Ohta, Y., N. Suzuki, S. Nakamura, J.H. Hartwig, and T.P. Stossel. 1999. The small GTPase RalA targets filamin to induce filopodia. *Proceedings of the National Academy of Sciences of the United States of America*. 96:2122-2128.

Okabe, S., and N. Hirokawa. 1988. Microtubule dynamics in nerve cells: analysis using microinjection of biotinylated tubulin into PC12 cells. *The Journal of cell biology*. 107:651-664.

Okabe, S., and N. Hirokawa. 1990. Turnover of fluorescently labelled tubulin and actin in the axon. *Nature*. 343:479-482.

Okabe, S., and N. Hirokawa. 1992. Differential behavior of photoactivated microtubules in growing axons of mouse and frog neurons. *The Journal of cell biology*. 117:105-120.

Okabe, S., and N. Hirokawa. 1993. Do photobleached fluorescent microtubules move?: re-evaluation of fluorescence laser photobleaching both in vitro and in growing Xenopus axon. *The Journal of cell biology*. 120:1177-1186.

Oster, G.F., and A.S. Perelson. 1987. The physics of cell motility. *J Cell Sci Suppl*. 8:35-54.

Pak, C.W., K.C. Flynn, and J.R. Bamburg. 2008. Actin-binding proteins take the reins in growth cones. *Nature reviews. Neuroscience*. 9:136-147.

Pantaloni, D., R. Boujemaa, D. Didry, P. Gounon, and M.F. Carlier. 2000. The Arp2/3 complex branches filament barbed ends: functional antagonism with capping proteins. *Nature cell biology*. 2:385-391.

Paschal, B.M., H.S. Shpetner, and R.B. Vallee. 1987. MAP 1C is a microtubule-activated ATPase which translocates microtubules in vitro and has dynein-like properties. *The Journal of cell biology*. 105:1273-1282.

Paschal, B.M., and R.B. Vallee. 1987. Retrograde transport by the microtubule-associated protein MAP 1C. *Nature*. 330:181-183.

Peng, J., B.J. Wallar, A. Flanders, P.J. Swiatek, and A.S. Alberts. 2003. Disruption of the Diaphanous-related formin Drf1 gene encoding mDia1 reveals a role for Drf3 as an effector for Cdc42. *Current biology : CB*. 13:534-545.

Peskin, C.S., G.M. Odell, and G.F. Oster. 1993. Cellular motions and thermal fluctuations: the Brownian ratchet. *Biophysical journal*. 65:316-324.

Pfister, B.J., D.P. Bonislawski, D.H. Smith, and A.S. Cohen. 2006. Stretch-grown axons retain the ability to transmit active electrical signals. *FEBS Lett*. 580:3525-3531.

Pfister, B.J., A. Iwata, D.F. Meaney, and D.H. Smith. 2004. Extreme stretch growth of integrated axons. *The Journal of neuroscience : the official journal of the Society for Neuroscience*. 24:7978-7983.

Pfister, K.K. 1999. Cytoplasmic dynein and microtubule transport in the axon: the action connection. *Mol Neurobiol*. 20:81-91.

Pilling, A.D., D. Horiuchi, C.M. Lively, and W.M. Saxton. 2006. Kinesin-1 and Dynein are the primary motors for fast transport of mitochondria in Drosophila motor axons. *Mol Biol Cell*. 17:2057-2068.

Pollard, T.D. 1986. Rate constants for the reactions of ATP- and ADP-actin with the ends of actin filaments. *The Journal of cell biology*. 103:2747-2754.

Pollard, T.D., and G.G. Borisy. 2003. Cellular motility driven by assembly and disassembly of actin filaments. *Cell*. 112:453-465.

Pollard, T.D., and E.D. Korn. 1973. Acanthamoeba myosin. I. Isolation from Acanthamoeba castellanii of an enzyme similar to muscle myosin. *The Journal of biological chemistry*. 248:4682-4690.

Porter, M.E., and K.A. Johnson. 1983. Transient state kinetic analysis of the ATP-induced dissociation of the dynein-microtubule complex. *The Journal of biological chemistry*. 258:6582-6587.

Pryer, N.K., R.A. Walker, V.P. Skeen, B.D. Bourns, M.F. Soboeiro, and E.D. Salmon. 1992. Brain microtubule-associated proteins modulate microtubule dynamic instability in vitro. Real-time observations using video microscopy. *Journal of cell science*. 103 (Pt 4):965-976.

Qiu, W., N.D. Derr, B.S. Goodman, E. Villa, D. Wu, W. Shih, and S.L. Reck-Peterson. 2012. Dynein achieves processive motion using both stochastic and coordinated stepping. *Nat Struct Mol Biol*. 19:193-200.

Ramon Y Cajal, S. 1890. A quelle epoque apparaissent les expansions des cellule nerveuses de la moelle epinere du poulet. *Anat Anzerger*. 5:609-613.

Rayment, I., H.M. Holden, M. Whittaker, C.B. Yohn, M. Lorenz, K.C. Holmes, and R.A. Milligan. 1993a. Structure of the actin-myosin complex and its implications for muscle contraction. *Science (New York, N.Y.* 261:58-65.

Rayment, I., W.R. Rypniewski, K. Schmidt-Base, R. Smith, D.R. Tomchick, M.M. Benning, D.A. Winkelmann, G. Wesenberg, and H.M. Holden. 1993b. Three-dimensional structure of myosin subfragment-1: a molecular motor. *Science (New York, N.Y.* 261:50-58.

Reck-Peterson, S.L., A. Yildiz, A.P. Carter, A. Gennerich, N. Zhang, and R.D. Vale. 2006. Single-molecule analysis of dynein processivity and stepping behavior. *Cell*. 126:335-348.

Reinsch, S.S., T.J. Mitchison, and M. Kirschner. 1991. Microtubule polymer assembly and transport during axonal elongation. *The Journal of cell biology*. 115:365-379.

Renaudin, A., M. Lehmann, J. Girault, and L. McKerracher. 1999. Organization of point contacts in neuronal growth cones. *J Neurosci Res*. 55:458-471.

Richards, T.A., and T. Cavalier-Smith. 2005. Myosin domain evolution and the primary divergence of eukaryotes. *Nature*. 436:1113-1118.

Ridley, A.J., M.A. Schwartz, K. Burridge, R.A. Firtel, M.H. Ginsberg, G. Borisy, J.T. Parsons, and A.R. Horwitz. 2003. Cell migration: integrating signals from front to back. *Science (New York, N.Y.* 302:1704-1709.

Rinnerthaler, G., M. Herzog, M. Klappacher, H. Kunka, and J.V. Small. 1991. Leading edge movement and ultrastructure in mouse macrophages. *J Struct Biol*. 106:1-16.

Roberts, A.J., T. Kon, P.J. Knight, K. Sutoh, and S.A. Burgess. 2013. Functions and mechanics of dynein motor proteins. *Nature reviews. Molecular cell biology*. 14:713-726.

Roberts, A.J., B. Malkova, M.L. Walker, H. Sakakibara, N. Numata, T. Kon, R. Ohkura, T.A. Edwards, P.J. Knight, K. Sutoh, K. Oiwa, and S.A. Burgess. 2012. ATP-driven remodeling of the linker domain in the dynein motor. *Structure*. 20:1670-1680.

Roberts, A.J., N. Numata, M.L. Walker, Y.S. Kato, B. Malkova, T. Kon, R. Ohkura, F. Arisaka, P.J. Knight, K. Sutoh, and S.A. Burgess. 2009. AAA+ Ring and linker swing mechanism in the dynein motor. *Cell*. 136:485-495.

Robinson, R.C., K. Turbedsky, D.A. Kaiser, J.B. Marchand, H.N. Higgs, S. Choe, and T.D. Pollard. 2001. Crystal structure of Arp2/3 complex. *Science (New York, N.Y.* 294:1679-1684.

Rochlin, M.W., K. Itoh, R.S. Adelstein, and P.C. Bridgman. 1995. Localization of myosin II A and B isoforms in cultured neurons. *Journal of cell science*. 108 (Pt 12):3661-3670.

Rochlin, M.W., K.M. Wickline, and P.C. Bridgman. 1996. Microtubule stability decreases axon elongation but not axoplasm production. *The Journal of neuroscience : the official journal of the Society for Neuroscience*. 16:3236-3246.

Rodriguez, O.C., A.W. Schaefer, C.A. Mandato, P. Forscher, W.M. Bement, and C.M. Waterman-Storer. 2003. Conserved microtubule-actin interactions in cell movement and morphogenesis. *Nature cell biology*. 5:599-609.

Rosenblatt, J., P. Peluso, and T.J. Mitchison. 1995. The bulk of unpolymerized actin in Xenopus egg extracts is ATP-bound. *Mol Biol Cell*. 6:227-236.

Rottner, K., A. Hall, and J.V. Small. 1999. Interplay between Rac and Rho in the control of substrate contact dynamics. *Current biology : CB*. 9:640-648.

Rusan, N.M., U.S. Tulu, C. Fagerstrom, and P. Wadsworth. 2002. Reorganization of the microtubule array in prophase/prometaphase requires cytoplasmic dynein-dependent microtubule transport. *The Journal of cell biology*. 158:997-1003.

Sabry, J., T.P. O'Connor, and M.W. Kirschner. 1995. Axonal transport of tubulin in Ti1 pioneer neurons in situ. *Neuron*. 14:1247-1256.

Sabry, J.H., T.P. O'Connor, L. Evans, A. Toroian-Raymond, M. Kirschner, and D. Bentley. 1991. Microtubule behavior during guidance of pioneer neuron growth cones in situ. *The Journal of cell biology*. 115:381-395.

Sale, W.S., and P. Satir. 1977. Direction of active sliding of microtubules in Tetrahymena cilia. *Proceedings of the National Academy of Sciences of the United States of America*. 74:2045-2049.

Saxton, W.M., and P.J. Hollenbeck. 2012. The axonal transport of mitochondria. *Journal of cell science*. 125:2095-2104.

Schaefer, A.W., N. Kabir, and P. Forscher. 2002. Filopodia and actin arcs guide the assembly and transport of two populations of microtubules with unique dynamic parameters in neuronal growth cones. *The Journal of cell biology*. 158:139-152.

Schaefer, A.W., V.T. Schoonderwoert, L. Ji, N. Mederios, G. Danuser, and P. Forscher. 2008. Coordination of actin filament and microtubule dynamics during neurite outgrowth. *Developmental cell*. 15:146-162.

Schmidt, D.J., D.J. Rose, W.M. Saxton, and S. Strome. 2005. Functional analysis of cytoplasmic dynein heavy chain in Caenorhabditis elegans with fast-acting temperature-sensitive mutations. *Mol Biol Cell*. 16:1200-1212.

Schnapp, B.J., and T.S. Reese. 1989. Dynein is the motor for retrograde axonal transport of organelles. *Proceedings of the National Academy of Sciences of the United States of America*. 86:1548-1552.

Scholey, J.M., K.A. Taylor, and J. Kendrick-Jones. 1980. Regulation of non-muscle myosin assembly by calmodulin-dependent light chain kinase. *Nature*. 287:233-235.

Schroer, T.A. 2004. Dynactin. *Annual review of cell and developmental biology*. 20:759-779.

Schroer, T.A., and M.P. Sheetz. 1991. Two activators of microtubule-based vesicle transport. *The Journal of cell biology*. 115:1309-1318.

Schroer, T.A., E.R. Steuer, and M.P. Sheetz. 1989. Cytoplasmic dynein is a minus end-directed motor for membranous organelles. *Cell*. 56:937-946.

Shaw, G., and D. Bray. 1977. Movement and extension of isolated growth cones. *Exp Cell Res*. 104:55-62.

Sheetz, M.P., D.B. Wayne, and A.L. Pearlman. 1992. Extension of filopodia by motor-dependent actin assembly. *Cell motility and the cytoskeleton*. 22:160-169.

Small, J.V., G. Isenberg, and J.E. Celis. 1978. Polarity of actin at the leading edge of cultured cells. *Nature*. 272:638-639.

Smith, D.H. 2009. Stretch growth of integrated axon tracts: extremes and exploitations. *Progress in neurobiology*. 89:231-239.

Smith, S.J., and R.O. McCann. 2007. A C-terminal dimerization motif is required for focal adhesion targeting of Talin1 and the interaction of the Talin1 I/LWEQ module with F-actin. *Biochemistry*. 46:10886-10898.

Smolensky, A.V., J. Ragozzino, S.H. Gilbert, C.Y. Seow, and L.E. Ford. 2005. Length-dependent filament formation assessed from birefringence increases during activation of porcine tracheal muscle. *J Physiol*. 563:517-527.

Spudich, J.A. 2001. The myosin swinging cross-bridge model. *Nature reviews. Molecular cell biology*. 2:387-392.

Stepanova, T., J. Slemmer, C.C. Hoogenraad, G. Lansbergen, B. Dortland, C.I. De Zeeuw, F. Grosveld, G. van Cappellen, A. Akhmanova, and N. Galjart. 2003. Visualization of microtubule growth in cultured neurons via the use of EB3-GFP (end-binding protein 3-green fluorescent protein). *The Journal of neuroscience : the official journal of the Society for Neuroscience*. 23:2655-2664.

Stiess, M., and F. Bradke. 2011. Neuronal polarization: the cytoskeleton leads the way. *Developmental neurobiology*. 71:430-444.

Straight, A.F., A. Cheung, J. Limouze, I. Chen, N.J. Westwood, J.R. Sellers, and T.J. Mitchison. 2003. Dissecting temporal and spatial control of cytokinesis with a myosin II Inhibitor. *Science (New York, N.Y.* 299:1743-1747.

Strasser, G.A., N.A. Rahim, K.E. VanderWaal, F.B. Gertler, and L.M. Lanier. 2004. Arp2/3 is a negative regulator of growth cone translocation. *Neuron*. 43:81-94.

Summers, K., and M.W. Kirschner. 1979. Characteristics of the polar assembly and disassembly of microtubules observed in vitro by darkfield light microscopy. *The Journal of cell biology*. 83:205-217.

Sun, H.Q., M. Yamamoto, M. Mejillano, and H.L. Yin. 1999. Gelsolin, a multifunctional actin regulatory protein. *The Journal of biological chemistry*. 274:33179-33182.

Suter, D.M., L.D. Errante, V. Belotserkovsky, and P. Forscher. 1998. The Ig superfamily cell adhesion molecule, apCAM, mediates growth cone steering by substrate-cytoskeletal coupling. *The Journal of cell biology*. 141:227-240.

Suter, D.M., and P. Forscher. 2000. Substrate-cytoskeletal coupling as a mechanism for the regulation of growth cone motility and guidance. *Journal of neurobiology*. 44:97-113.

Suter, D.M., and K.E. Miller. 2011. The emerging role of forces in axonal elongation. *Progress in neurobiology*. 94:91-101.

Tanaka, E., T. Ho, and M.W. Kirschner. 1995. The role of microtubule dynamics in growth cone motility and axonal growth. *The Journal of cell biology*. 128:139-155.

Tanaka, E., and J. Sabry. 1995. Making the connection: cytoskeletal rearrangements during growth cone guidance. *Cell*. 83:171-176.

Tanaka, E.M., and M.W. Kirschner. 1991. Microtubule behavior in the growth cones of living neurons during axon elongation. *The Journal of cell biology*. 115:345-363.

Tanentzapf, G., M.D. Martin-Bermudo, M.S. Hicks, and N.H. Brown. 2006. Multiple factors contribute to integrin-talin interactions in vivo. *Journal of cell science*. 119:1632-1644.

Terada, S., M. Kinjo, and N. Hirokawa. 2000. Oligomeric tubulin in large transporting complex is transported via kinesin in squid giant axons. *Cell*. 103:141-155.

Theriot, J.A., and T.J. Mitchison. 1991. Actin microfilament dynamics in locomoting cells. *Nature*. 352:126-131.

Tonges, L., J.C. Koch, M. Bahr, and P. Lingor. 2011. ROCKing Regeneration: Rho Kinase Inhibition as Molecular Target for Neurorestoration. *Frontiers in molecular neuroscience*. 4:39.

Tosney, K.W., and N.K. Wessells. 1983. Neuronal motility: the ultrastructure of veils and microspikes correlates with their motile activities. *Journal of cell science*. 61:389-411.

Totsukawa, G., Y. Yamakita, S. Yamashiro, D.J. Hartshorne, Y. Sasaki, and F. Matsumura. 2000. Distinct roles of ROCK (Rho-kinase) and MLCK in spatial regulation of MLC phosphorylation for assembly of stress fibers and focal adhesions in 3T3 fibroblasts. *The Journal of cell biology*. 150:797-806.

Trinczek, B., J. Biernat, K. Baumann, E.M. Mandelkow, and E. Mandelkow. 1995. Domains of tau protein, differential phosphorylation, and dynamic instability of microtubules. *Mol Biol Cell*. 6:1887-1902.

Tullio, A.N., P.C. Bridgman, N.J. Tresser, C.C. Chan, M.A. Conti, R.S. Adelstein, and Y. Hara. 2001. Structural abnormalities develop in the brain after ablation of the gene encoding nonmuscle myosin II-B heavy chain. *The Journal of comparative neurology*. 433:62-74.

Turney, S.G., and P.C. Bridgman. 2005. Laminin stimulates and guides axonal outgrowth via growth cone myosin II activity. *Nature neuroscience*. 8:717-719.

Vale, R.D. 2003. The molecular motor toolbox for intracellular transport. *Cell*. 112:467-480.

Valetti, C., D.M. Wetzel, M. Schrader, M.J. Hasbani, S.R. Gill, T.E. Kreis, and T.A. Schroer. 1999. Role of dynactin in endocytic traffic: effects of dynamitin overexpression and colocalization with CLIP-170. *Mol Biol Cell*. 10:4107-4120.

Vallee, R.B., G.E. Seale, and J.W. Tsai. 2009. Emerging roles for myosin II and cytoplasmic dynein in migrating neurons and growth cones. *Trends Cell Biol*. 19:347-355.

Vaughan, K.T., S.H. Tynan, N.E. Faulkner, C.J. Echeverri, and R.B. Vallee. 1999. Colocalization of cytoplasmic dynein with dynactin and CLIP-170 at microtubule distal ends. *Journal of cell science*. 112 (Pt 10):1437-1447.

Vaughan, K.T., and R.B. Vallee. 1995. Cytoplasmic dynein binds dynactin through a direct interaction between the intermediate chains and p150Glued. *The Journal of cell biology*. 131:1507-1516.

Vaughan, P.S., P. Miura, M. Henderson, B. Byrne, and K.T. Vaughan. 2002. A role for regulated binding of p150(Glued) to microtubule plus ends in organelle transport. *The Journal of cell biology*. 158:305-319.

Vicente-Manzanares, M., X. Ma, R.S. Adelstein, and A.R. Horwitz. 2009. Non-muscle myosin II takes centre stage in cell adhesion and migration. *Nature reviews. Molecular cell biology*. 10:778-790.

Vinson, V.K., E.M. De La Cruz, H.N. Higgs, and T.D. Pollard. 1998. Interactions of Acanthamoeba profilin with actin and nucleotides bound to actin. *Biochemistry*. 37:10871-10880.

Wang, F., M. Kovacs, A. Hu, J. Limouze, E.V. Harvey, and J.R. Sellers. 2003. Kinetic mechanism of non-muscle myosin IIB: functional adaptations for tension generation and maintenance. *The Journal of biological chemistry*. 278:27439-27448.

Wang, L., and A. Brown. 2002. Rapid movement of microtubules in axons. *Current biology : CB*. 12:1496-1501.

Waterman-Storer, C.M., A. Desai, J.C. Bulinski, and E.D. Salmon. 1998. Fluorescent speckle microscopy, a method to visualize the dynamics of protein assemblies in living cells. *Current biology : CB*. 8:1227-1230.

Waterman-Storer, C.M., S. Karki, and E.L. Holzbaur. 1995. The p150Glued component of the dynactin complex binds to both microtubules and the actin-related protein centractin (Arp-1). *Proceedings of the National Academy of Sciences of the United States of America*. 92:1634-1638.

Weisenberg, R.C., W.J. Deery, and P.J. Dickinson. 1976. Tubulin-nucleotide interactions during the polymerization and depolymerization of microtubules. *Biochemistry*. 15:4248-4254.

Weiss, P., and H. Hiscoe. 1948. Experiments on the mechanism of nerve growth. *J Exp Zoo*. 107:315-395.

Wendt, T., D. Taylor, K.M. Trybus, and K. Taylor. 2001. Three-dimensional image reconstruction of dephosphorylated smooth muscle heavy meromyosin reveals asymmetry in the interaction between myosin heads and placement of subfragment 2. *Proceedings of the National Academy of Sciences of the United States of America*. 98:4361-4366.

Wessells, N.K., S.R. Johnson, and R.P. Nuttall. 1978. Axon initiation and growth cone regeneration in cultured motor neurons. *Exp Cell Res*. 117:335-345.

Wessels, D., D.R. Soll, D. Knecht, W.F. Loomis, A. De Lozanne, and J. Spudich. 1988. Cell motility and chemotaxis in Dictyostelium amebae lacking myosin heavy chain. *Developmental biology*. 128:164-177.

White, L.A., P.W. Baas, and S.R. Heidemann. 1987. Microtubule stability in severed axons. *J Neurocytol*. 16:775-784.

Wittmann, T., and T. Hyman. 1999. Recombinant p50/dynamitin as a tool to examine the role of dynactin in intracellular processes. *Methods Cell Biol*. 61:137-143.

Woo, S., and T.M. Gomez. 2006. Rac1 and RhoA promote neurite outgrowth through formation and stabilization of growth cone point contacts. *J Neurosci*. 26:1418-1428.

Wuhr, M., E.S. Tan, S.K. Parker, H.W. Detrich, 3rd, and T.J. Mitchison. 2010. A model for cleavage plane determination in early amphibian and fish embryos. *Current biology : CB*. 20:2040-2045.

Yamada, K.M., B.S. Spooner, and N.K. Wessells. 1970. Axon growth: roles of microfilaments and microtubules. *Proceedings of the National Academy of Sciences of the United States of America*. 66:1206-1212.

Yamada, K.M., B.S. Spooner, and N.K. Wessells. 1971. Ultrastructure and function of growth cones and axons of cultured nerve cells. *The Journal of cell biology*. 49:614-635.

Yi, J.Y., K.M. Ori-McKenney, R.J. McKenney, M. Vershinin, S.P. Gross, and R.B. Vallee. 2011. High-resolution imaging reveals indirect coordination of opposite motors and a role for LIS1 in high-load axonal transport. *The Journal of cell biology*. 195:193-201.

Yu, P., L.Y. Santiago, Y. Katagiri, and H.M. Geller. 2012. Myosin II activity regulates neurite outgrowth and guidance in response to chondroitin sulfate proteoglycans. *Journal of neurochemistry*. 120:1117-1128.

Zamir, E., and B. Geiger. 2001. Molecular complexity and dynamics of cell-matrix adhesions. *Journal of cell science*. 114:3583-3590.

Zhang, X.F., A.W. Schaefer, D.T. Burnette, V.T. Schoonderwoert, and P. Forscher. 2003. Rho-dependent contractile responses in the neuronal growth cone are independent of classical peripheral retrograde actin flow. *Neuron*. 40:931-944.

Zhou, F.Q., C.M. Waterman-Storer, and C.S. Cohan. 2002. Focal loss of actin bundles causes microtubule redistribution and growth cone turning. *The Journal of cell biology*. 157:839-849.

CHAPTER 2:

Drosophila Growth Cones Advance by Forward Translocation of the Neuronal Cytoskeletal Meshwork *In vivo*

Douglas H. Roossien, Phillip Lamoureux, David Van Vactor & Kyle E. Miller

Reprinted from "*Drosophila* Growth Cones Advance by Forward Translocation of the Neuronal Cytoskeletal Meshwork *In vivo*". PLOS One. 2013 Nov 11;8(11):e80136.

Contributions: DHR performed experiments and analyzed data in Fig. 2.1A-D and Fig. 2.3. PL performed experiments and analyzed data in Fig. 2.1E-K and Fig. 2.2. DVV supplied reagents and equipment. KEM and DHR wrote manuscript.

2.1 Abstract

In vitro studies conducted in *Aplysia* and chick sensory neurons indicate that in addition to microtubule assembly, long microtubules in the C-domain of the growth cone move forward as a coherent bundle during axonal elongation. Nonetheless, whether this mode of microtubule translocation contributes to growth cone motility *in vivo* is unknown. To address this question, we turned to the model system *Drosophila*. Using docked mitochondria as fiduciary markers for the translocation of long microtubules, we first examined motion along the axon to test if the pattern of axonal elongation is conserved between *Drosophila* and other species *in vitro*. When *Drosophila* neurons were cultured on *Drosophila* extracellular matrix proteins collected from the *Drosophila* Kc167 cell line, docked mitochondria moved in a pattern indicative of bulk microtubule translocation, similar to that observed in chick sensory neurons grown on laminin. To investigate whether the C-domain is stationary or advances *in vivo,* we tracked the movement of mitochondria during elongation of the aCC motor neuron in stage 16 *Drosophila* embryos. We found docked mitochondria moved forward along the axon shaft and in the growth cone C-domain. This work confirms that the physical mechanism of growth cone advance is similar between *Drosophila* and vertebrate neurons and suggests forward translocation of the microtubule meshwork in the axon underlies the advance of the growth cone C-domain *in vivo*. These results highlight the need for incorporating en masse microtubule translocation, in addition to assembly, into models of axonal elongation.

2.2 Introduction

While there has been immense success in identifying the proteins that control and contribute to axonal elongation (Lowery and Van Vactor, 2009; O'Donnell et al., 2009), the mechanical process of growth cone motility has received comparatively little attention. Recent studies now suggest that that in addition to microtubule assembly, growth cone advance is paired with forward translocation of the entire microtubule bundle along the axon and in the growth cone (Lee and Suter, 2008; Miller and Sheetz, 2006; Schaefer et al., 2008). This opens the exciting possibility of developing new models of axonal elongation (Suter and Miller, 2011). Yet because growth is sensitive to the context of the extracellular environment, whether these new findings *in vitro* are relevant to growth cone motility *in vivo* is unknown.

Growth cones are typically divided into three major structural regions: an actin rich peripheral domain (P-domain) that undergoes retrograde flow, a microtubule and organelle rich central domain (C-domain) that advances at the same rate as axons elongate, and a transition zone (T-zone) between these domains where the plus ends of microtubules interact with actin arcs (Lowery and Van Vactor, 2009). The adjoining axon consists of a meshwork of cortical actin filaments and spectrin (Hammarlund et al., 2007; Hirokawa, 1982; Xu et al., 2013) that surrounds a core of cross-linked microtubules (Peter and Mofrad, 2012). Embedded within this meshwork are organelles that are stably linked to microtubules (Kang et al., 2008), actin (Pathak et al., 2010), and neurofilaments (Wagner et al., 2003; Walter and Biessmann, 1984) which is beautifully illustrated in classic electron micrographs (Hirokawa, 1982). While the dynamics of actin in the peripheral domain of the growth cone are relatively well understood in terms of a molecular clutch (Bard et al., 2008) that links (Kanchanawong et al., 2010) actin retrograde flow with the generation of traction forces (Chan and Odde, 2008; Koch et al., 2012) and protrusion at

the leading edge, the movement patterns of microtubules in the C-domain and axon (Suter and Miller, 2011) are still poorly understood.

The prevailing theory of axonal elongation, called the Protrusion, Engorgement, and Consolidation (PEC) hypothesis (Goldberg and Burmeister, 1986; Lowery and Van Vactor, 2009) classically proposed that the meshwork of cytoskeletal elements in the C-domain and along the axon is stationary (Aletta and Greene, 1988; Goldberg and Burmeister, 1986) and growth cone advance is directly coupled with microtubule assembly in the growth cones (Bamburg et al., 1986; Mitchison and Kirschner, 1988) as well as Kinesin / Dynein based delivery of new cytoskeletal elements and organelles to the tip of the axon (Bradke and Dotti, 1997; Conde and Caceres, 2009; Liu et al., 2010; Martenson et al., 1993). The Stretch and Intercalated (SAI) growth hypothesis (Lamoureux et al., 2010a; Suter and Miller, 2011), extends this model by proposing that in addition to microtubule polymerization, forces pull and / or push the axonal microtubule mass forward causing the C-domain to move forward relative to the substrate (Suter and Miller, 2011). In the SAI model at a microscopic level, much like the stop-and-go transport hypothesis (Baas et al., 2005; Liu et al., 2010), translocation occurs because forces cause microtubules and other cytoskeletal filaments to slide apart (Chetta et al., 2010). But to be clear there is a dramatic difference between the microtubule translocation that occurs by SAI and Stop-and-Go transport. During Stop-and-Go microtubules move at a rate of approximately 0.1 - 1 μm/sec (i.e. 360 – 3600 μm / h) as short filaments down long microtubules (Baas et al., 2005). In SAI, long microtubules move as a cross-linked meshwork at the slow rate of 1 – 50 μm / h in the distal axon (Lamoureux et al., 2010a).

While microtubules have been a central focus in the study of axonal elongation, their slow translocation is difficult to track using photoactivation or photobleaching because they are

dynamic (Chang et al., 1998). While fluorescent speckle microscopy could potentially overcome this limitation (Chang et al., 1999), because it requires high levels of illumination the resulting photo-damage makes it difficult to routinely image microtubules over extended periods of time. Our approach to this problem has been to use docked mitochondria as a fiduciary marker for the movement of the cytoskeletal meshwork (Miller and Sheetz, 2006; O'Toole et al., 2008a; Suter and Miller, 2011). Following fast transport by Kinesin-1 and dynein (Pilling et al., 2006), mitochondria 'dock' to microtubules (Kang et al., 2008), actin filaments (Pathak et al., 2010), and in vertebrates directly to neurofilaments (Wagner et al., 2003; Walter and Biessmann, 1984). Once mitochondria are docked they remain in position for hours. Facilitating the analysis of mitochondria transport, they are easy to label with fluorescent dyes (Miller and Sheetz, 2004) and GFP targeted to mitochondria (Pilling et al., 2006). Furthermore, they can be monitored using low levels of illumination that minimally impair axonal elongation (Lamoureux et al., 2010a). The use of mitochondria to track the movement of the cytoskeletal meshwork has been validated in prior studies that have demonstrated that beads bound to the axonal actin cortex, axonal branch points, and docked mitochondria all translocate forward during axonal elongation (Lamoureux et al., 2010a). For all three this occurs in a pattern that is consistent with the axon behaving mechanically like a piece of "silly putty" that is stretching with a fixed end at the cell body and a pulled end at the growth cone (O'Toole et al., 2008a). In addition, forward translocation of microtubules is paired with forward advance of the organelles in the C-domain of the growth cone in *Aplysia* neurons (Lee and Suter, 2008; Schaefer et al., 2008). Taken together, these data indicate that docked mitochondria are a reliable and convenient marker for tracking the translocation of the axonal meshwork and microtubules in the growth cone C-domain.

An important goal in neuronal cell biology is to be able to translate *in vitro* observations to *in vivo* axonal elongation and regeneration (Kerschensteiner et al., 2005; Pan et al., 2003). In the context of microtubule translocation, there has not yet been a systematic comparison of *in vivo* and *in vitro* observations where substrate and conservation between species have been considered. To determine if *Drosophila* neurons elongate in the same pattern as *Aplysia* and chick sensory neurons (Suter and Miller, 2011), we grew them on poly-ornithine and *Drosophila* extracellular matrix proteins (DECM) *in vitro* and monitored the pattern of docked mitochondrial movement. To investigate growth cone mediated axonal elongation *in vivo*, we tracked the movement of docked mitochondria during the elongation of the aCC motor neuron in stage 16 *Drosophila* embryos. We found in all cases, docked mitochondria in the growth cones and along the axon advanced in a pattern consistent with the SAI model. These data suggest that the biophysical mechanism of axonal elongation is widely conserved and occurs by a combination of microtubule assembly and forward translocation of C-domain of the growth cone *in vivo*.

2.3 Materials and methods

2.3.1 Fly stocks

Either *elav^{C155}-Gal4;;UAS-mitoGFP, dmiro^{B682}/TM6B$_{Tb,Sb}$* (a kind gift from Gregory Macleod and Konrad Zinsmaier) (Guo et al., 2005) or *elav^{C155}-Gal4;;UAS-mitoGFP* were crossed with *w;;10xUAS-IVS-myr-tdTomato* (Bloomington Stock Collection; Bloomington, IN, USA) to yield *+/elav^{C155}-Gal4;;UAS-mitoGFP, dmiro^{B682}/ 10XUAS-IVS-myr-tdTomato* or *+/elav^{C155}-Gal4;;10xUAS-IVS-myr-tdTomato/UAS-mitoGFP* for the *in vivo* imaging experiments. For all other experiments, the w^{1118} line was used as wild-type.

2.3.2 Preparation of *Drosophila* Extracellular Matrix (DECM)

The *Drosophila* cell line Kc167, acquired from the *Drosophila* Genomics Resource Center, was grown at log phase in HyClone SFX Insect media (Thermo Scientific; Waltham, MA, USA). Note: The *Drosophila* Genomics Resource Center recommends this brand of serum-free media. We found that though the cells grow in serum-free Schneider's they did so poorly. After 4 d of growth, conditioned media rich in DECM was collected and centrifuged at 500 g for 10 min. Media was decanted and stored at -70°C until further processing. Conditioned media (1.7 L) was processed through Millipore (Billerica, MA, USA) Centricon Plus-70 100kDa Ultracel-PL membrane filter devices at 3000 g down to a final volume of 50 ml (34x concentration) and stored at -70°C. DECM samples were analysed for quantity using the Pierce 660 nm Protein Assay (Thermo Scientific; Waltham, MA, USA) and for quality using SDS-PAGE. Samples were run on a 5-20% polyacrylamide gel at 125 V for 1.5 h and stained with Coomassie Blue.

2.3.3 Mass spectroscopy

Prominent bands on the SDS-PAGE gel were subjected to in-gel tryptic digestion. The extracted peptides were then loaded for 5 min onto a Waters Symmetry C18 peptide trap (5 µm, 180 µm x 20 mm) at 4 µL/min in 5% ACN/0.1% formic acid. The bound peptides were then eluted onto a MICHROM Bioresources 0.1 x 150 mm column packed with 3 units 200A Magic C18AQ material over 15 minutes.

2.3.4 Neuronal cultures

Wild-type *Drosophila* neurons, isolated from embryos of either sex, were used as described (Sicaeros and O'Dowd, 2007). Cells were grown at 25°C and imaged at room temperature in L-15 medium (Life Technologies, Item # 41300039; Grand Island, NY, USA) pH 7.1 supplemented with 0.6% glucose, 1 mM glutamine, 100 U/ml penicillin, 136 µg/ml streptomycin sulfate, 10% fetal calf serum, and N9 growth supplement (Lamoureux et al., 2010a). Note neuronal outgrowth is more reliable using the powdered version of L-15 noted above, rather than premade liquid L-15. The culture surface (35 mm cell culture dishes, Corning # 430165; Tewksbury, MA, USA) was treated with 0.01% poly-ornithine for 30 min then washed 3x with dH_2O for 5 min, or with 5 µg/ml DECM for 1 h and rinsed with dH_2O. Dishes were used immediately following coating.

2.3.5 Phase imaging

Axonal length measurements as a function of DECM concentration. Ten fields of cells of *Drosophila* neurons grown on plastic dishes for 24 h were acquired at each concentration of

DECM on the Leica DM IRB using a N Plan L 20x / 0.4 Corr Ph1 ∞ / 0 - 2 / c objective. The length of each neurite longer than the average cell diameter (approximately 10 µm) in the field was measured as the distance between the cell body and tip of the growth cone using ImageJ.

Continuous Measurement of Axonal Elongation. Drosophila neurons were plated on plastic dishes coated with either poly-ornithine or DECM and then phase images were captured every 5 min at room temperature for 24 h using either a Leica DM IRB with a N Plan L 20x / 0.4 Corr Ph1 ∞ / 0 - 2 / c objective and an Orca-ER digital camera CCD, model #CA742-95, (Hamamatsu; Hamamatsu, Japan) or a Nikon Diaphot with a Ph2 20x DL 0.4 160 / 0-2 objective and a Spot Diagnostic Instruments RT monochrome Model 2.1.1 camera. In both cases Micro-Manager was used to control the acquisition. Axonal length was measured by tracing the full length of the axon at 30 min intervals in ImageJ.

2.3.6 Mitochondria imaging

Mitochondria were labelled in wild-type neurons by adding MitoTracker Red CMX-Ros directly to the culture dish (Invitrogen; Carlsbad, CA, USA) at a final concentration of 5 nM. Cultures were observed with an N Plan L 40x / 0.55 corr Ph2 with an adjustable collar infinity / 0 – 2 / c objective on a Leica DM IRB. Cells were illuminated with a 100 W Xenon lamp attenuated 98% with neutral density filters and visualized with a 49008 ET – mCherry, Texas Red cube (Chroma; Bellows Falls, VT, USA) for MitoTracker. On the Leica DM IRB transmitted light exposure was controlled with a VMM-D3 controller and CS25 shutter (Vincent Associates; Rochester, NY, USA). Fluorescent light exposure was controlled with a Lambda 10-C (Sutter Instruments). Micro-manager software was used to control the shutters and camera

(Orca-ER digital camera CCD, model #CA742-95, Hamamatsu; Hamamatsu, Japan). Exposure times were set between 100 to 200 msec.

2.3.7 *In vivo* imaging

Stage 14-15 embryos of either sex were collected from timed egg lays and manually dechorionated. Embryos were oriented at a slight angle with the dorsal surface down on a #1 coverslip lightly coated with embryo glue made by mixing 19:1 chloroform:Spray Mount (3M, St. Paul, MN) and were then lightly coated with 20% chloroform in halocarbon oil 700 (Sigma; St. Louis, MO, USA) to minimize desiccation and muscle contraction. The coverslips were placed directly on a 60x oil immersion objective (NA 1.4) of the Nikon swept field confocal microscope (on a TE2000 platform) and covered with a humidity chamber. After scanning a series of embryos to find one at the correct developmental stage (mid stage 16) and optimal orientation, images were acquired every 2 min at 5% power (set in the NIS software) for the 488 nm line and 100% power for the 561 nm line. Exposure times were 1 s and 20 z-planes with a 0.7 µm step were collected at each time point. ImageJ was used for image analysis as follows. The multiple image planes were Z-projected using the maximum intensity setting at each time point. The limit of the stack was set to exclude the dp1-2 dorsal sensory neurons. In some cases, images were aligned using the Stackreg plugin and axons were straightened using the built-in ImageJ function. To generate kymographs these stacks were resliced and Z-projected using the standard deviation setting. Growth cones advancing faster than 3 µm/h were considered elongating. Mitochondria in the most distal portion of the axons were measured for the rate of advance if they could be tracked for at least 4 frames (i.e. docked for 8 min).

2.4 Results

2.4.1 *Drosophila* extracellular matrix proteins secreted from the Kc167 cell line promote robust axonal elongation.

In order to test whether the SAI model is applicable to a wider range of species and to examine axonal elongation *in vivo,* we turned to the model system *Drosophila* (Prokop et al., 2013). Because the composition of the substrate has a significant effect on the translocation of long microtubules (Chang et al., 1998), which is likely to occur through both signalling (Reichardt and Prokop, 2011) and differences in adhesiveness (O'Toole et al., 2008a), we wanted to examine elongation of *Drosophila* neurons *in vitro* on both poly-amines and ECM proteins. While techniques for culturing embryonic *Drosophila* neurons are gradually advancing (Prokop et al., 2012; Sicaeros and O'Dowd, 2007), vertebrate laminin does not support the growth of *Drosophila* cells (Gullberg et al., 1994; Hirano et al., 1991) and there are currently no commercial sources of *Drosophila* laminin. To acquire *Drosophila* ECM proteins we used the *Drosophila* Kc167 cell line. It secretes the three laminin chains, tiggrin, collagen IV and glutactin (Kumagai et al., 1997), and purified laminin isolated from this cell line has been used to culture *Drosophila* cells, neuronal cell lines and neurons (Takagi et al., 1996; Takagi et al., 1998). Because we were more interested in developing *in vitro* growth conditions that approximated the *in vivo* environment rather than specifically testing how neurons grow on laminin, we characterized the effectiveness of the mixture of DECM proteins produced by Kc167 cells in promoting axonal elongation.

To verify the composition of the proteins secreted by Kc167 cells, we ran concentrated cell culture supernatant on protein gels and then used mass spectroscopy to indentify the bands with the largest amount of protein (Fig. 2.1A) (Kumagai et al., 1997). To test the effectiveness of

DECM in promoting axonal elongation, we collected serum free cell culture supernatant from Kc167 cells, concentrated the total protein to 20 µg/ml, and then compared axonal length of neurons 24 h after plating when cultured on poly-ornithine (Fig. 2.1B) and a series of concentrations of DECM (Fig. 2.1C). We found a concentration of 4 µg/ml DECM causes axonal length to approximately double (91.7 µm +/- 54.3 s.d. n= 103 axons) as compared to poly-ornithine (48.8 µm +/- 26.8 s.d. n= 259 axons), whereas increasing the concentration of DECM to 20 µg/ml did not significantly increase the length of the axons measured at 24 h (Fig. 2.1D; post-hoc Dunnett's test). Using these numbers to make an estimate of average growth indicates elongation rates of 4 µm/h on poly-ornithine and 7.6 µm/h on 4 µg/ml DECM. The significantly higher rates of growth on DECM are consistent with the well-accepted observation that neurons grow more rapidly on endogenous substrates than poly-amines (Evans, 2007).

2.4.2 *Drosophila* elongation *in vitro* occurs at rates comparable to rates *in vivo*

While axons of primary embryonic *Drosophila* neurons elongate more rapidly on DECM than poly-ornithine *in vitro*, the rate is slow as compared to the growth of *Drosophila* motoneurons navigating through the periphery *in vivo* (Murray et al., 1998) (i.e. ~ 20 µm/h). The reason for the slow rate of growth could fall into one of three broad categories. The first is that *Drosophila* neurons *in vitro* are 'sick' because key components found *in vivo* are missing in the cell culture media. The second is that while the neurons are healthy, the substrate conditions *in vitro* so poorly match those *in vivo* that rapid rates of elongation are not possible. The third, a more subtle point, is that *Drosophila* neurons do grow rapidly *in vitro*, but this is obscured because of the way growth rates are measured. To address these questions, we continuously monitored fields of neurons for up to 3 days with frames acquired every five min using phase

optics to unambiguously track the position of individual growth cones. Our first question was whether a delay in the time of axonal initiation could explain the slow average rates of growth. We considered this as a possibility because in contrast to most systems, the culture of embryonic *Drosophila* neurons involves the plating of neuronal precursors (Jacob et al., 2008; Prokop et al., 2012; Salvaterra et al., 1987) instead of post-mitotic cells. We found axonal initiation occurred in a 24 hour window after plating, with half of the neurons sprouting axons at 11.5 h after plating (i.e. 16 hours after egg lay (hAEL)) and that substrate had no obvious effect on the average time of initiation (Fig. 2.1E). This suggests that population averages of axonal length will tend to underestimate growth rates because the initiation of axonal elongation in primary embryonic *Drosophila* neurons is asynchronous.

We then directly assessed the 'instantaneous' rate of axonal elongation by tracking the movement of individual growth cones. We found growth cones advanced at a rapid rate following axonal initiation that slowed until axons reached a final stable length. Figures 2.1F and 2.1G show representative data for individual neurons grown on poly-ornithine and DECM where growth cone position was monitored for 48 h (n= 68 and 56 axons respectively). Simply averaging the raw data in Figs. 2.1F and 2.1G produces an average growth graph (Fig. 2.1J) that is very similar to previously reported growth *in vitro* on poly-ornithine (Wu et al., 1983). To determine the average instantaneous growth rates, we aligned the time of axonal initiation for each axon as illustrated in Figs. 2.1H and 2.1I and averaged growth cone position (Fig. 2.1K). For neurons grown on poly-ornithine, elongation initially occurred at 11.1 +/- 1.5 μm/h (ave. +/- 95% c.i., n = 291 measurements of change in growth cone position over 30 min intervals) and then gradually slowed over the next 12 h with length plateauing at 60 μm (Fig. 2.1K). For neurons grown on DECM axonal elongation initially occurred at 20.9 +/- 2.5 μm/h (ave. +/- 95%

c.i., n = 736 measurements) and then gradually slowed over the next 30 h with the average length reaching 200 µm (Fig. 2.1K). These data demonstrate that embryonic *Drosophila* neurons *in vitro* elongate at instantaneous rates comparable to *Drosophila* neurons in the periphery *in vivo* (Murray et al., 1998).

2.4.3 Anterograde translocation of microtubules during axonal elongation is conserved

As a means to assess if *Drosophila* neurons elongate by microtubule assembly at the tip of a stationary array of microtubules or by combination of microtubule assembly and translocation as is seen in other species (Suter and Miller, 2011) we monitored the movement of docked mitochondria in neurons plated on poly-ornithine and DECM at 1 min intervals for 1 to 2 hours. As the transport velocity of kinesin and dynein occurs at a characteristic rate of ~ 0.1 – 1 µm/s (i.e. 360 – 3600 µm/h) whereas axonal elongation and stretching occurs at 1-50 µm/h, distinguishing between fast transported and slowly moving docked mitochondria is straightforward (Miller and Sheetz, 2006). Examples of what we defined as either docked or fast transported mitochondria are shown as green and blue arrows, respectively, in the mitochondrial kymographs (Figs. 2.2E and 2.2J). On poly-ornithine (18 neurons analyzed), we found docked mitochondria along the axon moved at a rate of 2 to 3 µm/h (Fig. 2.2B, D, E, and K). In contrast, on DECM (40 neurons analyzed), mitochondria along the length of the axon moved at 5 – 10 µm/h in a velocity gradient that was highest at the growth cone (Fig. 2.2G, 2I, J, and K). On both poly-ornithine and DECM, we observed that mitochondria in the growth cone advanced with the growth cone, though at a higher rate on DECM. Therefore, similarly to what is found in *Xenopus* neurons on laminin (Chang et al., 1998), DECM increases translocation of the axonal

cytoskeletal meshwork. Together this suggests that substrate effects on neuronal outgrowth are conserved (Suter and Miller, 2011).

2.4.4 Growth cones advance by anterograde translocation of the axonal meshwork *in vivo*

We next tested whether microtubule translocation in the growth cone and distal portion of the axon occurs similarly *in vivo* by monitoring docked mitochondrial movement in the aCC pioneer neuron in stage 16 *Drosophila* embryos (Campos-Ortega and Hartenstein, 1997). This neuron (Van Vactor et al., 1993) originates in the CNS in stage 10 embryos, approximately 10 hours after egg lay. The elongation of the aCC axon occurs over a time and distance of approximately 6 hours and 200 μm (Sanchez-Soriano et al., 2007) over a basal lamina consisting of roughly a dozen proteins secreted by the fat body and hemocytes including laminin, tiggrin, glutactin and perlecan (Broadie et al., 2011). The focus of our studies was in the region of muscles 1 and 2, past the synaptic termination point of the RP2 motor neuron. We chose to follow the aCC growth cone in this region because growth occurs along a plane close to the body wall through a region in the embryo that allows visual isolation of the growth cone (Fig. 2.3A).

To track axonal elongation and the movement of docked mitochondria in the distal axon and growth cone, we co-expressed the plasma membrane marker myr-tdTomato and mitochondrially targeted GFP (Pilling et al., 2006) using the pan-neuronal Gal4 driver *elav*. Docked mitochondria were defined as those that maintained their relative position along the axon for at least 8 minutes and moved at a velocity of less than 100 μm/h. In our initial observations using +/*elav*-Gal4;;*UAS-mitoGFP*/*IVS-10XUAS-myr-tdTom* embryos, we observed only 1 – 2 docked mitochondria per axon. We therefore sought a genetic means to increase the number of docked mitochondria. $dmiro^{B682}$ mutants have reduced fast mitochondrial transport (Guo et al.,

2005), which we reasoned would increase the frequency of mitochondria docking to the axonal meshwork. We used heterozygous *dmiro*^{B682} embryos, which increased the number of docked mitochondria to 2-3 per axon (Table 3.1). In total we imaged 35 growth cones (21 with the genotype +/*elav*-Gal4;;*UAS-mitoGFP*/*IVS-10XUAS-myr-tdTom* and 14 with the genotype +/*elav*-Gal4;;*UAS-mitoGFP, dmiro*^{B682}/*IVS-10XUAS-myr-tdTom*). We found no differences in the rates of growth cone advance or docked mitochondrial movement between *dmiro*^{wt} and heterozygous *dmiro*^{B682} so the data were pooled (Table 3.1). The pooled average rate of growth cone advance was 20.0 +/- 3.0 μm/h (ave +/- 95% c.i., n = 35). Likewise the movement of docked mitochondria in the growth cone, defined as the distal most 5 μm of the axon, had the same average rate of advance (Fig. 2.3E). Along the next 20 μm of axon, docked mitochondria advanced at an average rate of ~30 μm/h. The higher rate of docked mitochondrial movement, as compared to the rate of growth cone advance (Fig. 2.3E), appears to occur because translocation of docked mitochondria continues when growth cones briefly pause (Miller and Sheetz, 2006; Reinsch et al., 1991). For example, the triangle in Figure 2.3C points out a docked mitochondrion that is advancing more rapidly than the growth cone. In all instances where a mitochondrion was found in the growth cone it advanced simultaneously with the growth cone (arrow, Fig. 2.3B-D). These data indicate that growth cones of *Drosophila* motor neurons advance by forward translocation of the axonal cytoskeletal meshwork and organelle rich C-domain.

2.5 Discussion

By monitoring the movement patterns of docked mitochondria to track the subcellular movement of the axonal meshwork during axonal elongation, our data suggest that the influence of substrate on microtubule translocation during axonal elongation is shared between species and that the forward translocation of microtubules in the axon contributes to the advance of the C-domain and hence axon elongation, both in culture and *in vivo*.

2.5.1 Extracellular matrix proteins from the Kc167 cell line provide useful culture substrates to study neuronal processes.

There has been a surge of interest in the development of *in vitro* neuronal culture techniques in *Drosophila* (Ayali, 2012; Bai et al., 2009; Beadle, 2006; Sanchez-Soriano et al., 2010; Sicaeros and O'Dowd, 2007). This provides new avenues to combine well established molecular /genetic tools with timelapse microscopy (Miller and Sheetz, 2006), super-resolution microscopy (Shtengel et al., 2009), ultrastructural analysis (Svitkina et al., 1997), *in vitro* RNAi (Sepp et al., 2008), and biophysical approaches (Suter and Miller, 2011). In terms of developing *in vitro* culture systems that allow the exploration of the wider range of parameters known to be present *in vivo*, the inclusion of physiologically relevant ECM proteins is important (Broadie et al., 2011). Our work here demonstrates a straightforward means to concentrate and apply DECM in tissue culture and describes the concentration range over which axonal elongation is promoted. We also note DECM can be stored at -70°C for at least a year, which is both convenient and decreases experimental variability; two advantages that are important for both small and high throughput gene disruption experiments. While supernatant collected from Kc167 cells is a convenient source of *Drosophila* extracellular matrix proteins, it contains a complex mixture of

proteins (Kumagai et al., 1997). While we view this as an advantage in our studies, in the context of understanding the process of axonal elongation, it will be important to systematically analyze the function of the individual ECM proteins and their receptors to assess their roles in mediating adhesion (Bard et al., 2008) and their modulation of signaling pathways (Broadie et al., 2011).

2.5.2 *Drosophila* neurons elongate robustly but briefly *in vitro*

Based on our experience with chick and rat neurons (Lamoureux et al., 2010a; Lamoureux et al., 2010b), we were initially struck by the slow growth of *Drosophila* neurons *in vitro*. We found (Fig. 2.1J), as others have reported (Salvaterra et al., 1987; Sanchez-Soriano et al., 2010; Wu et al., 1983), an average rate of growth of ~ 3 – 5 μm/h. In contrast, *Drosophila* growth cones advance at a rate of 20-30 μm/h *in vivo* (Murray et al., 1998) (Fig. 2.3E). By unambiguously tracking individual growth cones and accounting for asynchronous axon initiation in culture (Fig. 2.1E), we found instantaneous growth rates of ~10 μm/h on poly-ornithine and ~20 μm/h on DECM (Fig. 2.1K), the latter of which is within the window of growth rates observed *in vivo*. DECM will thus be an important tool in future *in vitro* studies to achieve the higher velocities observed *in vivo.*

While we found *Drosophila* neurons grow rapidly *in vitro*, for individual neurons this occurred for a time period of less than 24 h (Fig. 2.1K). While it is well accepted that as neurons mature they lose their capacity for elongation and regeneration, what controls the intrinsic decrease in growth potential is poorly understood. Two of several possibilities are that neurons have a means to measure axonal length (Albus et al., 2013) and switch off growth when a set distance has been reached. In addition, there may be an internal clock that acts independently of axonal length and activates maturation after a set time. While we have previously suggested that

a length sensor controls axonal transport in *Drosophila* larvae (O'Toole et al., 2008b), our data here suggest a clock, similar to that which controls differentiation, electrophysiological properties, and neuronal process morphologies (Kuppers-Munther et al., 2004), may regulate the transition to maturity for *Drosophila* neurons *in vitro* (Salvaterra et al., 1987). In support of this we note that if a length sensor solely regulated the cessation of elongation, neurons grown on poly-ornithine would be predicted to sustain elongation for a longer time than neurons grown on DECM (Fig. 2.1K). *Drosophila* provides an excellent platform for studying changes in gene and protein expression and because their neurons develop rapidly, this system has the potential to be useful for studying why neurons lose their capacity for growth over time.

2.5.3 The pattern of axonal elongation is similar between *Drosophila* and other species *in vitro*

As a prerequisite to analyzing the pattern of axonal elongation *in vivo*, we felt that it was important to establish that *Drosophila* neurons grow in a manner similar to other types of neurons *in vitro*. If they did it would suggest that regardless of the results we observed *in vivo*, they would applicable to other species. Closely related to this question was the issue of whether *in vitro* axonal elongation recapitulates growth *in vivo*. While this is an unspoken assumption, it has not been systematically validated in terms of whether microtubules are stationary or translocate forward during axonal elongation. Two important aspects of this problem are that the rate of microtubule translocation varies along the length of the axon and the adhesiveness of the substrate modulates translocation velocity (O'Toole et al., 2008a). Thus to characterize microtubule translocation in *Drosophila* neurons, examination of one point along the axon on one type of substrate is not sufficient. To address these issues we grew *Drosophila* neurons on poly-ornithine and DECM *in vitro* and monitored the pattern of docked mitochondrial movement

along the length of the axon (Fig. 2.2K). On both substrates, we observed that the rate of forward translocation was higher in the growth cone than along the length of the axon. In addition, the overall velocity was higher in neurons grown on DECM than on poly-ornithine. This movement pattern and response to growth on ECM protein have both been observed in chick sensory (O'Toole et al., 2008a) and *Xenopus* neurons (Chang et al., 1998; Reinsch et al., 1991). Together these observations indicate that the pattern physical mechanism underlying microtubule translocation (Suter and Miller, 2011) *in vitro* is similar between *Drosophila* and other species.

2.5.4 Growth cones advance by forward translocation of the axonal meshwork *in vivo*

While our analysis of mitochondrial movement (Fig. 2.2K) confirms that *Drosophila* neurons, like chick (Miller and Sheetz, 2006), rat (Lamoureux et al., 2010b), and *Aplysia* neurons (Lee and Suter, 2008; Schaefer et al., 2008), elongate by forward translocation of microtubules, these experiments were all carried out *in vitro*. *In vivo* analysis of microtubule translocation in Zebrafish and grasshopper Ti1 pioneer neurons, in contrast revealed microtubules are stationary along the axon (Sabry et al., 1995; Takeda et al., 1995). One possibility that can explain these differing results is that microtubule translocation only occurs *in vitro* and because axonal elongation is a highly conserved process this is an ‘artifact’ that is seen in various species. To investigate we tracked the movement of docked mitochondria in the growth cone and distal axon in *Drosophila* embryos *in vivo* (Fig. 2.3). We found mitochondria advanced in a pattern consistent with anterograde translocation of the axonal meshwork, but in turn this raises the question of why the *in vivo* data conflict. We suggest the underlying reason is that we examined translocation near the growth cone (Fig. 2.3), whereas the previous studies (Sabry et al., 1995; Takeda et al., 1995) focused on the region of the axon closer to the cell body to test a now

defunct theory about slow axonal transport called the Structural Hypothesis (Hoffman and Lasek, 1975; Miller and Heidemann, 2008; Miller and Joshi, 1996). Previous *in vitro* studies in chick (Miller and Sheetz, 2006) and *Xenopus* neurons (Chang et al., 1998; Reinsch et al., 1991), as well as our *in vitro* studies here (Fig. 2.2K), all show that the cytoskeletal meshwork moves more slowly or is stationary close to the cell body, but moves forward near the growth cone (Suter and Miller, 2011). Biophysical analysis suggests this occurs because axons stretch and forces that move the axonal meshwork forward are dissipated along the axon through adhesions (O'Toole et al., 2008a). Thus we see no conflict between our *in vivo* observations and prior studies in Zebrafish and grasshopper (Sabry et al., 1995; Takeda et al., 1995). While the similarity between the pattern of elongation we observe *in vitro* (Fig. 2.2K) between *Drosophila* and chick neurons (Miller and Sheetz, 2006) suggests our *in vivo* findings may be relevant to other species, because of the complexity of axonal elongation *in vivo* it will be important to explicitly examine growth cone motility in other systems (e.g. Zebrafish, grasshopper, chick, mouse) and cell-types.

2.5.5 Toward a comprehensive model of axonal elongation.

While microtubule assembly is critical for axonal elongation (Conde and Caceres, 2009; Geraldo and Gordon-Weeks, 2009; Tanaka et al., 1995), the contribution of microtubule translocation has only recently become appreciated (Suter and Miller, 2011). Moving beyond the debates of whether long microtubules are stationary or move, understanding the mechanisms that underlie their translocation is the next major question. In the context of the findings noted above, we propose two highly speculative models that can account for microtubule translocation. In both, forces generated by molecular motors such as myosin (Suter, 2011), dynein (Vallee et al., 2009), mitotic kinesins (Liu et al., 2010), and Kinesin-1 (Lu et al., 2013), not only move short

microtubules by stop-and-go transport (Liu et al., 2010), but also drive the slow advance of the long microtubule array (Prokop, 2013; Suter and Miller, 2011). In the first, these motors generate a net force that pushes microtubules along the axon forward and myosin II driven actin retrograde flow in the growth cone acts as a dynamic barrier that blocks their advance (Forscher and Smith, 1988; Hur et al., 2011; Ketschek et al., 2007; Stiess and Bradke, 2011; Zhou et al., 2002). Part of the appeal of this model is that it has been known for decades that axons can elongate when actin is disrupted (Marsh and Letourneau, 1984). In addition, recent experiments in *Drosophila* have revealed that Kinesin-1 is capable of sliding microtubules out of the neuronal body during the process of neurite initiation (Lu et al., 2013). Nonetheless, this model of axonal elongation seems incomplete. When the actin cytoskeleton is intact, detachment of growth cones from the substrate (Condic and Bentley, 1989) or axonal severing (Gallo, 2004) leads to axonal retraction driven by actomyosin contractile forces generated along the axon (Bernal et al., 2007; Joshi et al., 1985). Furthermore, it is well accepted that when actin is intact growth cones pull (Lamoureux et al., 1989) the substrate rearwards while pulling the C-domain forward (Suter and Miller, 2011). To explain these observations we suggest that while microtubules along the axon push forward, contractile forces generated along the axon are larger (Bernal et al., 2007; Joshi et al., 1985) and thus retraction of the axon occurs when the growth cone is detached from the substrate (Condic and Bentley, 1989). In the growth cone, coupling between actin and microtubules (Lowery and Van Vactor, 2009) sweeps microtubules that polymerize or translocate into the P-domain back (Dent et al., 1999; Rauch et al., 2013; Schaefer et al., 2002), yet the net force generated by the growth cone pulls microtubules in the C-domain (Lee and Suter, 2008; Schaefer et al., 2008) and along the axon forward (Miller and Sheetz, 2006). The key difference between the two models is that in the first the net force generated along the axon

by the combined actions of the microtubule and actin cytoskeleton pushes forward and forces generated in the growth cone restrain this advance. In the second, the net forces generated along the axon pull the growth cone rearwards, while the growth cone pulls forwards. In summary, our work suggests models of growth cone motility need to incorporate microtubule translocation in addition to assembly, raises the question of what powers translocation, and provides tools for testing various models.

Acknowledgements: We thank Andreas Prokop, Peter Hollenbeck and Steve Heidemann for their thoughtful comments and helpful suggestions.

APPENDIX

Table 2.1 Rates of growth cone and docked mitochondrial advance are the same in *dmiro*^{wt} and heterozygous *dmiro*^{B682} axons *in vivo*.

Genotype	**GC rate (µm/h)**	**Mito rate (µm/h)**	**Mito per axon**
***dmiro*$^{+/+}$**	20.5 +/- 3.7 (21)	29.0 +/- 7.5 (32)	1.6 +/- 0.6 (21)
***dmiro*$^{+/-}$**	19.3 +/- 5.9 (14)	31.0 +/- 8.1 (38)	2.4 +/- 0.6 (14)
combined	20.0 +/- 3.0 (35)	30.1 +/- 5.4 (70)	

All values reported as ave +/- 95% CI. Values in parenthesis represent *n* values. No significant differences were found between growth cone or mitochondria rates of advance (P = 0.707 and 0.732, respectively, by unpaired two tail, t-test). The number of docked mitochondria in the distal 30 µm of the axon was significantly higher in the heterozygous *dmiro*^{B682} axons (P = 0.05).

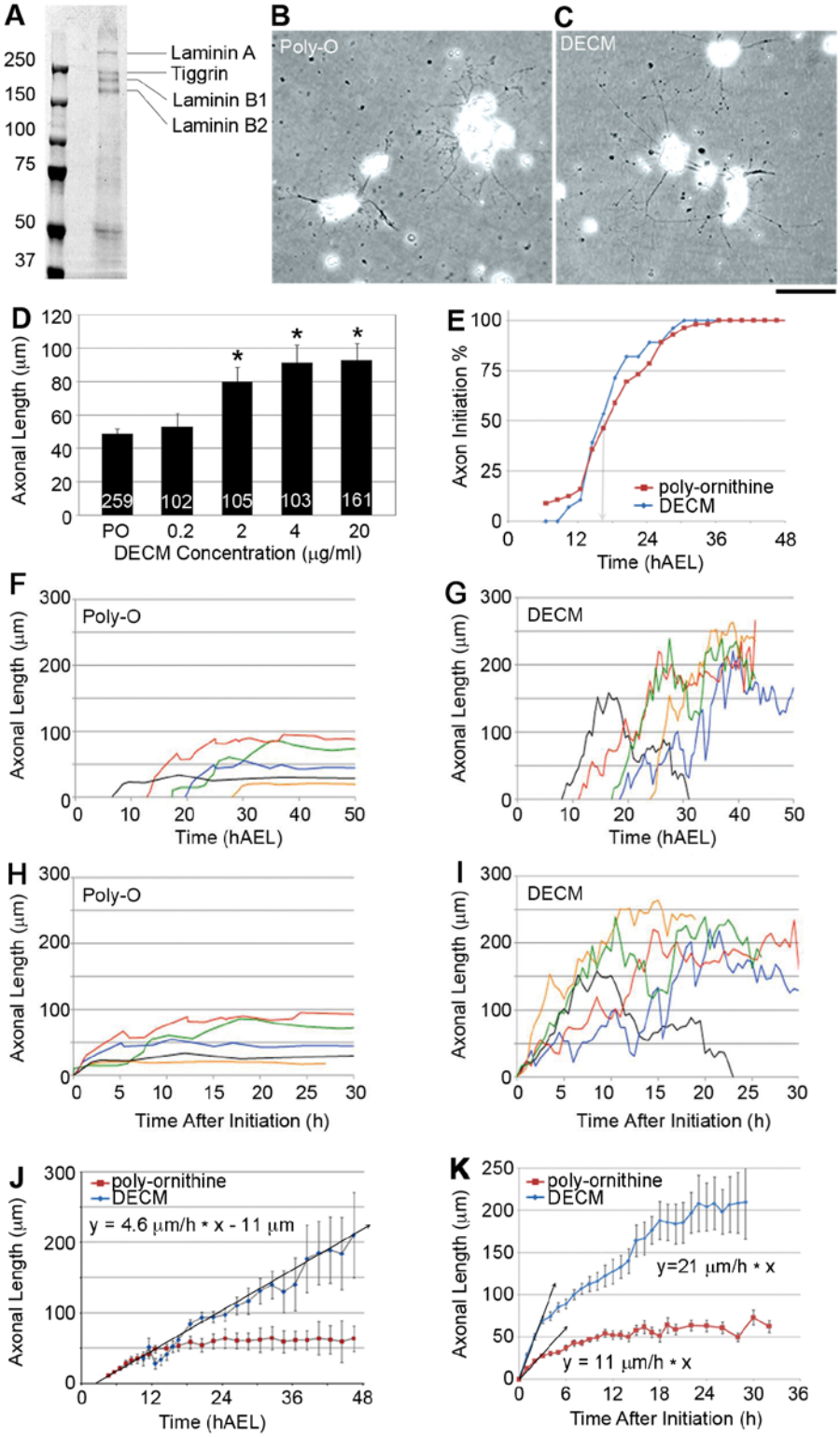

Figure 2.1. ***Drosophila*** **neurons grow at physiological rates *in vitro*.** (**A**) Coomassie stain of DECM purified from Kc167 conditioned media. Bands identified as Laminin A, Tiggrin,

Figure 2.1 (cont'd)

Laminin B1, and Laminin B2 by mass spectroscopy. Unsequenced band at 50 kDa corresponds to glutactin based on previous reports (Kumagai et al., 1997). Phase images of *Drosophila* neurons grown *in vitro* on (**B**) poly-ornithine and (**C**) DECM. Axonal length at 24 hours increases with concentrations of DECM at 2 µg/ml and higher (**D**). The numbers in the bars in (**D**) represent *n* for each group. The graph in (**E**) shows axonal initiation is asynchronous, occurring over a period of ~12 hours, and is not substrate dependent. The arrow marks the time point where 50% of the neurons had initiated axons. Representative examples of growth cone position over time are shown for neurons grown on (**F**) poly-ornithine and (**G**) DECM. By aligning individual growth cone positions so initiation is at t = 0, accurate depictions of cone advance can be more clearly seen. (**H**) poly-ornithine alignment, (**I**) DECM alignment. Averaging axonal length over time without accounting for differences in initiation (**J**) yields rates of elongation similar to previous reports, whereas analysis of synchronized average axonal length (**K**) reveals elongation occurs at rates similar to those observed *in vivo*. All error bars are 95% CI. Scale bar = 70 µm.

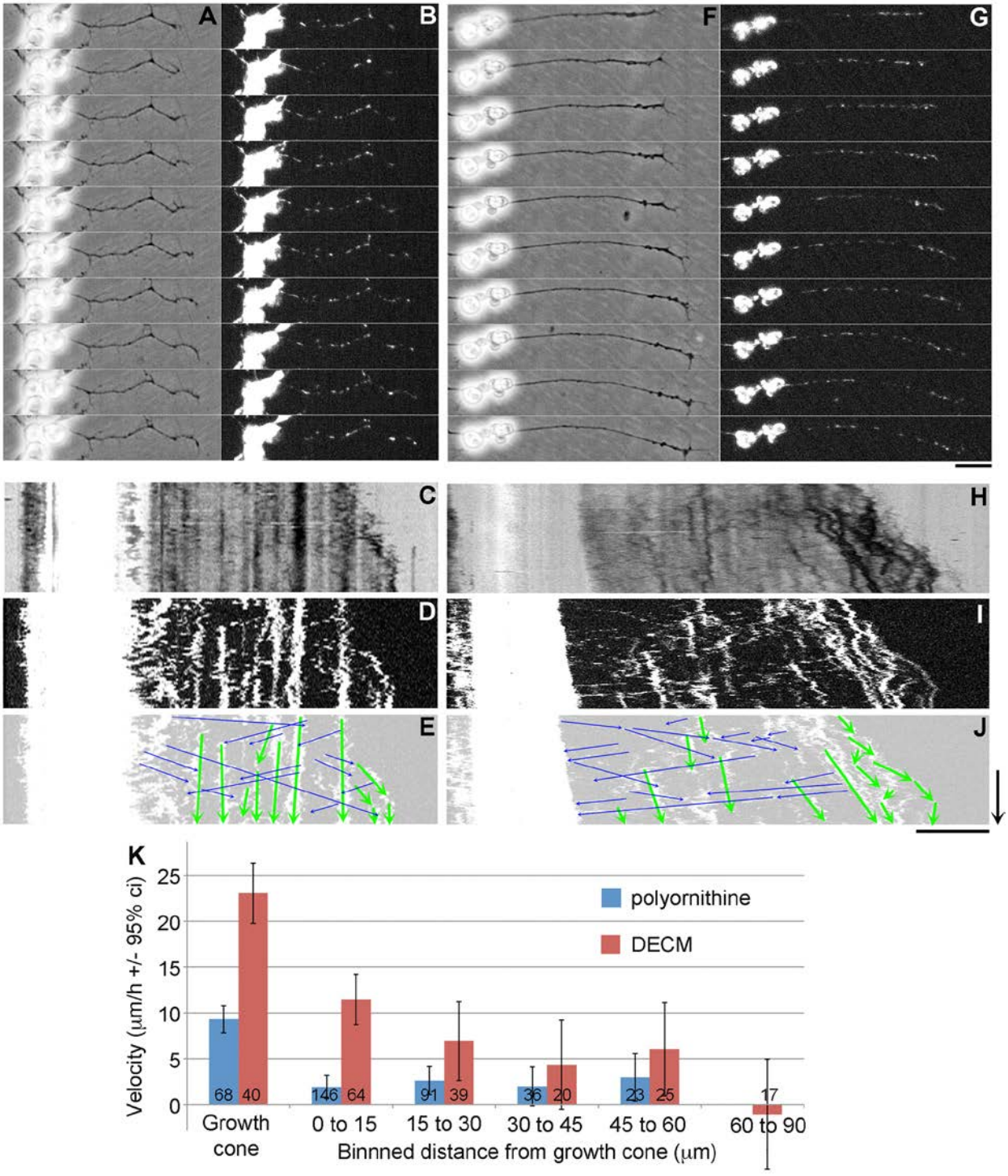

Figure 2.2. Growth cones advance by forward translocation of the C-domain and axonal framework *in vitro*. (**A**) Phase and (**B**) fluorescent images over 1 h of MitoTracker labelled *Drosophila* neurons grown on poly-ornithine. Kymographs of the phase images (**C**) and fluorescent images (**D**) show the position of the growth cone and mitochondria over time. (**E**) Green arrows overlaid on the kymograph illustrate the movement of docked mitochondria and

Figure 2.2 (cont'd)

the blue arrows show the tracks of fast transported mitochondria. The corresponding images from a neuron grown on DECM are shown in panels (**F-J**). Time arrow = 30 min and scale bar is 10 μm for both the time-lapse images and kymographs. (**K**) Quantitative analysis of the velocity of docked mitochondria plotted against distance from the growth cone. Errors bars are 95% confidence intervals. The numbers at the base of the bars denote the number of mitochondria analyzed in each bin. The growth cone is defined as the first 5 μm of axon.

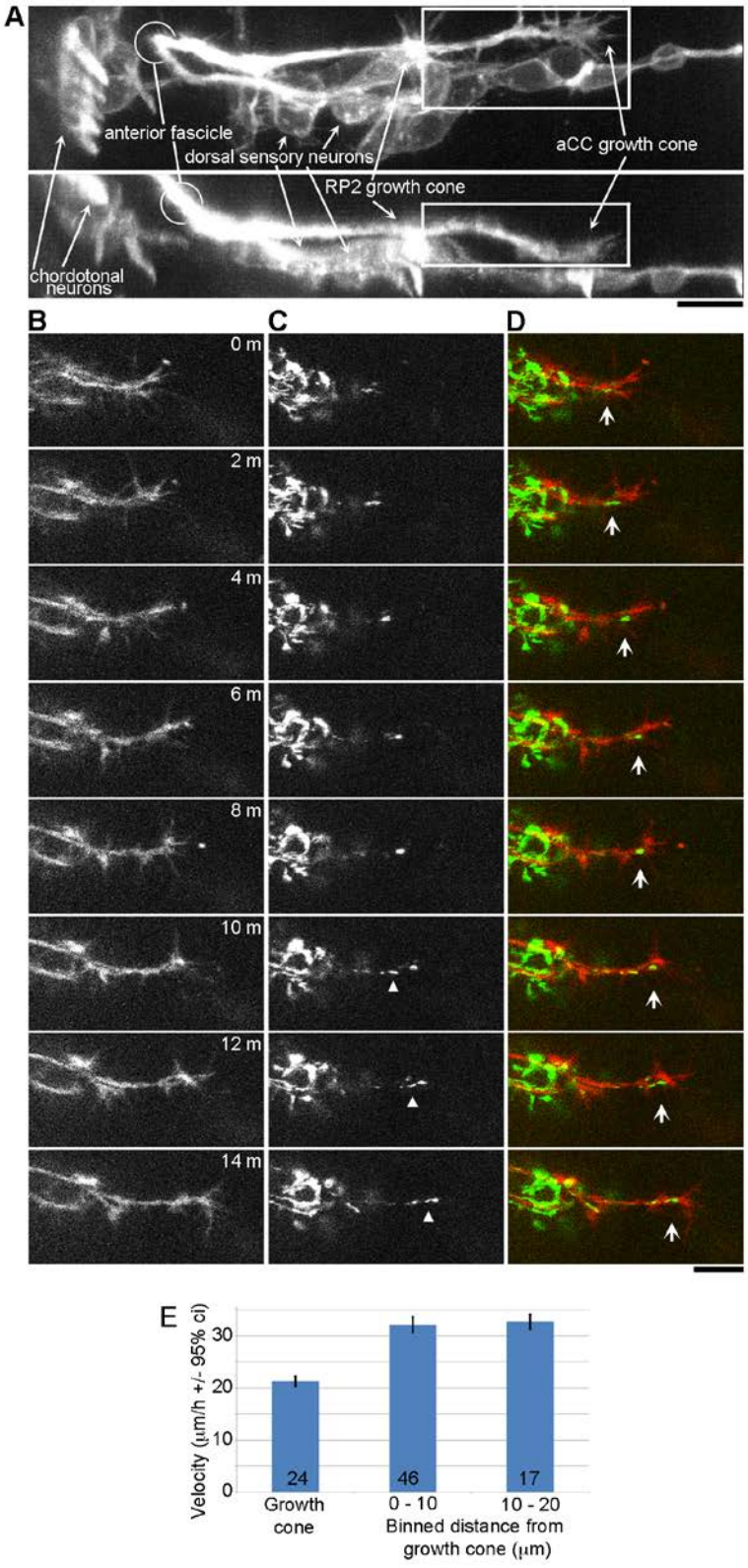

Figure 2.3. Growth cones advance by forward translocation of the C-domain and axonal framework *in vivo*. (**A**) A 3D reconstruction of late stage 16 embryo expressing the membrane

Figure 2.3 (cont'd)

marker myr-tdTomato in the nervous system via *elav-Gal4*. After the intersegmental axon of the aCC neuron passes the point where the RP2 axon forms a synapse on muscle 2, it is in a region free of other axons and the cell bodies of surrounding sensory neurons. The box indicates the region of the aCC motor axon that was used for 3D analysis of mitochondrion advance. (**B - D**) Time-lapse series of an elongating *Drosophila* aCC motor neuron in stage 16 embryo of the genotype +/*elav*-Gal4;;*UAS-mtGFP*, *dmiro*^{B682}/ *IVS-10XUAS-myr-tdTom*, shown at 2 min intervals. (**B**) myr-tdTomato (red in **D**) labels neuronal plasma membranes. (**C**) mitoGFP (green in **D**) labels mitochondria. The arrow shows a mitochondrion in growth cone. In the last half of the series a mitochondrion docks in the distal axon (triangle in **B**) and advances. (**E**) Average velocity of docked mitochondria in the growth cone, defined as the last five µm of the axon, and in binned regions along the distal axon. Because the RP2 axon is fasciculated with the aCC axon (**A**), only mitochondria in the last 25 µm of the aCC axon were analyzed. Error bars show the 95% confidence intervals. The number at the base of the bar is the number of docked mitochondria that were analyzed. Scale bars = 10 µm.

REFERENCES

REFERENCES

Albus, C.A., I. Rishal, and M. Fainzilber. 2013. Cell length sensing for neuronal growth control. *Trends Cell Biol*. 23:305-310.

Aletta, J.M., and L.A. Greene. 1988. Growth cone configuration and advance: a time-lapse study using video-enhanced differential interference contrast microscopy. *J Neurosci*. 8:1425-1435.

Ayali, A. 2012. Editorial: models of invertebrate neurons in culture. *J Mol Histol*. 43:379-381.

Baas, P.W., A. Karabay, and L. Qiang. 2005. Microtubules cut and run. *Trends Cell Biol*. 15:518-524.

Bai, J., K.J. Sepp, and N. Perrimon. 2009. Culture of Drosophila primary cells dissociated from gastrula embryos and their use in RNAi screening. *Nat Protoc*. 4:1502-1512.

Bamburg, J.R., D. Bray, and K. Chapman. 1986. Assembly of microtubules at the tip of growing axons. *Nature*. 321:788-790.

Bard, L., C. Boscher, M. Lambert, R.M. Mege, D. Choquet, and O. Thoumine. 2008. A molecular clutch between the actin flow and N-cadherin adhesions drives growth cone migration. *J Neurosci*. 28:5879-5890.

Beadle, D.J. 2006. Insect neuronal cultures: an experimental vehicle for studies of physiology, pharmacology and cell interactions. *Invert Neurosci*. 6:95-103.

Bernal, R., P.A. Pullarkat, and F. Melo. 2007. Mechanical properties of axons. *Physical review letters*. 99:018301.

Bradke, F., and C.G. Dotti. 1997. Neuronal polarity: vectorial cytoplasmic flow precedes axon formation. *Neuron*. 19:1175-1186.

Broadie, K., S. Baumgartner, and A. Prokop. 2011. Extracellular matrix and its receptors in Drosophila neural development. *Dev Neurobiol*. 71:1102-1130.

Campos-Ortega, J.A., and V. Hartenstein. 1997. The embryonic development of Drosophila melanogaster. Springer, Berlin ; New York. xvii, 405 p. pp.

Chan, C.E., and D.J. Odde. 2008. Traction dynamics of filopodia on compliant substrates. *Science (New York, N.Y.* 322:1687-1691.

Chang, S., V.I. Rodionov, G.G. Borisy, and S.V. Popov. 1998. Transport and turnover of microtubules in frog neurons depend on the pattern of axonal growth. *J Neurosci*. 18:821-829.

Chang, S., T.M. Svitkina, G.G. Borisy, and S.V. Popov. 1999. Speckle microscopic evaluation of microtubule transport in growing nerve processes. *Nat Cell Biol*. 1:399-403.

Chetta, J., C. Kye, and S.B. Shah. 2010. Cytoskeletal dynamics in response to tensile loading of mammalian axons. *Cytoskeleton (Hoboken)*. 67:650-665.

Conde, C., and A. Caceres. 2009. Microtubule assembly, organization and dynamics in axons and dendrites. *Nat Rev Neurosci*. 10:319-332.

Condic, M.L., and D. Bentley. 1989. Removal of the basal lamina in vivo reveals growth cone-basal lamina adhesive interactions and axonal tension in grasshopper embryos. *J Neurosci*. 9:2678-2686.

Dent, E.W., J.L. Callaway, G. Szebenyi, P.W. Baas, and K. Kalil. 1999. Reorganization and movement of microtubules in axonal growth cones and developing interstitial branches. *J Neurosci*. 19:8894-8908.

Evans, A.R. 2007. Laminin and fibronectin modulate inner ear spiral ganglion neurite outgrowth in an in vitro alternate choice assay. *Dev. Neurobiol.* 67:1721-1730.

Forscher, P., and S.J. Smith. 1988. Actions of cytochalasins on the organization of actin filaments and microtubules in a neuronal growth cone. *The Journal of cell biology*. 107:1505-1516.

Gallo, G. 2004. Myosin II activity is required for severing-induced axon retraction in vitro. *Experimental neurology*. 189:112-121.

Geraldo, S., and P.R. Gordon-Weeks. 2009. Cytoskeletal dynamics in growth-cone steering. *J Cell Sci*. 122:3595-3604.

Goldberg, D.J., and D.W. Burmeister. 1986. Stages in axon formation: observations of growth of Aplysia axons in culture using video-enhanced contrast-differential interference contrast microscopy. *The Journal of cell biology*. 103:1921-1931.

Gullberg, D., L.I. Fessler, and J.H. Fessler. 1994. Differentiation, extracellular matrix synthesis, and integrin assembly by Drosophila embryo cells cultured on vitronectin and laminin substrates. *Dev Dyn*. 199:116-128.

Guo, X., G.T. Macleod, A. Wellington, F. Hu, S. Panchumarthi, M. Schoenfield, L. Marin, M.P. Charlton, H.L. Atwood, and K.E. Zinsmaier. 2005. The GTPase dMiro is required for axonal transport of mitochondria to Drosophila synapses. *Neuron*. 47:379-393.

Hammarlund, M., E.M. Jorgensen, and M.J. Bastiani. 2007. Axons break in animals lacking beta-spectrin. *J Cell Biol*. 176:269-275.

Hirano, S., K. Ui, T. Miyake, T. Uemura, and M. Takeichi. 1991. Drosophila PS integrins recognize vertebrate vitronectin and function as cell-substratum adhesion receptors in vitro. *Development*. 113:1007-1016.

Hirokawa, N. 1982. Cross-linker system between neurofilaments, microtubules, and membranous organelles in frog axons revealed by the quick-freeze, deep-etching method. *The Journal of cell biology*. 94:129-142.

Hoffman, P.N., and R.J. Lasek. 1975. The slow component of axonal transport. Identification of major structural polypeptides of the axon and their generality among mammalian neurons. *J Cell Biol*. 66:351-366.

Hur, E.M., I.H. Yang, D.H. Kim, J. Byun, Saijilafu, W.L. Xu, P.R. Nicovich, R. Cheong, A. Levchenko, N. Thakor, and F.Q. Zhou. 2011. Engineering neuronal growth cones to promote axon regeneration over inhibitory molecules. *Proceedings of the National Academy of Sciences of the United States of America*. 108:5057-5062.

Jacob, J., C. Maurange, and A.P. Gould. 2008. Temporal control of neuronal diversity: common regulatory principles in insects and vertebrates? *Development*. 135:3481-3489.

Joshi, H.C., D. Chu, R.E. Buxbaum, and S.R. Heidemann. 1985. Tension and compression in the cytoskeleton of PC 12 neurites. *The Journal of cell biology*. 101:697-705.

Kanchanawong, P., G. Shtengel, A.M. Pasapera, E.B. Ramko, M.W. Davidson, H.F. Hess, and C.M. Waterman. 2010. Nanoscale architecture of integrin-based cell adhesions. *Nature*. 468:580-584.

Kang, J.S., J.H. Tian, P.Y. Pan, P. Zald, C. Li, C. Deng, and Z.H. Sheng. 2008. Docking of axonal mitochondria by syntaphilin controls their mobility and affects short-term facilitation. *Cell*. 132:137-148.

Kerschensteiner, M., M.E. Schwab, J.W. Lichtman, and T. Misgeld. 2005. In vivo imaging of axonal degeneration and regeneration in the injured spinal cord. *Nat Med*. 11:572-577.

Ketschek, A.R., S.L. Jones, and G. Gallo. 2007. Axon extension in the fast and slow lanes: substratum-dependent engagement of myosin II functions. *Developmental neurobiology*. 67:1305-1320.

Koch, D., W.J. Rosoff, J. Jiang, H.M. Geller, and J.S. Urbach. 2012. Strength in the periphery: growth cone biomechanics and substrate rigidity response in peripheral and central nervous system neurons. *Biophysical journal*. 102:452-460.

Kumagai, C., T. Kadowaki, and Y. Kitagawa. 1997. Disulfide-bonding between Drosophila laminin beta and gamma chains is essential for alpha chain to form alpha betagamma trimer. *FEBS Lett*. 412:211-216.

Kuppers-Munther, B., J.J. Letzkus, K. Luer, G. Technau, H. Schmidt, and A. Prokop. 2004. A new culturing strategy optimises Drosophila primary cell cultures for structural and functional analyses. *Dev Biol*. 269:459-478.

Lamoureux, P., R.E. Buxbaum, and S.R. Heidemann. 1989. Direct evidence that growth cones pull. *Nature*. 340:159-162.

Lamoureux, P., S.R. Heidemann, N.R. Martzke, and K.E. Miller. 2010a. Growth and elongation within and along the axon. *Developmental neurobiology*. 70:135-149.

Lamoureux, P.L., M.R. O'Toole, S.R. Heidemann, and K.E. Miller. 2010b. Slowing of axonal regeneration is correlated with increased axonal viscosity during aging. *BMC neuroscience*. 11:140.

Lee, A.C., and D.M. Suter. 2008. Quantitative analysis of microtubule dynamics during adhesion-mediated growth cone guidance. *Developmental neurobiology*. 68:1363-1377.

Liu, M., V.C. Nadar, F. Kozielski, M. Kozlowska, W. Yu, and P.W. Baas. 2010. Kinesin-12, a mitotic microtubule-associated motor protein, impacts axonal growth, navigation, and branching. *J Neurosci*. 30:14896-14906.

Lowery, L.A., and D. Van Vactor. 2009. The trip of the tip: understanding the growth cone machinery. *Nat Rev Mol Cell Biol*. 10:332-343.

Lu, W., P. Fox, M. Lakonishok, M.W. Davidson, and V.I. Gelfand. 2013. Initial neurite outgrowth in Drosophila neurons is driven by kinesin-powered microtubule sliding. *Curr Biol*. 23:1018-1023.

Marsh, L., and P.C. Letourneau. 1984. Growth of neurites without filopodial or lamellipodial activity in the presence of cytochalasin B. *J Cell Biol*. 99:2041-2047.

Martenson, C., K. Stone, M. Reedy, and M. Sheetz. 1993. Fast axonal transport is required for growth cone advance. *Nature*. 366:66-69.

Miller, K.E., and S.R. Heidemann. 2008. What is slow axonal transport? *Exp Cell Res*. 314:1981-1990.

Miller, K.E., and H.C. Joshi. 1996. Tubulin transport in neurons. *The Journal of cell biology*. 133:1355-1366.

Miller, K.E., and M.P. Sheetz. 2004. Axonal mitochondrial transport and potential are correlated. *J Cell Sci*. 117:2791-2804.

Miller, K.E., and M.P. Sheetz. 2006. Direct evidence for coherent low velocity axonal transport of mitochondria. *The Journal of cell biology*. 173:373-381.

Mitchison, T., and M. Kirschner. 1988. Cytoskeletal dynamics and nerve growth. *Neuron*. 1:761-772.

Murray, M.J., D.J. Merritt, A.H. Brand, and P.M. Whitington. 1998. In vivo dynamics of axon pathfinding in the Drosophilia CNS: a time-lapse study of an identified motorneuron. *J Neurobiol*. 37:607-621.

O'Donnell, M., R.K. Chance, and G.J. Bashaw. 2009. Axon growth and guidance: receptor regulation and signal transduction. *Annu Rev Neurosci*. 32:383-412.

O'Toole, M., P. Lamoureux, and K.E. Miller. 2008a. A physical model of axonal elongation: force, viscosity, and adhesions govern the mode of outgrowth. *Biophysical journal*. 94:2610-2620.

O'Toole, M., R. Latham, R.M. Baqri, and K.E. Miller. 2008b. Modeling mitochondrial dynamics during in vivo axonal elongation. *Journal of theoretical biology*. 255:369-377.

Pan, Y.A., T. Misgeld, J.W. Lichtman, and J.R. Sanes. 2003. Effects of neurotoxic and neuroprotective agents on peripheral nerve regeneration assayed by time-lapse imaging in vivo. *Journal of Neuroscience*. 23:11479-11488.

Pathak, D., K.J. Sepp, and P.J. Hollenbeck. 2010. Evidence that myosin activity opposes microtubule-based axonal transport of mitochondria. *J Neurosci*. 30:8984-8992.

Peter, S.J., and M.R. Mofrad. 2012. Computational modeling of axonal microtubule bundles under tension. *Biophys J*. 102:749-757.

Pilling, A.D., D. Horiuchi, C.M. Lively, and W.M. Saxton. 2006. Kinesin-1 and Dynein are the primary motors for fast transport of mitochondria in Drosophila motor axons. *Mol Biol Cell*. 17:2057-2068.

Prokop, A. 2013. The intricate relationship between microtubules and their associated motor proteins during axon growth and maintenance. *Neural Dev*. 8:17-27.

Prokop, A., R. Beaven, Y. Qu, and N. Sanchez-Soriano. 2013. Using fly genetics to dissect the cytoskeletal machinery of neurons during axonal growth and maintenance. *J Cell Sci*. 126:2331-2341.

Prokop, A., B. Kuppers-Munther, and N. Sanchez-Soriano. 2012. Using primary neuron cultures of Drosophila to analyze neuronal circuit formation and function. *In* The making and un-making of neuronal circuits in Drosophila. Springer. 225-247.

Rauch, P., P. Heine, B. Goettgens, and J.A. Kas. 2013. Forces from the rear: deformed microtubules in neuronal growth cones influence retrograde flow and advancement. *New Journal of Physics*. 15:015007.

Reichardt, L.F., and A. Prokop. 2011. Introduction: the role of extracellular matrix in nervous system development and maintenance. *Dev Neurobiol*. 71:883-888.

Reinsch, S.S., T.J. Mitchison, and M. Kirschner. 1991. Microtubule polymer assembly and transport during axonal elongation. *The Journal of cell biology*. 115:365-379.

Sabry, J., T.P. O'Connor, and M.W. Kirschner. 1995. Axonal transport of tubulin in Ti1 pioneer neurons in situ. *Neuron*. 14:1247-1256.

Salvaterra, P.M., N. Bournias-Vardiabasis, T. Nair, G. Hou, and C. Lieu. 1987. In vitro neuronal differentiation of Drosophila embryo cells. *J Neurosci*. 7:10-22.

Sanchez-Soriano, N., C. Goncalves-Pimentel, R. Beaven, U. Haessler, L. Ofner-Ziegenfuss, C. Ballestrem, and A. Prokop. 2010. Drosophila growth cones: a genetically tractable platform for the analysis of axonal growth dynamics. *Developmental neurobiology*. 70:58-71.

Sanchez-Soriano, N., G. Tear, P. Whitington, and A. Prokop. 2007. Drosophila as a genetic and cellular model for studies on axonal growth. *Neural Develop*. 2:9.

Schaefer, A.W., N. Kabir, and P. Forscher. 2002. Filopodia and actin arcs guide the assembly and transport of two populations of microtubules with unique dynamic parameters in neuronal growth cones. *The Journal of cell biology*. 158:139-152.

Schaefer, A.W., V.T. Schoonderwoert, L. Ji, N. Mederios, G. Danuser, and P. Forscher. 2008. Coordination of actin filament and microtubule dynamics during neurite outgrowth. *Developmental cell*. 15:146-162.

Sepp, K.J., P. Hong, S.B. Lizarraga, J.S. Liu, L.A. Mejia, C.A. Walsh, and N. Perrimon. 2008. Identification of neural outgrowth genes using genome-wide RNAi. *PLoS Genet*. 4:e1000111.

Shtengel, G., J.A. Galbraith, C.G. Galbraith, J. Lippincott-Schwartz, J.M. Gillette, S. Manley, R. Sougrat, C.M. Waterman, P. Kanchanawong, M.W. Davidson, R.D. Fetter, and H.F. Hess. 2009. Interferometric fluorescent super-resolution microscopy resolves 3D cellular ultrastructure. *Proc Natl Acad Sci U S A*. 106:3125-3130.

Sicaeros, B., and D.K. O'Dowd. 2007. Preparation of neuronal cultures from midgastrula stage Drosophila embryos. *J Vis Exp*:226.

Stiess, M., and F. Bradke. 2011. Neuronal polarization: the cytoskeleton leads the way. *Developmental neurobiology*. 71:430-444.

Suter, D.M. 2011. Functions of Myosin Motor Proteins in the Nervous System. *In* Neurobiology of Actin. Springer. 45-72.

Suter, D.M., and K.E. Miller. 2011. The emerging role of forces in axonal elongation. *Progress in neurobiology*. 94:91-101.

Svitkina, T.M., A.B. Verkhovsky, K.M. McQuade, and G.G. Borisy. 1997. Analysis of the actin-myosin II system in fish epidermal keratocytes: mechanism of cell body translocation. *The Journal of cell biology*. 139:397-415.

Takagi, Y., M. Nomizu, D. Gullberg, A.J. MacKrell, D.R. Keene, Y. Yamada, and J.H. Fessler. 1996. Conserved neuron promoting activity in Drosophila and vertebrate laminin alpha1. *J Biol Chem*. 271:18074-18081.

Takagi, Y., K. Ui-Tei, T. Miyake, and S. Hirohashi. 1998. Laminin-dependent integrin clustering with tyrosine-phosphorylated molecules in a Drosophila neuronal cell line. *Neurosci Lett*. 244:149-152.

Takeda, S., T. Funakoshi, and N. Hirokawa. 1995. Tubulin dynamics in neuronal axons of living zebrafish embryos. *Neuron*. 14:1257-1264.

Tanaka, E., T. Ho, and M.W. Kirschner. 1995. The role of microtubule dynamics in growth cone motility and axonal growth. *The Journal of cell biology*. 128:139-155.

Vallee, R.B., G.E. Seale, and J.W. Tsai. 2009. Emerging roles for myosin II and cytoplasmic dynein in migrating neurons and growth cones. *Trends Cell Biol*. 19:347-355.

Van Vactor, D., H. Sink, D. Fambrough, R. Tsoo, and C.S. Goodman. 1993. Genes that control neuromuscular specificity in Drosophila. *Cell*. 73:1137-1153.

Wagner, O.I., J. Lifshitz, P.A. Janmey, M. Linden, T.K. McIntosh, and J.F. Leterrier. 2003. Mechanisms of mitochondria-neurofilament interactions. *J Neurosci*. 23:9046-9058.

Walter, M.F., and H. Biessmann. 1984. Intermediate-sized filaments in Drosophila tissue culture cells. *J Cell Biol*. 99:1468-1477.

Wu, C.F., N. Suzuki, and M.M. Poo. 1983. Dissociated neurons from normal and mutant Drosophila larval central nervous system in cell culture. *J Neurosci*. 3:1888-1899.

Xu, K., G. Zhong, and X. Zhuang. 2013. Actin, spectrin, and associated proteins form a periodic cytoskeletal structure in axons. *Science (New York, N.Y.* 339:452-456.

Zhou, F.Q., C.M. Waterman-Storer, and C.S. Cohan. 2002. Focal loss of actin bundles causes microtubule redistribution and growth cone turning. *The Journal of cell biology*. 157:839-849.

CHAPTER 3:

A Tug of War Between Growth Cone and Axonal Myosin II Controls Neuronal Growth

Douglas H. Roossien, Phillip Lamoureux, Erica A. Melkonian, Matthew O'Toole, & Kyle E. Miller

This chapter is currently under review at PLOS One. As such this, this may not represent final published form.

Contributions: DHR performed experiments and analyzed data in Fig. 3.2 and Fig. 3.4. PL performed experiments and analyzed data in Fig. 3.1 and 3.3. EAM assisted with experiments in Fig. 3.2. MO performed mathematical modeling and analysis. KEM developed model presented in Fig. 3.5 and wrote manuscript together with DHR.

3.1 Abstract

While current therapies to promote neuronal regeneration are largely ineffective, disruption of non-muscle myosin II (NMII) is emerging as an exciting approach because it can dramatically increase the rate of axonal elongation. Although the mechanics of NMII in the growth cone have been characterized in terms of driving retrograde actin flow and the generation of traction forces required for growth cone motility, a clear explanation of how NMII disruption leads to an increase in elongation remains elusive. To understand the mechanistic basis of this effect we combined tracking of the *en masse* movement of the cytoskeletal meshwork along the axon (using docked mitochondria as fiduciary markers) with biophysical analysis and pharmacological NMII disruption in chick sensory neurons and genetic mutations in primary *Drosophila* neurons. We found that under conditions where disruption of NMII increases elongation that axons are under tension and strong contractile forces are generated in the growth cone that pull the cytoskeletal meshwork forward. Disruption of NMII at the growth cone using focal application of blebbistatin induces growth cone retraction, while global disruption of NMII increases elongation by reducing the apparent viscosity of the axon and the strength of adhesions to the substrate. Based on these observations we develop a model of elongation that incorporates the push and pull of microtubules and actin in both the growth cone and along the axon. In the context of this model, inhibition of NMII increases elongation because it makes the axon easier to stretch and allows unknown force generating mechanisms to move the growth cone forward *en masse* more rapidly. These findings are important for understanding the mechanical process of growth cone motility and will be helpful for developing rational approaches to promote axonal regeneration following spinal cord injury, stroke, neuronal degeneration and trauma.

3.2 Introduction

Disruption of Non-muscle Myosin II (NMII) dramatically increases the rate of axonal elongation of neurons grown on substrates such as chondroitin sulfate proteoglycans (Hur et al., 2011; Yu et al., 2012), polyamines (Ketschek et al., 2007; Turney and Bridgman, 2005) and low concentrations of laminin (Hur et al., 2011). Understanding the mechanism underlying this response is important because current therapies to promote functional neuronal regeneration are largely ineffective (Lu et al., 2012). Growth cone advance occurs by a multi-step process that involves protrusion of the actin cytoskeleton (Lowery and Van Vactor, 2009) at the leading edge of the peripheral domain (P-domain) paired with forward advance of microtubules. While a series of studies once suggested long microtubules embedded in the cytoskeletal meshwork are stationary along the axon and elongation occurs via microtubule assembly at the growth cone (Bamburg et al., 1986; Bray, 1970; Liu et al., 2010; Miller and Joshi, 1996; Okabe and Hirokawa, 1990), recent work indicates that in addition to assembly microtubules move forward *en masse* in the growth cone and along the distal section of the axon (Lee and Suter, 2008; Schaefer et al., 2008; Suter and Miller, 2011). Paired with the bulk forward advance of the growth cone, axons stretch and new material is added along the axon to prevent it from thinning (Lamoureux et al., 2010; Miller and Sheetz, 2006; O'Toole et al., 2008; Suter and Miller, 2011). NMII is among the most active force-generating molecular motors in neurons. When it is disrupted, peak traction stresses generated by growth cones drop by as much as 80% (Bridgman et al., 2001; Koch et al., 2012) and retrograde actin flow in the P-domain slows by at least 50% (Lin et al., 1996; Medeiros et al., 2006). Because NMII is a dominant cellular motor, it is a natural candidate for modulating the *en masse* movement of cytoskeletal components that occur during axonal stretching and elongation. In an early model of growth cone mechanics, called the

substrate coupling hypothesis (Suter et al., 1998), it was proposed that a mechanical continuum exists between the substrate and the C-domain. This mechanical linkage allows contractile forces in the growth cone to be applied to extracellular substrates. If the substrate is stationary, tension builds in this linkage and the C-domain will tend to be pulled forward. In terms of the role of NMII, it was suggested that actomyosin contractility localized to the T-zone may provide the motive force for both retrograde flow and cell translocation. Nonetheless, it was not clear if actomyosin in the growth cone primarily promoted or acted as a barrier to microtubule advance.

In addition, an alternative model was proposed where coupling between actin and the substrate slows retrograde actin flow and allows actin-recycling to clear F-actin away from distal microtubule ends. This would relieve restraints on microtubule advance associated with retrograde F-actin flow. This model is appealing based on the observations that retrograde actin flow sweeps back microtubules that enter into the P-domain (Schaefer et al., 2002) and depolymerization of actin (Forscher and Smith, 1988) and disruption of NMII (Ketschek et al., 2007; Myers et al., 2006) both lead to a forward advance of microtubules into the P-domain. In the first of these two models disruption of NMII would decrease the advance of the C-domain by reducing the forward pulling force of the growth cone. In support of this, disruption of NMII, either by knockout of NMIIB (Bridgman et al., 2001; Tullio et al., 2001; Turney and Bridgman, 2005) or blebbistatin (Ketschek et al., 2007), decreases the rate of growth cone advance when neurons are grown on high concentrations of laminin. In terms of the second model, disruption of NMII would increase elongation because it reduces retrograde actin flow. This has been used to explain why disruption of NMII increases growth on low concentrations of laminin (Hur et al., 2011), poly-ornithine (PO) (Ketschek et al., 2007; Turney and Bridgman, 2005; Yu et al., 2012),

and non-permissive substrates such as chondroitin sulfate proteoglycans (Hur et al., 2011; Yu et al., 2012).

Nonetheless, these are diametric models for the role of NMII in the growth cone (Roossien et al., 2013). In the first, NMII generates force that pulls microtubules forward and promotes elongation. In the second, NMII generates force that pushes microtubules back and inhibits growth. Here we tested these models by combining biophysical analysis and pharmacological NMII disruption in chick sensory neurons and genetic mutations in primary *Drosophila* neurons. Looking specifically at growth on substrate conditions where disruption of NMII increases growth, we found that net NMII activity in the growth cone promotes elongation and that disruption of NMII increases elongation because it decreases the apparent viscosity of the axon and the strength of axonal adhesions to the substrate. As a result of these changes, unknown force generating mechanisms are able to more rapidly pull the axonal cytoskeletal meshwork forward. Acknowledging the importance of the forward push associated with microtubule assembly and the rearward push of retrograde actin flow, we develop a biophysical model of axonal elongation that incorporates these forces along with contractile force generation by NMII in the growth cone and along the axon. Our findings are consistent with NMII activity acting as a dynamic barrier to growth, but indicates that this occurs because it is important for the generation of both active and passive forces along the axon that impede elongation.

3.3 Materials and methods

3.3.1 Cell culture.

Chick sensory neurons were isolated from embryonic day 10-11 embryos obtained from the Michigan State University Poultry Farm. Dorsal root ganglia were removed from the spinal cord and placed in L-15 medium pH 7.1 made from powder (Life Technologies, Item # 41300039; Grand Island, NY, USA). After excess tissue was removed with forceps, the ganglia were placed in 0.25% trypsin for 8-10 min at 37°C and allowed to settle to the bottom of tube. The trypsin solution was then removed, replaced with supplemented L-15 and triturated slowly until the tissue had dispersed into a homogenous solution. This was then dripped into substrate coated culture dishes containing supplemented L-15 media. L-15 is supplemented with 0.6% glucose, 1 mM glutamine, 100 U/ml penicillin, 136 μg/ml streptomycin sulfate, 10% fetal calf serum, 50 ng/ml 7S nerve growth factor (Harlan Bioproducts, Indianapolis, IN) and N9 growth supplement (Lamoureux et al., 2010). Neurons were grown on three different substrates. For poly-ornithine (PO) treated dishes (35 mm cell culture dishes, Corning # 430165; Tewksbury, MA, USA), the culture surface was treated with 0.01% poly-L-ornithine for 1 h then rinsed three times with sterile dH_2O. High laminin (HiLn) dishes were coated with 25 μg/ml laminin (that had been thawed on ice) and incubated at 37°C overnight. Combined PO and low laminin (LoLnPO) dishes were coated with 0.01% PO solution for 1 h at RT, rinsed 3x with sterile dH_2O and incubated with 250 ng/ml laminin at 37°C for 1 h. For both HiLn and LoLnPO conditions, cells were plated into the dish without the removal of the laminin. Cells were grown and imaged at 37°C in supplemented L-15 medium. Unless otherwise noted, reagents were purchased from Sigma (St. Louis, MO, USA).

3.3.2 Tension assays.

Micropipettes were calibrated for their bending spring constant and dipped in 0.01% PO for 30 min, followed by 30 min in concanavalin A (1 mg/ml). Growth cones were allowed to adhere to the substrate-coated pipet and then the growth cone was raised above the surface of the culture dish. After allowing 30 to 50 min for force equilibration, the deflection of the micropipette was used to calculate neuronal force generation. For a detailed description of this method see (Lamoureux et al., 2011).

3.3.3 Mitochondrial labeling, imaging and motion analysis in chick sensory neurons.

Mitochondria in chick sensory neurons were labeled with 0.1 μM MitoTracker Red CMXRos (Invitrogen, Carlsbad, CA), incubated for 2 min, and recovered in fresh L-15 for 2 h (Lamoureux et al., 2010). Cultures were maintained in a ringcubator to warm the dish at 37°C on the stage of a Leica DM IRB inverted microscope and observed with an N Plan L 40x/0.55 corrPh2 with an adjustable collar infinity/0-2/c objective. Cells were illuminated with a 100 W Xenon lamp attenuated 98% with neutral density filters through a Texas Red 49008 ET cube (Chroma, Rockingham, VT) for visualization of Mito-Tracker. On the Leica DM IRB transmitted light exposure was controlled with a VMM-D3 controller and CS25 shutter (Vincent Associates; Rochester, NY, USA). Fluorescent light exposure was controlled with a Lambda 10-C (Sutter Instruments). Micro-manager (US National Institutes of Health) software (Edelstein et al., 2010) was used to control the shutters and camera (Orca-ER digital camera CCD, model #CA742-95, Hamamatsu; Hamamatsu, Japan). Exposure times were set between 100 to 200 msec. Docked mitochondrial velocities were measured by change in position over 10 min

intervals on the kymographs and plotted against their initial position along the axon in relation to the growth cone using ImageJ (US National Institutes of Health).

3.3.4 Blebbistatin treatments.

For all experiments, (-)-blebbistatin was initially made as a 50 mM stock in DMSO. Prior to global bath application it was pre-warmed and diluted 330 fold in L-15, this was sonicated for 1 min, and then further incubated for at least 1 h at 37°C. This was then added to the culture dish at a 1:3 dilution to make a final concentration of 50 μM blebbistatin. For focal application, 50 mM stock blebbistatin was diluted to100 μM in PBS containing either 0.1 μg/ml FITC-dextran (148 kDa) (Sigma, St. Louis, MO) or 1 mg/ml TexasRed-dextran (10 kDa) (Invitrogen, Carlsbad, CA), sonicated for 10 min, incubated for 30 min at 37°C, passed through a 0.22 μm PVDF syringe filter (Millipore, Billerica, MA), then stored at 37°C until use. Solutions were back loaded into TW100F-4 glass micropipettes (World Precision Instruments, Sarasota, FL). Micropipettes were pulled on a Sutter Instruments P-97 Flaming / Brown micropipette puller using the following settings: Heat = 484, Pull = 60, Vel. = 60, Time = 250. To maximize focal application at the growth cone, the micropipette tips were positioned within 10 μm of the growth cone within a flow chamber that had a flow rate of approximately 0.5 ml/min and a volume of 10 ml. This resulted in drug application that was highest at the growth cone and tapered away over the adjoining 20 to 30 μm of the axon. Pressure was manually applied to the micropipette using a 10 ml syringe connected through Tygon tubing. Manual pressure, in combination with monitoring the fluid as it comes out of the pipette by fluorescence, was used instead of a Picospritzer because it allows for tighter control of fluid flow out of the pipette. Phase images were captured every 10 s, and fluorescent images were captured every 1 min using 100 ms

exposures. A FITC cube 41001 (Chroma, Rockingham, VT) was used to image FITC-dextran and a Texas Red 49008 ET cube (Chroma, Rockingham, VT) was used to image TexasRed-dextran. Change in growth cone position was measured by tracking the position of the widest aspect of the C-domain at 1 min intervals over 20 min and calling initial position 0.

3.3.5 Mathematical model and determination of parameters.

Mechanically there are two simple ways an axon can stretch (O'Toole et al., 2008): like a solid where the application of a constant force results in a length that is constant over time (i.e. the spring equation; $F = k$ x that relates force, the spring constant, and distance) or as a fluid where application of constant force results in a length that increases at constant rate over time (i.e. the viscosity equation; $F = \gamma v$ that relates force, the viscosity coefficient and velocity) (Howard, 2001). Because chick sensory neurons lengthen at a constant rate when under the influence of a constant force over long periods of time, they behave like viscous fluids (O'Toole et al., 2008). At a molecular level, viscosity arises because spring-like cross-links cyclically attach and detach with characteristic K_{on} and K_{off} rates (Howard, 2001). Over periods of time shorter than K_{off}, cross-links do not have time to detach and fluids behave like solids. Over longer time periods, the disassociation of cross-links releases energy and thus when a force is applied over a long period of time an object deforms at a constant rate. For an excellent description of the molecular basis of viscosity see (Howard, 2001). Adhesions are conceptually similar to viscosity, differing primarily in that the cross-links are between the object and some external structure. Thus when an object slides across a surface as cross-links form and break energy is dissipated and a constant force results in a constant velocity. Disruption of NMII could increase axonal stretching because it disrupts NMII based cross-links between actin filaments in

the axon, it reduces contractile forces within the axon that opposes stretching, or because it reduces the strength of attachment of the axon to the substrate. To quantify the effects of NMII on axonal viscosity and cell-substrate adhesion, we applied our previously developed mathematical model that describes the velocity profile of bulk movement of the axonal cytoskeletal framework as a function of growth cone force F_0, viscosity G, and friction due to cell-substrate adhesions η (O'Toole et al., 2008). The function that models the velocity along the axon is

$$v[x, L(t)] = \frac{F_0 \sinh(x\sqrt{\eta/G})}{\sqrt{\eta G}\cosh(L(t)\sqrt{\eta/G})} \quad \text{Eq. 1}$$

In each case (before and after the addition of blebbistatin) the force generated by the growth cone F_0 and the length $L(t)$ were measured. The Nonlinear Curve Fit option, which uses an iterative least squares algorithm, in the software package Origin was then used to find values for G and η that best fit the velocity data for docked mitochondria along the axon. In Eq. 1 G is in units of (g μm h^{-1}). To convert this into the most commonly used units for viscosity, G is divided by the cross-sectional area of the axon to give intrinsic viscosity (g) in units of Pa sec. For the conversion of G to g in this manuscript, we used our measurements of axonal diameter from (O'Toole et al., 2008). Viscosity is also discussed in units of μdynes h / μm where it is denoted as γ. G, g and γ are related as follows (A, axonal cross-sectional area; L, axon length):

$$g = \frac{G}{A} = \gamma\frac{L}{A} \quad \text{Eq. 2}$$

3.3.6 Fly stocks.

For disruption of NMII, $Zip^1/CyO_{TWI\text{-}GFP}$ flies (Franke et al., 2010; Halfon et al., 2002) were crossed with $Df(3L)BSC608/CyO_{TWI\text{-}GFP}$ flies to produce embryos used for screening and

neuronal cultures. The *Df(3L)BSC608* allele is denoted throughout the text as Zip^{Df}. w^{1118}*;+/+;+/+* were used as the wild-type stock. All *Drosophila* stocks were obtained from the Bloomington Stock Collection.

Drosophila neurons were grown at 25°C and imaged at room temperature in supplemented L-15 medium as described for the chick sensory neurons, except NGF was not added to the media. Note *Drosophila* neuronal outgrowth is more reliable using the powdered version of L-15 rather than premade liquid L-15. The culture surface (35 mm cell culture dishes, Corning # 430165; Tewksbury, MA, USA) was treated with 5 μg/ml *Drosophila* Extracellular Matrix Proteins (DECM) (Roossien et al., 2013) for 1 h and rinsed with dH_2O. The isolation of DECM is described in detail in (Roossien et al., 2013). In brief, DECM was isolated from the *Drosophila* Kc167 cell line (*Drosophila* Genomics Resource Center). Cells were grown at log phase in HyClone SFX Insect media (Thermo Scientific; Waltham, MA, USA). After 4 d, conditioned media rich in DECM was collected and centrifuged at 500 g for 10 min. Media was decanted and stored at -70°C until further processing. Conditioned media (1.7 L) was processed through Millipore (Billerica, MA, USA) Centricon Plus-70 100kDa Ultracel-PL membrane filter devices at 3000 g down to a final volume of 50 ml (34 x concentration) and stored at -70°C. Dishes were used immediately following coating with DECM. To harvest NMII null neurons, $Zip^{1}/CyO_{TWI\text{-}GFP}$ x $Df(2R)BSC608/CyO_{TWI\text{-}GFP}$ fly crosses were used to generate embryos (denoted in text as Zip^{1}/Zip^{Df}). At developmental stage 10 (8 h after egg lay) and later, GFP from the $CyO_{TWI\text{-}GFP}$ balancer was expressed at levels that could be visualized (Halfon et al., 2002) and non-fluorescent Zip^{1}/Zip^{Df} embryos were used to isolate neurons as described (Roossien et al., 2013; Sicaeros and O'Dowd, 2007). The neurons were stored in a tube containing 6 μl supplemented L-15 / embryo at 18°C for 3 d prior to plating to reduce the level of maternally

loaded NMII protein (Prokop et al., 2012; Sanchez-Soriano et al., 2010). For NMII mutant neurons, MitoTracker Red CMX-Ros was added directly to the neurons in the storage tube such that the final concentration in the culture dish after plating was 0.01 μM and incubated for 1 hr at 25°C prior to plating. Imaging conditions and mitochondrial measurements were the same as for chick sensory neurons.

3.3.7 Immunocytochemistry.

Drosophila neurons were grown for 24 h on # 1 glass coverslips (Corning 2865-22; Tewksbury, MA, USA) coated with DECM as described above, then fixed with 4% formaldehyde / 3% sucrose / 50 mM EGTA for 20 min at RT. Staining for NMII was performed with antisera against *Drosophila* NMII (Kiehart and Feghali, 1986), a kind gift from Daniel Kiehart, at a 1:500 dilution and visualized with goat anti-rabbit Alexa 488 secondary antibody (Invitrogen A-11008; Carlsbad, CA, USA). Neuronal plasma membranes were stained with an antibody against HRP conjugated to Texas Red (Jackson Immunoresearch Labs; West Grove, PA), which interacts with glycoproteins found on *Drosophila* neurons (Jan and Jan, 1982; Snow et al., 1987). Fixed coverslips were mounted using Vectashield (Vector Laboratories, Burlingame, CA) onto glass slides, then placed directly on a 60x oil immersion objective (NA 1.4) of the Nikon swept field confocal microscope (on a TE2000 platform). Image stacks were acquired with 12 slices at 1.0 μm spacing and 1 s exposure times. The laser was set to 10% power (set in the NIS software) for the 488 nm line of 200 mW Argon laser (Melles Griot, Carlsbad, CA, USA) and 100% power for the 561 nm line of a 50 mW DPSS laser (Cobalt, Stockholm, Sweden). ImageJ was used to Z-project the image stacks using the maximum intensity setting for each neuron. NMII staining intensity was measured by plotting pixel

intensities using the Plot Profile command in ImageJ across 40 pixel lines in both cell bodies and axons and comparing the average intensities between the two genotypes.

3.4 Results

Previous studies have reported varying effects of NMII disruption on axonal elongation based upon the growth substrate. When neurons are grown on high concentrations of laminin NMII disruption decreases elongation (Bridgman et al., 2001; Ketschek et al., 2007; Tullio et al., 2001; Turney and Bridgman, 2005), yet on polyamines or low concentrations of laminin it increases elongation (Hur et al., 2011; Ketschek et al., 2007; Turney and Bridgman, 2005; Yu et al., 2012). To confirm the substrate dependent effect of NMII disruption, we plated chick sensory neurons in plastic tissue culture dishes treated with 3 different substrates: 0.01% poly-ornithine incubated for 1 h (PO); 0.01% poly-ornithine incubated for 1 h and then 0.25 μg/ml laminin for 1h (LoLnPO); and 25 μg/ml laminin incubated overnight (HiLn) (Fig. 3.1A). Blebbistatin was added to the dishes at 50 μM 2 hrs after plating. We then waited 24 h and measured axonal length. As previously reported, disruption of NMII with blebbistatin led to a dramatic increase in axonal length when neurons were grown on either PO or LoLnPO (Hur et al., 2011; Ketschek et al., 2007; Yu et al., 2012), but significantly decreased length when neurons were grown on HiLn (Ketschek et al., 2007). Of these findings, the observation that disruption of NMII increases axonal elongation is most exciting because of its therapeutic potential to augment axonal regeneration.

One proposal for a mechanistic explanation of this effect is that inhibition of NMII releases microtubules from a compressed state and thus allows microtubule extension toward the leading edge (Hur et al., 2011). In terms of mechanics, for microtubules to push forward they must push material towards the cell body backwards (Fig. 3.1B). Likewise, for actin to push microtubules back it must push the leading edge of the cell forward (Fig. 3.1B). This implies the axon as a whole is under compression and it follows that axons lengthen by pushing forward, a

prediction consistent with the model of NMII forces impeding the forward push of microtubules. While many prior studies have indicated that neurons are under tension as the result of pulling forces generated in the growth cone, the net forces generated by neurons have never been explicitly measured under conditions where disruption of NMII increases elongation. To test this, we attached the growth cones of chick sensory neurons plated on LoLnPO to force-calibrated towing needles. We then lifted the distal section of the axon (i.e. the last 50 to 100 μm) off of the substrate, while measuring the direction and magnitude of force generation by monitoring the bending of the needle (Fig. 3.1C) (Lamoureux et al., 2011). Before taking force measurements, we waited for at least 30 minutes to allow the system to come to a steady state force balance. At this point the force generated by the neuron is equal to the force on the towing needle, while the position of the growth cone and the force generated by the neuron is constant over time. At steady state, we found growth cones pulled the towing needle towards the cell body with an average force of 132 +/- 30 μdynes (ave +/- 95% CI, n = 20 neurons). To account for our observation that neurons are under tension, contractile forces must be generated either in the growth cone, along the axon, or in both locations. As a means to assess the primary site of contractile force generation in neurons, we tracked the motion of docked mitochondria (Fig. 3.1D-E) that are stably associated with microtubules, actin filaments and neurofilaments (Roossien et al., 2013; Saxton and Hollenbeck, 2012) and thus serve as a fiduciary marker for their bulk movement (Lamoureux et al., 2010; Morris and Hollenbeck, 1993; Roossien et al., 2013). We hypothesized that if the growth cone was the primary site of tension generation in the neuron, material along the axon would move towards the growth cone. For control neurons, we monitored the docked mitochondrial velocity profiles over 10 min periods for 20 neurons that were at steady state tension and in total tracked the movement of 462 mitochondria. The

velocities of mitochondria were then binned at 20 μm intervals versus distance from the growth cone with the number of mitochondria tracked in each bin shown in the figure panel (Fig. 3.1G). We found that docked mitochondria move forward along the length of the axon, with velocity increasing closer to the growth cone while mitochondria in the growth cone are stationary. This pattern is consistent with contractile force generation in the growth cone that pulls material along the axon forward and thus stretches the axon. While these experiments demonstrate that control growth cones pull, they leave open the possibility that when NMII is disrupted neurons switch to growth by microtubules pushing forward. Support for such a mechanism is indicated by the observation that when actin is depolymerized and microtubules are stabilized with taxol, growth cones elongate by pushing forward (Letourneau et al., 1987). To test this, we repeated our force analysis in the presence of blebbistatin (50 μM) (Fig. 3.1H-J). We found tension decreased significantly to 62 +/- 12 μdyne (ave +/- 95% CI, n = 32 neurons; $p < 0.0001$ vs. control data from above), but the axons remained under tension. Furthermore, docked mitochondria along the axon (n = 32 axons and 575 mitochondria) continued to advance in the same pattern as the controls (Fig. 3.1E, I). This indicates that when NMII is disrupted contractile forces continue to be generated in the growth cone by unknown motors. These experiments demonstrate that when neurons are grown under conditions where disruption of NMII dramatically increases axonal elongation, they are under tension and strong contractile forces are generated in the growth cone that pull material along the length of the axon forward.

These biophysical experiments in no way exclude the possibility that microtubules push forward and NMII acts as a barrier to their advance. Nonetheless, they indicate the net forces in the growth cone are contractile and pull material along the axon forward. To directly test if NMII in the growth cone promotes or prohibits elongation, we focally applied blebbistatin to the

growth cone of neurons grown on PO. Here, 100 μM blebbistatin was mixed with either 0.1 μg/ml FITC-dextran or 1.0 mg/ml TexasRed-dextran to visualize the fluid and backloaded into micropipettes. Because these experiments were conducted in a flow chamber, drug application was highest at the growth cone and decreased rapidly over the last 20 μm of the axon as visualized with fluorescent tracers. As a control, DMSO was applied directly to the growth cone with either FITC-dextran or TexasRed-dextran. We found no significant difference in the rate of growth cone advance between the two dyes in these controls, so the data were pooled (Table 3.1). On average, control growth cones advanced at a rate of 15.5 +/- 8.9 μm/hr (n = 16) (Table 3.1; Fig. 3.2A; Fig. 3.2C, red lines). On the contrary, when blebbistatin was focally applied to the growth cones they retracted at an average rate of -13.1 +/- 6.1 μm/hr (n = 21), significantly lower than DMSO controls ($p < 0.01$) (Table 3.1; Fig. 3.2B; Fig. 3.2C, blue lines). The graph in Fig. 3.2C shows growth cones to retract when treated with blebbistatin. Combined with the biophysical analysis above these experiments indicate that NMII activity in the growth cone is not a barrier to elongation.

While the biophysical analysis (Fig. 3.1) and focal application experiments (Fig. 3.2) suggest NMII in the growth cone promotes axonal elongation, they do not explain why global disruption of NMII increases elongation. Because NMII is present along the axon (Rochlin et al., 1995) and growth cone advance is paired with axonal stretching (Suter and Miller, 2011), this suggested to us that NMII may restrain growth cone advance by opposing axonal stretching. To test this, we measured the rate of axonal stretching (in mathematical terms the derivative of velocity versus distance) by tracking docked mitochondria along the length of the axon of freely growing neurons cultured on PO in the presence and absence of bath-applied blebbistatin (Fig. 3.3). Before disruption of NMII we found docked mitochondria advanced in a non-linear

velocity gradient that rose along the axon as distance from the growth cone decreased (Fig. 3.3C, red lines; Fig. 3.3D, Pre-blebbistatin) (Miller and Sheetz, 2006). In response to global disruption of NMII using bath-applied 50 μM blebbistatin, we found the velocity profile shifted in two ways. First we found the rate of advance of docked mitochondria in the last 5 μm of the axon (which we defined as the growth cone) moved forward significantly more rapidly than in the controls (i.e. 33.4 +/- 5 μm/h vs. 22.4 +/- 4.3; ave +/- 95% CI, $n = 22$; $p < 0.05$). In addition, we found that along the length of the axon the velocity of forward translocation decreased significantly following blebbistatin addition (Fig. 3.3C, blue lines; Fig. 3.3D). Examining the red and blue curve fits in Fig. 3.3D shows that following blebbistatin, the steepness of the velocity curve along the axon increases. The increased rate of change in velocity over distance is analogous to an increased rate of axonal stretching. To provide a more intuitive illustration of axonal stretching, we calculated the difference in the velocity of forward advance between adjacent regions of the axon (Fig. 3.3E, error bars are the 95% CI). We found that in the first 25 μm of the axon it stretched at 8 μm/h before versus 16 μm/h after blebbistatin addition. This indicates that global disruption of NMII increases axonal elongation by increasing axonal stretching.

To more systematically analyze axonal stretching and axonal adhesion strength, we used our previously developed equation (O'Toole et al., 2008) that describes the relationship between forces, axonal stretching, viscosity, and substrate adhesion. For a brief explanation of this model and the molecular basis of viscosity (as well as a comparison of the various viscosity calculations) see the methods section. Because the data shown in Fig. 3.3 were collected from neurons grown on PO, as part of this analysis we repeated our axonal rest tension measurements on neurons grown on PO. In the controls, we found growth cones pulled the towing needle

towards the cell body with an average force of 79.4 +/- 22.5 μdyne (ave +/- 95% CI, n = 8). In the presence of blebbistatin, we found tension decreased significantly to 23.7 +/- 8.2 μdyne (ave +/- 95% CI, n = 8; $p < 0.01$) and again the force vectors generated by the neuron did not switch the direction. Inputting these forces, the length of the axon, and the velocity profiles along the axon from Fig. 3.3D into Eq. 1, we let the variables for apparent viscosity (g) and substrate attachment strength (η) vary using the Nonlinear Curve Fit option in Origin (O'Toole et al., 2008). We found g to be 2.3 x 10^6 Pa sec and 0.28 x 10^6 Pa sec and η to be 8700 Pa s and 2700 Pa s before and after blebbistatin addition respectively (red and blue lines in Fig 3.3D). These results indicate that disruption of NMII dramatically decreases both the apparent axonal viscosity and the strength of adhesions along the axon. As a second means to measure the effect of NMII on axonal viscosity, we also include a simple 'back of the envelope' calculation. Keeping in mind the viscosity equation is $F = \gamma v$ (γ, viscosity; v, velocity) (Howard, 2001), a direct way to estimate viscosity is to divide the force acting on the axon by the rate it stretches. In the control neurons grown on PO, we find the rest tension is 79 μdynes and over the last 25 μm of the axon it stretches at 8 μm/hr. This yields a value of γ = 9.8 μdynes h / μm. For the blebbistatin treated neurons the rest tension is 24 μdyne and the rate of stretching over the same region is 16 μm / hr, thus γ is 1.5 μdynes h / μm. To convert this into intrinsic apparent viscosity (g) in units of Pa sec, one multiplies γ by the length of the stretched region and then divides by cross-sectional area (Eq. 2). From above, the length of the region is 25 μm and the average cross sectional area of the last 25 μm of chick sensory neurons is ~ 3.14 μm^2 (O'Toole et al., 2008). While we do observe visible thinning of the axon following treatment with blebbistatin (compare the 2 h and 3 h phase images in Fig. 3.3A), we use the initial diameter of the axon for this calculation with the reasoning that blebbistatin changes the intrinsic viscosity of the axon, which then leads to

thinning. Using these values gives an intrinsic viscosity of 2.9 x 10^6 Pa sec for the controls and 0.5 x 10^6 Pa sec for the blebbistatin treated neurons. We note that this rough calculation is in close agreement with the results of 2.3 x 10^6 Pa sec and 0.28 x 10^6 Pa sec from the curve fitting above. Together this data indicates that disruption of NMII leads to an approximately 90% decrease in the apparent viscosity of the axon and a 70% drop in attachment strength to the substrate.

To control for the possibility that global blebbistatin addition has off-target effects; to verify that chronic disruption of NMII has the same effects as acute; and to determine if the role of NMII in axonal stretching is evolutionarily conserved, we examined the movement pattern of docked mitochondria in primary *Drosophila* neurons (Roossien et al., 2013). A motivation for conducting these experiments is that we recently reported that like chick sensory neurons, *Drosophila* neurons elongate by *en masse* forward translocation of the cytoskeletal meshwork and that this mechanism of elongation occurs *in vivo* (Roossien et al., 2013). For these experiments, we harvested neurons from *Drosophila* embryos with transheterozygous null mutations in *Zipper*, the *Drosophila* homolog of NMII (Young et al., 1993). After storing the neurons for 3 d in suspension to reduce maternally loaded protein (Prokop et al., 2012; Sanchez-Soriano et al., 2010), we were able to achieve a 48% reduction in NMII protein (Fig. 3.4A; $p < 0.01$). As seen in the chick neurons, the rate of mitochondria advance in the growth cone and distal 25 μm of the axon together increased significantly in Zip^1/Zip^{Df} axons (NMII null) from 25.8 +/- 4.7 (n = 131) to 58.1 +/- 9.7 (n = 43) μm/h (ave +/- 95% CI, $p < 0.05$) (Fig. 3.4B-C). Likewise, we found axonal tension in Zip^1/Zip^{Df} neurons to be approximately half of that in wild-type *Drosophila* neurons (6.16 +/- 0.78 μdyne (n = 27) vs. 12.6 +/- 1.6 μdyne (n = 36), respectively). Together this indicates that the elevated rate of elongation, increased bulk transport

and decrease in neuronal rest tension observed in chick sensory neurons are not off-target effects of blebbistatin nor transient in nature. This indicates that the function of NMII in the process of axonal elongation is broadly conserved between vertebrates and invertebrates.

3.5 Discussion

Understanding why disruption of NMII increases the rate of axonal elongation is important in terms of developing therapies that promote neuronal regeneration. One model to explain this effect (Hur et al., 2011) suggests NMII driven actin retrograde flow acts as dynamic barrier to the advance of microtubules. It is based on observations that microtubules are being simultaneously assembled in the growth cone while being transported rearwards by retrograde actin flow (Burnette et al., 2007), which suggests that microtubule-end position is determined by the sum of microtubule assembly and retrograde transport rates. It is appealing based on the observations that minutes after actin is disrupted using cytochalasin, microtubules surge forward into the P-domain (Forscher and Smith, 1988), disruption of NMII decreases retrograde flow by 50% (Medeiros et al., 2006) and this leads to an increase in the density of microtubules in the P-domain (Burnette et al., 2007; Ketschek et al., 2007). Here we have tested the biophysical aspects of this model. Contrary to the predictions of this model, our findings indicate NMII in the growth cone pulls the organelle rich C-domain of the growth cone forward, while NMII along the axon acts to inhibit axonal stretching. When NMII is disrupted the rate of axonal elongation increases because unknown force generating mechanisms generate contractile forces in the growth cone that are able to more easily pull the C-domain of the growth cone forward. Fully acknowledging the importance of the pushing forces associated with actin assembly and microtubule assembly, we propose below a biophysical model of axonal elongation that incorporates the forward push of microtubules in the C-domain of the growth cone, the forward push of actin assembly at the plasma membrane, NMII contractile force generation in the transition zone of the growth cone, NMII contractile force generation along the axon, and the

assembly and disassembly of adhesions in the growth cone that are important for traction force generation.

In terms of mechanics, the model where actin retrograde flow is a dynamic barrier to the forward advance of microtubules (Burnette et al., 2007; Hur et al., 2011) is predicated on the idea that the forward push of microtubules is opposed by the rearward push of retrograde flow. Since every force is balanced by an equal and opposite force, it follows that the forward push of microtubules (that could occur either through microtubule polymerization (Rauch et al., 2013) or motor driven sliding (Lu et al., 2013a)) is associated with a rearward push in the direction of the cell body. Likewise the rearward push of retrograde flow is paired with the forward push of actin at the leading edge (Pollard and Borisy, 2003) (Fig. 3.1B). This is illustrated schematically in Fig. 3.5A, where the push of microtubules (orange arrow), actin (magenta arrow) and membrane tension (Craig et al., 2012; Lieber et al., 2013; Raucher and Sheetz, 2000) (black arrows) are illustrated. In this model, if the force associated with retrograde flow is decreased (Fig. 3.5B, magenta arrow) the C-domain (vertical red line) would be expected to move forward at a higher rate. What is troublesome is summation of the force vectors in the axon and the growth cone indicates that the net forces (light blue arrow) generated by the neuron push forward (Fig. 3.5C), yet every prior analysis of growth cone traction forces (Betz et al., 2011; Bray, 1984; Brown and Bridgman, 2003; Chan and Odde, 2008; Koch et al., 2012; Lamoureux et al., 1989; O'Toole et al., 2008) and our work here (Fig. 3.1), indicates that growth cones normally pull the substrate rearwards even under conditions where disruption of NMII increases elongation. For the neuron as a whole to be under tension, strong contractile forces must be generated either in the growth cone, along the axon or in both locations. Thus based on our force / motion analysis (Fig. 3.1) to this model we first add strong contractile forces (green arrows) in the actin rich transition zone of

the growth cone that corresponds with the convergence zone in non-neuronal cells (Salmon et al., 2002) and couple these forces with an attachment point to the substrate that provides adhesive support for mechanical tension (grey dashpot) (Woo and Gomez, 2006) (Fig. 3.5D). Because of the geometry of the growth cone these contractile forces act in series with actin polymerization (magenta arrow) to respectively pull and push substrate linkages rearwards. While this model accounts for both the observed tension of the neuron and the forward advance of material along the axon (Fig. 3.1), it does not explain why local disruption of NMII via focal application of blebbistatin induces retraction of the C-domain (Fig. 3.2). Furthermore, it suggests that if NMII was disrupted neurons would switch from pulling to pushing forward, yet we find neurons remain under tension (Fig. 3.1). To accommodate these experimental observations we add moderate contractile forces along the axon (blue arrows) that are greater than the push associated with microtubules (Ahmad et al., 2000) (Fig. 3.5E). Taken together, this model accounts for the observations that neurons are under tension (Fig. 3.1) (Bray, 1979; Lamoureux et al., 1989; O'Toole et al., 2008), material along the axon moves towards the growth cone (Fig. 3.1, 3.3 and 3.4) (Miller and Sheetz, 2006; Reinsch et al., 1991), disruption of NMII force generation in the growth cone leads to retraction of the growth cone (Fig. 3.2) and that actin filament polymerization at the leading edge of the cell pushes the plasma membrane forward (Pollard and Borisy, 2003). In this model, disruption of NMII increases the rate of growth cone advance because it leads to a larger drop in the forces generated along the axon (blue arrow) than in the growth cone (green arrow) (Fig. 3.5F). To illustrate how the force arrows in Fig. 3.5F map onto the physical structure of the growth cone, we have color-coded the various regions (Fig. 3.5G). Note the symbol M stands for the aggregate activity of motors, not just NMII activity.

To illustrate how this static model translates into elongation, we propose a 3-step model where actin polymerization (magenta arrows) pushes substrate adhesions rearwards (grey dashpot) and the plasma membrane forward (Fig. 3.5I). Simultaneously new adhesions are formed towards the leading edge and are lost towards the rear of the growth cone as it moves forward (Fig. 3.5J) (Myers and Gomez, 2011; Santiago-Medina et al., 2013; Woo and Gomez, 2006). In parallel, contraction of the T-zone (green arrows) pulls rearwards on the substrate (grey dashpot) and forwards on microtubules (orange arrows) and actin (blue arrows) along the axon. This stretches the axon and the C-domain (red line) advances (Fig. 3.5K). In this model, actin retrograde flow in the P-domain can still act as a barrier to microtubule advance in the sense that when microtubules polymerize into the P-domain they are swept backwards (Burnette et al., 2007; Lin and Forscher, 1995; Schaefer et al., 2002; Zhou et al., 2002). Yet the net forces generated in the growth cone pull microtubules in the C-domain forward. While this may seem counterintuitive, in non-neuronal cells this is well accepted. There it is clear that even as microtubules move retrogradely in the P-domain, they move anterogradely in the cell body (Salmon et al., 2002). This occurs because microtubules are coupled to actin and actin in the cell body moves forward (Shao et al., 2012). We think this is an important point because it suggests that much about what is known in the context of non-neuronal cell migration (Gardel et al., 2010; Julicher et al., 2007; Wilson et al., 2010) may be applied to understanding growth cone motility.

To analyze how disruption of NMII alters the susceptibility of the axon to stretching, we applied our mathematical model to our observed mitochondria movements along the axon (O'Toole et al., 2008). Following disruption of NMII, we found a 90% drop in what we have previously called intrinsic axonal viscosity (g). We note though that in our measurement of g, the passive viscosity of the axon that arises through cross-links and the contractile forces generated

by NMII are mathematically intertwined. Thus, while g gives a straightforward numerical value for how easily a given level of force will stretch the axon, g is an overestimate of passive viscosity. In terms of relating the biophysical analysis to the biological data, the proposition that NMII makes both active and passive contributions to the integrity of the axon is quite plausible. NMII is present along the axon beneath the plasma membrane (Bridgman and Dailey, 1989) at an intensity that is equal to that found in the C-domain (Rochlin et al., 1995). In the axon, a meshwork of short actin filaments (Hirokawa, 1982; Xu et al., 2013) is associated with the generation of contractile forces that oppose the push associated with microtubules (Joshi et al., 1985) and activation of NMII can drive axonal retraction (Ahmad et al., 2000; Gallo, 2006). Furthermore, in non-neuronal cells NMII contributes to cytoskeletal coherence, which allows the long distance transmission of forces in non-neuronal cells (Cai et al., 2010; Cai and Sheetz, 2009). The decrease in apparent viscosity we observe also fits well with blebbistatin's pharmacological mechanism; it locks NMII in a transition state where it is detached from actin filaments (Kovacs et al., 2004). Thus blebbistatin not only decreases force generation it also disrupts NMII's ability to cross-link actin filaments together into a coherent framework. Furthermore, blebbistatin causes a 60% decrease in actin filament content in chick sensory neurons grown on poly-lysine (Ketschek et al., 2007). Together these changes provide a strong molecular explanation for the large drop in the apparent viscosity of the axon. It suggests that when NMII is disrupted axons elongate more rapidly because there is a reduction in the generation of contractile forces along the axon and the integrity of the actin cytoskeleton is reduced. Both effects allow contractile forces that are generated in the growth cone when NMII is disrupted to more easily pull the C-domain of the growth cone forward.

In addition to the drop in apparent viscosity, we found the strength of the frictional adhesions along the axon decreased by 70%. Because less force is required to move an object when the coefficient of friction is low, this provides an additional mechanistic explanation as to why disruption of NMII increases forward advance of microtubules in the C-domain of the growth cone. To get an intuitive understanding as to why our data indicates the strength of adhesions along the axon decreases, it is important to keep in mind that the shape of the velocity curve along the axon (Fig. 3.3D) is determined by the ratio of viscosity to adhesions (O'Toole et al., 2008). For each point along the axon force can either be transmitted to the next segment of the axon or to the substrate. In the presence of blebbistatin, we find that the viscosity of the axon decreases by almost 10 fold, yet there is only a modest change in shape of the velocity curve. This indicates that paired with the decrease in viscosity there is a similar, but not quite as dramatic, decrease in adhesions. This has interesting implications in the context of previous studies that have noted disruption of NMII decreases the strength by which cells can attach to each other and the substrate (Wylie and Chantler, 2001). Of particular importance to our work, when NMII is disrupted it decreases the attachment of the neurons to laminin, but has no effect on their binding to PO (Ketschek et al., 2007; Yu et al., 2012). This suggests that the decrease in frictional interaction we report is not occurring due to a change in how well cells are binding to the substrate external to the plasma membrane, but rather it is occurring because of changes in internal linkages to the substrate. This interpretation is consistent with observations that disruption of NMII significantly decreases vinculin and paxillin; two proteins that are important for linking cell adhesion receptors to the cytoskeletal framework (Ketschek et al., 2007; Woo and Gomez, 2006; Wylie and Chantler, 2001). Thus disruption of NMII allows microtubules in the axon to slide forward more easily.

While our data indicate that disruption of NMII increases the rate of axonal elongation because the axon is easier to stretch and frictional forces are smaller, it raises the important question of the identity of mechanisms that pull the growth cone forward in the absence of NMII activity. Within the myosin family 1, 2, 5 and 10 have all been implicated in the process of axonal elongation (Suter, 2011). Of the Kinesins, 1, 2, 5, and 12 have all been suggested as making either positive or negative contributions to growth (Hirokawa et al., 2009; Liu et al., 2010; Lu et al., 2013b; Myers and Baas, 2007). Likewise there is clear evidence that dynein is involved in growth cone motility (Ahmad et al., 2000; Grabham et al., 2007). With the expectation that most, if not all of these will make a contribution to neuronal force balance and growth cone motility, the challenge will be to quantitatively assess how these cooperate with or oppose the activity of NMII in pulling the growth cone forward. In sum, this model confirms previous models in which NMII generates traction force that pulls the growth cone forward (Bridgman et al., 2001; Suter et al., 1998), while providing an explanation for why its disruption globally increases growth cone advance.

In terms of therapeutics, our work suggests several approaches that may be used to increase the rate of axonal elongation. One could increase contractile force generation in the growth cone that pulls material forward via increasing the activity of NMII and other unknown motors that generate contractile forces (Fig. 3.5G, green arrows) or by increasing the dynamics of adhesions in the growth cone that are important for the generation of traction forces (Chan and Odde, 2008; Myers and Gomez, 2011; Santiago-Medina et al., 2013; Woo and Gomez, 2006) (Fig. 3.5G, gray dashpots). One could increase the forward push of microtubules at the growth cone by selectively increasing microtubule polymerization (Hellal et al., 2011) or by modulating the activity of motors that control microtubule sliding (Liu et al., 2010; Lu et al., 2013b) (Fig.

3.5G, orange arrows). Or one could decrease the active generation of forces along the axon that impede growth cone advance (Brown et al., 2009; Liu et al., 2010) or decrease the passive generation of reaction forces associated with axonal viscosity and the strength of adhesions along the axon (O'Toole et al., 2008) (Fig. 3.5G, blue arrows). It has been shown that Rho-kinase regulates a pool of NMII not associated with retrograde actin flow (Zhang et al., 2003) which, in the context of our model, suggests that indeed Rho-kinase inhibitors are potential candidates for nerve regeneration (Tonges et al., 2011) because they selectively inhibit NMII activity along the axon. Given the lack of effective treatments for spinal cord injury, stroke, neuronal degeneration and trauma, our work here is important because it provides an integrated physical model of growth cone motility that suggests several rational approaches to increasing neuronal regeneration.

Acknowledgements: We thank Dan Kiehart for supplying the NMII antisera and Peter Hollenbeck for helpful comments and stimulating discussions.

APPENDIX

Table 3.1: Blebbistatin causes growth cone retraction when mixed with either FITC- or TexasRed-dextran.

	FITC	TexRed		Pooled
DMSO	14.4 +/- 14.3 (8)	16.5 +/- 14.7 (8)	p = 0.815	15.5 +/- 8.9 (16)
Blebbistatin	-13.7 +/- 10.6 (10)	-12.5 +/- 2.7 (11)	p = 0.837	-13.1 +/- 6.1 (21)
				p < 0.01

Both DMSO and blebbistatin were mixed either with 0.1 μg/ml FITC-dextran or 1.0 mg/ml TexasRed-dextran and focally applied to growth cones. Rates of movement in the table were obtained by tracking position of the C-domain over time. Numbers presented as ave. +/- 95% CI (n) in μm/hr. All p-values presented in table obtained from two-tailed, unpaired t-test.

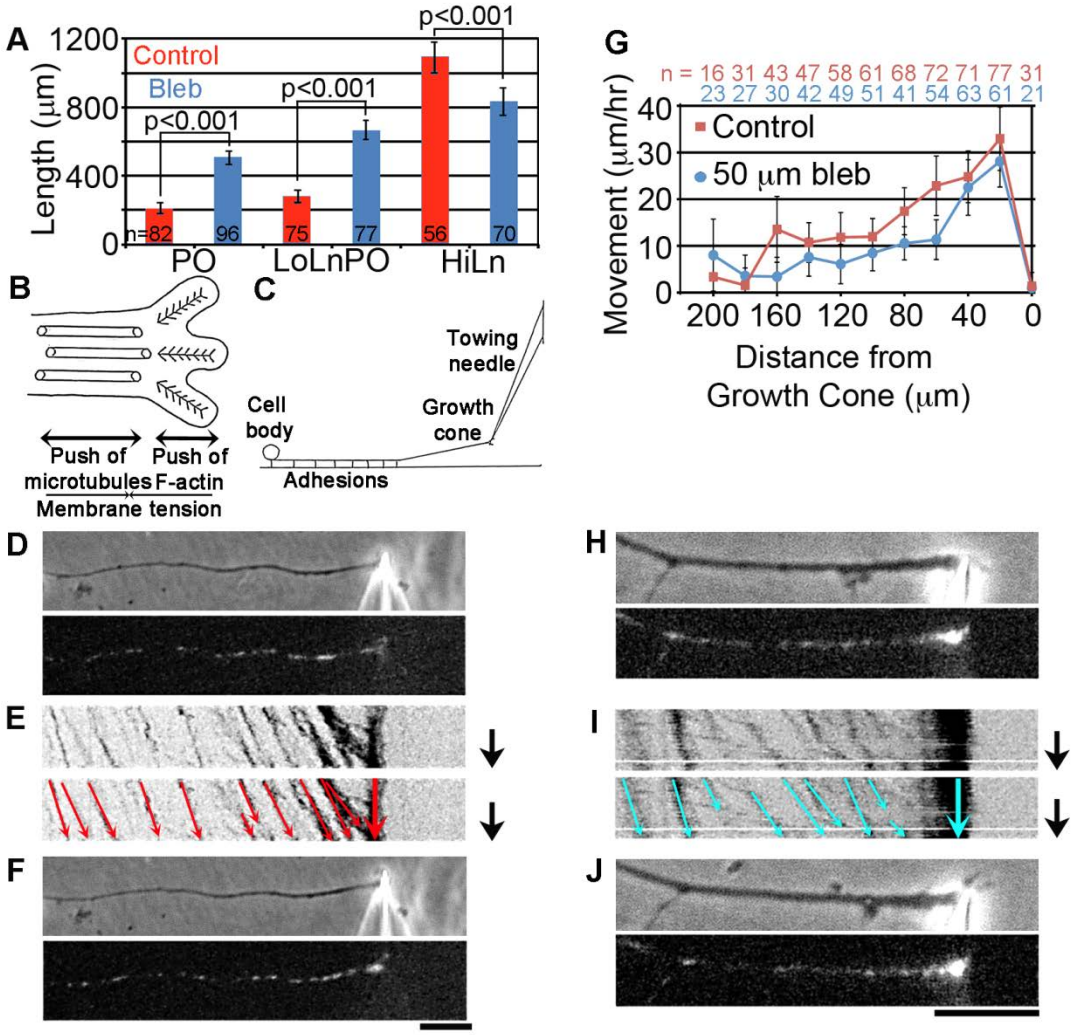

Figure 3.1 Contractile forces in the growth cone pull the axon forward. (**A**). To verify that disruption of NMII increases and decreases elongation in ways consistent with previous reports, we plated chick sensory neurons on three substrates, treated them with 50 μM blebbistatin and measured axonal length 24 h later. The *n* for each group is at the base of the columns. Significance was calculated using a two-tailed Student's *t* test. (**B**) Schematic of a growth cone illustrating a model where microtubules push forward and actin filaments push back. (**C**) Illustration of our method for measuring neuronal forces using a force calibrated towing needle. (**D**) A phase and fluorescent image of Mitotracker labeled mitochondria in a chick sensory neuron grown on LoLnPO. The growth cone is attached to a towing needle, which appears as a phase bright triangle on the right hand side of the image. (**E**) Fluorescent images of docked mitochondria were acquired every 10 seconds and converted into a color-inverted kymograph (time arrow 10 min) to track movement along the axon. The kymograph with the red arrows, is a duplicate of the kymograph above, and illustrates the movement of docked mitochondria used in this analysis. (**F**) The final phase and fluorescent images at the end of the experiment; bar, 20 μm. The velocity profile of docked mitochondria along the axon when the growth cone was held

Figure 3.1 (cont'd)

at steady state rest tension attached to a towing needle are shown in red in (**G**); averages are displayed with 95% confidence interval error bars versus their distance from the growth cone. *n* values are color coded and listed above each bin. (**H**, **I**, and **J**) To characterize how disruption of NMII alters force generation and bulk transport (blue arrows in I), the experiment was repeated in the presence of 50 μM blebbistatin; bar, 20 μm. The velocity profile in the presence of blebbistatin is shown in blue in (**G**).

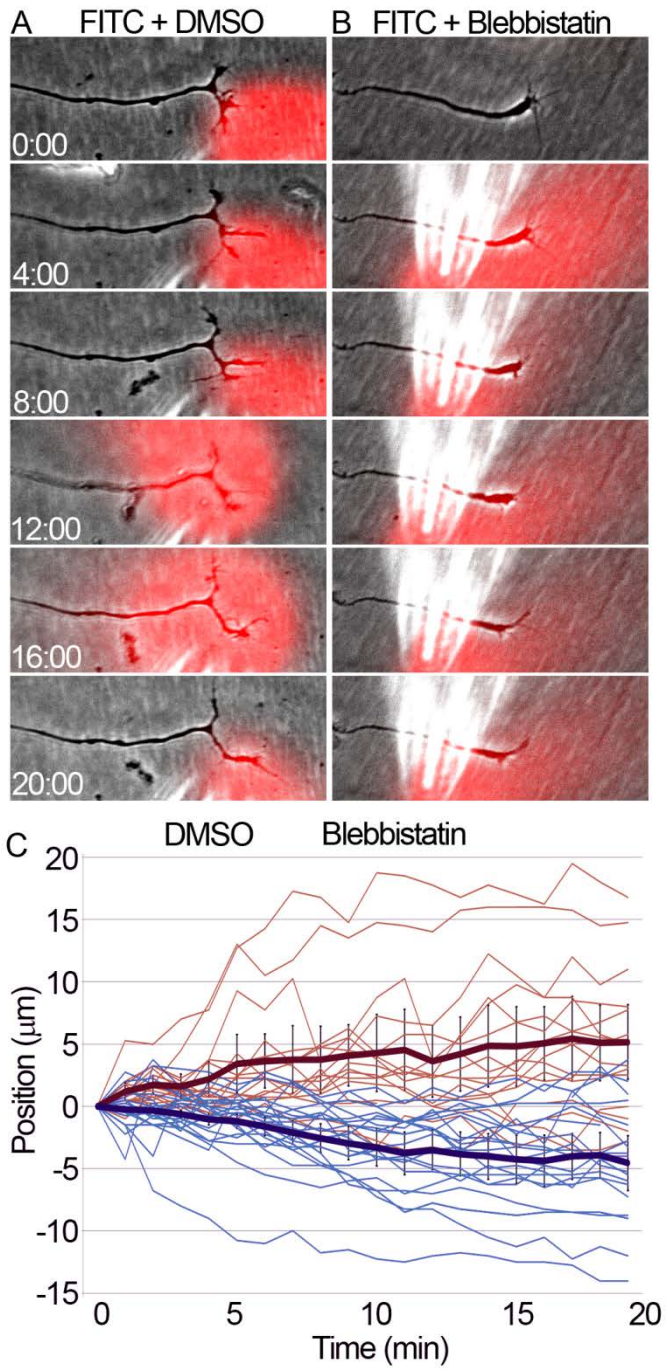

Figure 3.2 Local disruption of NMII in the growth cone induces retraction. Focal application of FITC-dextran plus DMSO (**A**) or FITC-dextran plus 100 μM blebbistatin (**B**) to the growth cone is shown as red overlay on a phase time series of 4 min intervals. Blebbistatin (B) causes the growth cone C-domain to move backward, whereas the growth cone advances when exposed to DMSO (A). Vertical white lines have been added to each series as a stationary reference. Individual growth cone positions (**C**) at 1 min intervals are shown in red for DMSO controls and blue for blebbistatin treated growth cones, where initial growth cone position at t =

Figure 3.2 (cont'd)

0 are aligned at position 0. The thick lines represent average position of each group for each time point. Error bars are 95% CI. Statistical significance was found at each time point by unpaired, two-tailed t-test ($p < 0.05$). Scale bar = 20 μm.

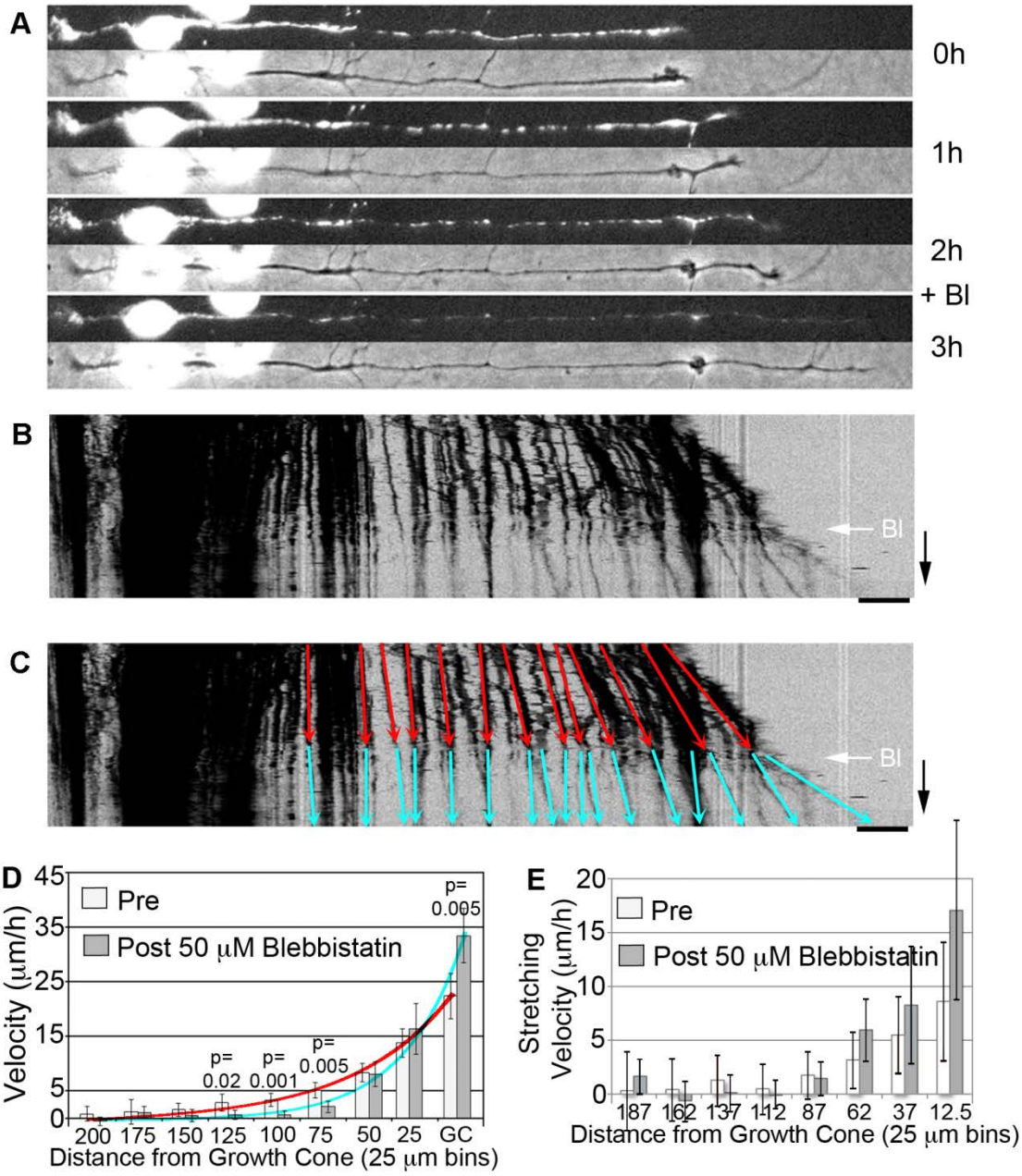

Figure 3.3 Global disruption of NMII in chick sensory neurons speeds elongation because it increases axonal stretching. Time series of an elongating axon with fluorescently labelled mitochondria shown as paired phase and inverted fluorescent images at 1 h intervals (**A**) and a color inverted kymograph of the mitochondria (**B**). Bl indicates 50 μM blebbistatin addition just after the 2h time point. Scale bar = 20 μm; time arrow = 1 h. (**C**) To illustrate the motion of docked mitochondria before and after Blebbistatin addition, the kymograph in (B) was duplicated and red and blue arrows were drawn over their paths. Mitochondria were grouped into 25 μm bins in relation to their distance from the growth cone and their velocities graphed in (**D**). The red line shows the curve fit for the control using Eq. 1 and the parameter values: F_0 = 80

Figure 3.3 (cont'd)

μdynes, G = 25 x 10^6 g μm h^{-1}, η = 8712 Pa sec, L = 200 μm. The blue line shows the curve fit when NMII is disrupted using the parameter values: F_0 = 23 μdynes, G = 3 x 10^6 g μm h^{-1}, η = 2685 Pa sec, L = 200 μm. (**E**) To illustrate the rate of stretching along the axon in the absence and presence of blebbistatin, the difference between the velocities in the bins shown in (D) is plotted.

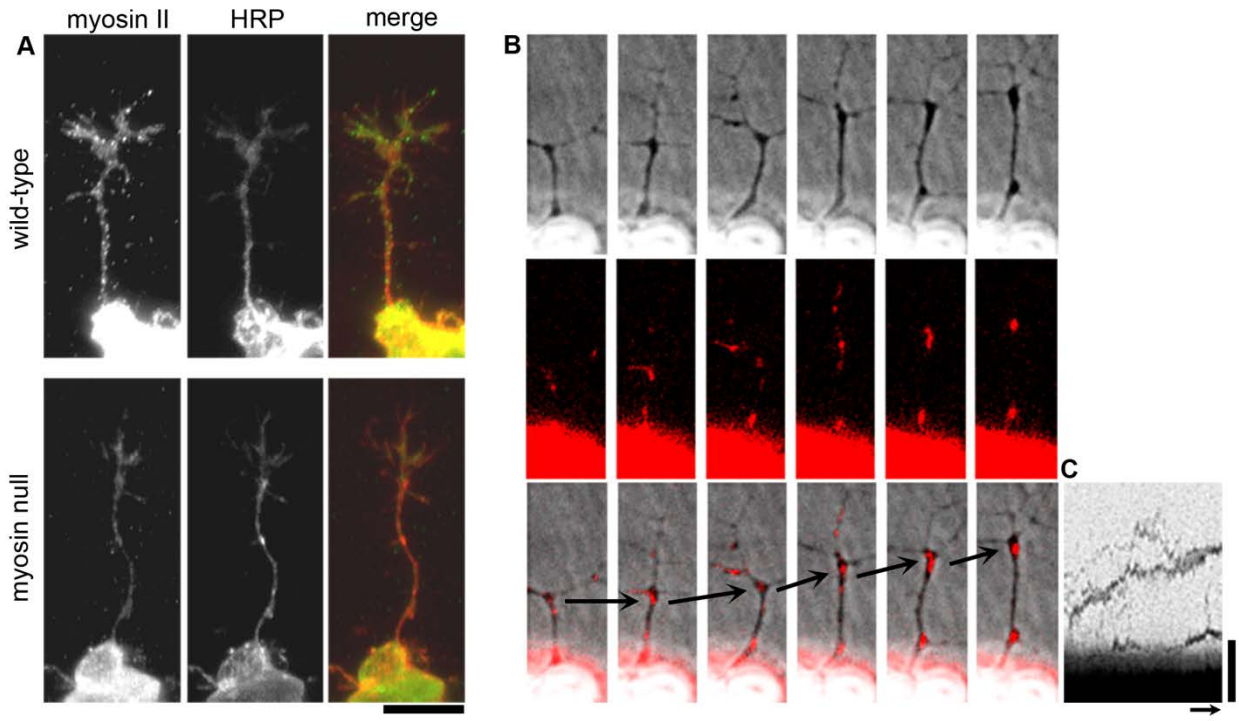

Figure 3.4 Genetic disruption of *Zipper* / NMII in *Drosophila* neurons increases anterograde translocation of docked mitochondria. (**A**) Immunostaining for NMII shows a 48% reduction in NMII levels in Zip^{1}/Zip^{Df} mutant neurons compared to wild-type neurons. Neuronal plasma membranes are labelled with HRP-Texas Red. (**B**) Time-lapse series of a growing Zip^{1}/Zip^{Df} axon in 10 min intervals shows advance of an axonal branch point (phase in top and bottom row) together with a cluster of docked mitochondria at the branch point (red in middle and bottom row). (**C**) Kymograph constructed from the same time period as in (B), using 30 s intervals. Scale bars = 10 μm, time arrow = 10 min.

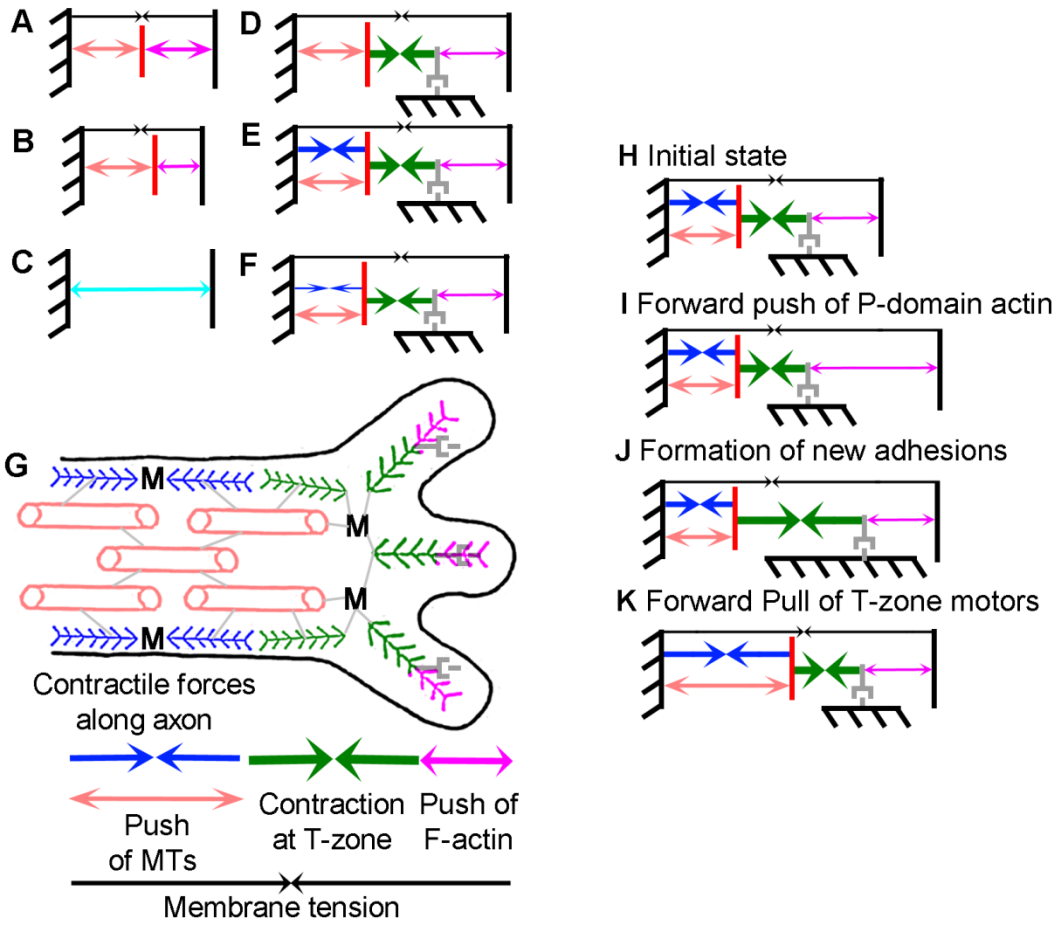

Figure 3.5 Biophysical models of neurons.
(**A**) A model where the push of microtubule assembly is countered by the push of retrograde actin flow. The vertical line with hash marks on the left is a stationary attachment point at the cell body. The orange double-headed arrows pointing outward indicate microtubule-associated forces. The red line is the boundary between the microtubule rich C-domain and actin in the T-zone. The magenta line is force associated with actin that pushes the plasma membrane forward and microtubules back. The black line on the right hand side represents the plasma membrane at the leading edge and the small black arrows are the force associated with membrane tension. (**B**) A reduction in the pushing force associated with actin retrograde flow allows microtubules to push forward more easily. (**C**) Summation of the forces in panel B yields a net force vector that pushes forward. (**D**) Actin based forces are divided into two sections: actin assembly that simultaneously pushes the plasma membrane forward (magenta arrow) and attachment sites to the extracellular matrix rearwards (grey dashpot); and contractile forces focused in the T-Zone (green arrow) that simultaneously pull microtubules in the C-domain forward and pull attachments to the substrate rearwards. (**E**) The addition of moderate contractile forces along the axon (blue arrows) that arise actively as the result of NMII activity and passively as reaction forces that result from viscosity and frictional adhesions to the substrate. (**F**) Disruption of NMII leads to large reduction in the restraining forces (blue arrow) along the axon and to a moderate decrease in the generation of contractile forces (green arrow) in the growth cone. (**G**) Cartoon of the growth cone and proximal axon, illustrating how the force vectors in panel E map to

Figure 3.5 (cont'd)

cytoskeletal structures. M stands for combined motor activity, not just NMII. (**H**-**K**) A schematic illustrates the steps in axonal elongation. Forces associated with actin polymerization (magenta arrow) push the plasma membrane forward and provide a region for the formation of new attachments (J, grey dashpot) to the substrate. Contraction of actin (K, green arrow) pulls actin and microtubules along the axon forward.

REFERENCES

REFERENCES

Ahmad, F.J., J. Hughey, T. Wittmann, A. Hyman, M. Greaser, and P.W. Baas. 2000. Motor proteins regulate force interactions between microtubules and microfilaments in the axon. *Nature cell biology*. 2:276-280.

Bamburg, J.R., D. Bray, and K. Chapman. 1986. Assembly of microtubules at the tip of growing axons. *Nature*. 321:788-790.

Betz, T., D. Koch, Y.B. Lu, K. Franze, and J.A. Kas. 2011. Growth cones as soft and weak force generators. *Proceedings of the National Academy of Sciences of the United States of America*. 108:13420-13425.

Bray, D. 1970. Surface movements during the growth of single explanted neurons. *Proceedings of the National Academy of Sciences of the United States of America*. 65:905-910.

Bray, D. 1979. Mechanical Tension Produced by Nerve-Cells in Tissue-Culture. *Journal of cell science*. 37:391-410.

Bray, D. 1984. Axonal growth in response to experimentally applied mechanical tension. *Dev Biol*. 102:379-389.

Bridgman, P.C., and M.E. Dailey. 1989. The organization of myosin and actin in rapid frozen nerve growth cones. *The Journal of cell biology*. 108:95-109.

Bridgman, P.C., S. Dave, C.F. Asnes, A.N. Tullio, and R.S. Adelstein. 2001. Myosin IIB is required for growth cone motility. *J Neurosci*. 21:6159-6169.

Brown, J.A., R.B. Wysolmerski, and P.C. Bridgman. 2009. Dorsal root ganglion neurons react to semaphorin 3A application through a biphasic response that requires multiple myosin II isoforms. *Mol Biol Cell*. 20:1167-1179.

Brown, M.E., and P.C. Bridgman. 2003. Retrograde flow rate is increased in growth cones from myosin IIB knockout mice. *Journal of cell science*. 116:1087-1094.

Burnette, D.T., A.W. Schaefer, L. Ji, G. Danuser, and P. Forscher. 2007. Filopodial actin bundles are not necessary for microtubule advance into the peripheral domain of Aplysia neuronal growth cones. *Nature cell biology*. 9:1360-1369.

Cai, Y., O. Rossier, N.C. Gauthier, N. Biais, M.A. Fardin, X. Zhang, L.W. Miller, B. Ladoux, V.W. Cornish, and M.P. Sheetz. 2010. Cytoskeletal coherence requires myosin-IIA contractility. *Journal of cell science*. 123:413-423.

Cai, Y., and M.P. Sheetz. 2009. Force propagation across cells: mechanical coherence of dynamic cytoskeletons. *Curr Opin Cell Biol*. 21:47-50.

Chan, C.E., and D.J. Odde. 2008. Traction dynamics of filopodia on compliant substrates. *Science (New York, N.Y.* 322:1687-1691.

Craig, E.M., D. Van Goor, P. Forscher, and A. Mogilner. 2012. Membrane tension, myosin force, and actin turnover maintain actin treadmill in the nerve growth cone. *Biophysical journal*. 102:1503-1513.

Edelstein, A., N. Amodaj, K. Hoover, R. Vale, and N. Stuurman. 2010. Computer control of microscopes using microManager. *Curr Protoc Mol Biol*. Chapter 14:Unit14 20.

Forscher, P., and S.J. Smith. 1988. Actions of cytochalasins on the organization of actin filaments and microtubules in a neuronal growth cone. *The Journal of cell biology*. 107:1505-1516.

Franke, J.D., R.A. Montague, and D.P. Kiehart. 2010. Nonmuscle myosin II is required for cell proliferation, cell sheet adhesion and wing hair morphology during wing morphogenesis. *Dev Biol*. 345:117-132.

Gallo, G. 2006. RhoA-kinase coordinates F-actin organization and myosin II activity during semaphorin-3A-induced axon retraction. *Journal of cell science*. 119:3413-3423.

Gardel, M.L., I.C. Schneider, Y. Aratyn-Schaus, and C.M. Waterman. 2010. Mechanical integration of actin and adhesion dynamics in cell migration. *Annu Rev Cell Dev Biol*. 26:315-333.

Grabham, P.W., G.E. Seale, M. Bennecib, D.J. Goldberg, and R.B. Vallee. 2007. Cytoplasmic dynein and LIS1 are required for microtubule advance during growth cone remodeling and fast axonal outgrowth. *J Neurosci*. 27:5823-5834.

Halfon, M.S., S. Gisselbrecht, J. Lu, B. Estrada, H. Keshishian, and A.M. Michelson. 2002. New fluorescent protein reporters for use with the Drosophila Gal4 expression system and for vital detection of balancer chromosomes. *Genesis*. 34:135-138.

Hellal, F., A. Hurtado, J. Ruschel, K.C. Flynn, C.J. Laskowski, M. Umlauf, L.C. Kapitein, D. Strikis, V. Lemmon, J. Bixby, C.C. Hoogenraad, and F. Bradke. 2011. Microtubule stabilization reduces scarring and causes axon regeneration after spinal cord injury. *Science*. 331:928-931.

Hirokawa, N. 1982. Cross-linker system between neurofilaments, microtubules, and membranous organelles in frog axons revealed by the quick-freeze, deep-etching method. *The Journal of cell biology*. 94:129-142.

Hirokawa, N., Y. Noda, Y. Tanaka, and S. Niwa. 2009. Kinesin superfamily motor proteins and intracellular transport. *Nat Rev Mol Cell Biol*. 10:682-696.

Howard, J. 2001. Mechanics of motor proteins and the cytoskeleton. Sinauer Associates, Publishers, Sunderland, Mass. xvi, 367 p. pp.

Hur, E.M., I.H. Yang, D.H. Kim, J. Byun, Saijilafu, W.L. Xu, P.R. Nicovich, R. Cheong, A. Levchenko, N. Thakor, and F.Q. Zhou. 2011. Engineering neuronal growth cones to promote axon regeneration over inhibitory molecules. *Proceedings of the National Academy of Sciences of the United States of America*. 108:5057-5062.

Jan, L.Y., and Y.N. Jan. 1982. Antibodies to horseradish peroxidase as specific neuronal markers in Drosophila and in grasshopper embryos. *Proceedings of the National Academy of Sciences of the United States of America*. 79:2700-2704.

Joshi, H.C., D. Chu, R.E. Buxbaum, and S.R. Heidemann. 1985. Tension and compression in the cytoskeleton of PC 12 neurites. *The Journal of cell biology*. 101:697-705.

Julicher, F., K. Kruse, J. Prost, and J.F. Joanny. 2007. Active behavior of the cytoskeleton. *Phys Rep*. 449:3-28.

Ketschek, A.R., S.L. Jones, and G. Gallo. 2007. Axon extension in the fast and slow lanes: substratum-dependent engagement of myosin II functions. *Developmental neurobiology*. 67:1305-1320.

Kiehart, D.P., and R. Feghali. 1986. Cytoplasmic myosin from Drosophila melanogaster. *The Journal of cell biology*. 103:1517-1525.

Koch, D., W.J. Rosoff, J. Jiang, H.M. Geller, and J.S. Urbach. 2012. Strength in the periphery: growth cone biomechanics and substrate rigidity response in peripheral and central nervous system neurons. *Biophysical journal*. 102:452-460.

Kovacs, M., J. Toth, C. Hetenyi, A. Malnasi-Csizmadia, and J.R. Sellers. 2004. Mechanism of blebbistatin inhibition of myosin II. *J Biol Chem*. 279:35557-35563.

Lamoureux, P., R.E. Buxbaum, and S.R. Heidemann. 1989. Direct evidence that growth cones pull. *Nature*. 340:159-162.

Lamoureux, P., S. Heidemann, and K.E. Miller. 2011. Mechanical Manipulation of Neurons to Control Axonal Development. *Journal of visualized experiments: JoVE*.

Lamoureux, P., S.R. Heidemann, N.R. Martzke, and K.E. Miller. 2010. Growth and elongation within and along the axon. *Developmental neurobiology*. 70:135-149.

Lee, A.C., and D.M. Suter. 2008. Quantitative analysis of microtubule dynamics during adhesion-mediated growth cone guidance. *Developmental neurobiology*. 68:1363-1377.

Letourneau, P.C., T.A. Shattuck, and A.H. Ressler. 1987. "Pull" and "push" in neurite elongation: observations on the effects of different concentrations of cytochalasin B and taxol. *Cell Motil Cytoskeleton*. 8:193-209.

Lieber, A.D., S. Yehudai-Resheff, E.L. Barnhart, J.A. Theriot, and K. Keren. 2013. Membrane tension in rapidly moving cells is determined by cytoskeletal forces. *Curr Biol*. 23:1409-1417.

Lin, C.H., E.M. Espreafico, M.S. Mooseker, and P. Forscher. 1996. Myosin drives retrograde F-actin flow in neuronal growth cones. *Neuron*. 16:769-782.

Lin, C.H., and P. Forscher. 1995. Growth cone advance is inversely proportional to retrograde F-actin flow. *Neuron*. 14:763-771.

Liu, M., V.C. Nadar, F. Kozielski, M. Kozlowska, W. Yu, and P.W. Baas. 2010. Kinesin-12, a mitotic microtubule-associated motor protein, impacts axonal growth, navigation, and branching. *J Neurosci*. 30:14896-14906.

Lowery, L.A., and D. Van Vactor. 2009. The trip of the tip: understanding the growth cone machinery. *Nat Rev Mol Cell Biol*. 10:332-343.

Lu, P., A. Blesch, L. Graham, Y. Wang, R. Samara, K. Banos, V. Haringer, L. Havton, N. Weishaupt, D. Bennett, K. Fouad, and M.H. Tuszynski. 2012. Motor axonal regeneration after partial and complete spinal cord transection. *J Neurosci*. 32:8208-8218.

Lu, W., P. Fox, M. Lakonishok, M.W. Davidson, and V.I. Gelfand. 2013a. Initial Neurite Outgrowth in Drosophila Neurons Is Driven by Kinesin-Powered Microtubule Sliding. *Curr Biol*.

Lu, W., P. Fox, M. Lakonishok, M.W. Davidson, and V.I. Gelfand. 2013b. Initial neurite outgrowth in Drosophila neurons is driven by kinesin-powered microtubule sliding. *Curr Biol*. 23:1018-1023.

Medeiros, N.A., D.T. Burnette, and P. Forscher. 2006. Myosin II functions in actin-bundle turnover in neuronal growth cones. *Nature cell biology*. 8:215-226.

Miller, K.E., and H.C. Joshi. 1996. Tubulin transport in neurons. *The Journal of cell biology*. 133:1355-1366.

Miller, K.E., and M.P. Sheetz. 2006. Direct evidence for coherent low velocity axonal transport of mitochondria. *The Journal of cell biology*. 173:373-381.

Morris, R.L., and P.J. Hollenbeck. 1993. The regulation of bidirectional mitochondrial transport is coordinated with axonal outgrowth. *Journal of cell science*. 104 (Pt 3):917-927.

Myers, J.P., and T.M. Gomez. 2011. Focal adhesion kinase promotes integrin adhesion dynamics necessary for chemotropic turning of nerve growth cones. *J Neurosci*. 31:13585-13595.

Myers, K.A., and P.W. Baas. 2007. Kinesin-5 regulates the growth of the axon by acting as a brake on its microtubule array. *The Journal of cell biology*. 178:1081-1091.

Myers, K.A., I. Tint, C.V. Nadar, Y. He, M.M. Black, and P.W. Baas. 2006. Antagonistic forces generated by cytoplasmic dynein and myosin-II during growth cone turning and axonal retraction. *Traffic (Copenhagen, Denmark)*. 7:1333-1351.

O'Toole, M., P. Lamoureux, and K.E. Miller. 2008. A physical model of axonal elongation: force, viscosity, and adhesions govern the mode of outgrowth. *Biophysical journal*. 94:2610-2620.

Okabe, S., and N. Hirokawa. 1990. Turnover of fluorescently labelled tubulin and actin in the axon. *Nature*. 343:479-482.

Pollard, T.D., and G.G. Borisy. 2003. Cellular motility driven by assembly and disassembly of actin filaments. *Cell*. 112:453-465.

Prokop, A., B. Kuppers-Munther, and N. Sanchez-Soriano. 2012. Using primary neuron cultures of Drosophila to analyze neuronal circuit formation and function. *In* The making and un-making of neuronal circuits in Drosophila. Springer. 225-247.

Rauch, P., P. Heine, B. Goettgens, and J.A. Kas. 2013. Forces from the rear: deformed microtubules in neuronal growth cones influence retrograde flow and advancement. *New Journal of Physics*. 15:015007.

Raucher, D., and M.P. Sheetz. 2000. Cell spreading and lamellipodial extension rate is regulated by membrane tension. *The Journal of cell biology*. 148:127-136.

Reinsch, S.S., T.J. Mitchison, and M. Kirschner. 1991. Microtubule polymer assembly and transport during axonal elongation. *The Journal of cell biology*. 115:365-379.

Rochlin, M.W., K. Itoh, R.S. Adelstein, and P.C. Bridgman. 1995. Localization of myosin II A and B isoforms in cultured neurons. *Journal of cell science*. 108 (Pt 12):3661-3670.

Roossien, D.H., P. Lamoureux, D. Van Vactor, and K.E. Miller. 2013. Drosophila growth cones advance by forward translocation of the neuronal cytoskeletal meshwork in vivo. *PLoS One*. 8:e80136.

Salmon, W.C., M.C. Adams, and C.M. Waterman-Storer. 2002. Dual-wavelength fluorescent speckle microscopy reveals coupling of microtubule and actin movements in migrating cells. *The Journal of cell biology*. 158:31-37.

Sanchez-Soriano, N., C. Goncalves-Pimentel, R. Beaven, U. Haessler, L. Ofner-Ziegenfuss, C. Ballestrem, and A. Prokop. 2010. Drosophila growth cones: a genetically tractable platform for the analysis of axonal growth dynamics. *Developmental neurobiology*. 70:58-71.

Santiago-Medina, M., K.A. Gregus, and T.M. Gomez. 2013. PAK-PIX interactions regulate adhesion dynamics and membrane protrusion to control neurite outgrowth. *Journal of cell science*. 126:1122-1133.

Saxton, W.M., and P.J. Hollenbeck. 2012. The axonal transport of mitochondria. *Journal of cell science*. 125:2095-2104.

Schaefer, A.W., N. Kabir, and P. Forscher. 2002. Filopodia and actin arcs guide the assembly and transport of two populations of microtubules with unique dynamic parameters in neuronal growth cones. *The Journal of cell biology*. 158:139-152.

Schaefer, A.W., V.T. Schoonderwoert, L. Ji, N. Mederios, G. Danuser, and P. Forscher. 2008. Coordination of actin filament and microtubule dynamics during neurite outgrowth. *Developmental cell*. 15:146-162.

Shao, D., H. Levine, and W.J. Rappel. 2012. Coupling actin flow, adhesion, and morphology in a computational cell motility model. *Proceedings of the National Academy of Sciences of the United States of America*. 109:6851-6856.

Sicaeros, B., and D.K. O'Dowd. 2007. Preparation of neuronal cultures from midgastrula stage Drosophila embryos. *Journal of visualized experiments: JoVE*.

Snow, P.M., N.H. Patel, A.L. Harrelson, and C.S. Goodman. 1987. Neural-specific carbohydrate moiety shared by many surface glycoproteins in Drosophila and grasshopper embryos. *J Neurosci*. 7:4137-4144.

Suter, D.M. 2011. Functions of Myosin Motor Proteins in the Nervous System. *In* Neurobiology of Actin. Springer. 45-72.

Suter, D.M., L.D. Errante, V. Belotserkovsky, and P. Forscher. 1998. The Ig superfamily cell adhesion molecule, apCAM, mediates growth cone steering by substrate-cytoskeletal coupling. *The Journal of cell biology*. 141:227-240.

Suter, D.M., and K.E. Miller. 2011. The emerging role of forces in axonal elongation. *Progress in neurobiology*. 94:91-101.

Tonges, L., J.C. Koch, M. Bahr, and P. Lingor. 2011. ROCKing Regeneration: Rho Kinase Inhibition as Molecular Target for Neurorestoration. *Frontiers in molecular neuroscience*. 4:39.

Tullio, A.N., P.C. Bridgman, N.J. Tresser, C.C. Chan, M.A. Conti, R.S. Adelstein, and Y. Hara. 2001. Structural abnormalities develop in the brain after ablation of the gene encoding nonmuscle myosin II-B heavy chain. *The Journal of comparative neurology*. 433:62-74.

Turney, S.G., and P.C. Bridgman. 2005. Laminin stimulates and guides axonal outgrowth via growth cone myosin II activity. *Nature neuroscience*. 8:717-719.

Wilson, C.A., M.A. Tsuchida, G.M. Allen, E.L. Barnhart, K.T. Applegate, P.T. Yam, L. Ji, K. Keren, G. Danuser, and J.A. Theriot. 2010. Myosin II contributes to cell-scale actin network treadmilling through network disassembly. *Nature*. 465:373-377.

Woo, S., and T.M. Gomez. 2006. Rac1 and RhoA promote neurite outgrowth through formation and stabilization of growth cone point contacts. *J Neurosci*. 26:1418-1428.

Wylie, S.R., and P.D. Chantler. 2001. Separate but linked functions of conventional myosins modulate adhesion and neurite outgrowth. *Nature cell biology*. 3:88-92.

Xu, K., G. Zhong, and X. Zhuang. 2013. Actin, spectrin, and associated proteins form a periodic cytoskeletal structure in axons. *Science (New York, N.Y.* 339:452-456.

Young, P.E., A.M. Richman, A.S. Ketchum, and D.P. Kiehart. 1993. Morphogenesis in Drosophila requires nonmuscle myosin heavy chain function. *Genes Dev*. 7:29-41.

Yu, P., L.Y. Santiago, Y. Katagiri, and H.M. Geller. 2012. Myosin II activity regulates neurite outgrowth and guidance in response to chondroitin sulfate proteoglycans. *Journal of neurochemistry*. 120:1117-1128.

Zhang, X.F., A.W. Schaefer, D.T. Burnette, V.T. Schoonderwoert, and P. Forscher. 2003. Rho-dependent contractile responses in the neuronal growth cone are independent of classical peripheral retrograde actin flow. *Neuron*. 40:931-944.

Zhou, F.Q., C.M. Waterman-Storer, and C.S. Cohan. 2002. Focal loss of actin bundles causes microtubule redistribution and growth cone turning. *The Journal of cell biology*. 157:839-849.

CHAPTER 4:

Cytoplasmic Dynein Pushes the Cytoskeletal Meshwork Forward During Axonal Elongation

Douglas H. Roossien, Phillip Lamoureux, & Kyle E. Miller

Contributions: PL performed the experiments and analyzed data presented in Figure 4.5. DHR performed all other experiments, analyzed all other data, and wrote the manuscript.

This chapter has been submitted in manuscript form to The Journal of Cell Science and may not represent the final published form.

4.1 Abstract

During development, neurons send out axonal processes that can reach lengths hundreds of times longer than the diameter of their cell bodies. While there has been great progress in identifying the proteins involved in axonal elongation, how they govern this biophysical process is poorly understood. Emerging models for elongation suggest *en masse* microtubule translocation, in addition to polymerization, contributes to axonal outgrowth. Cytoplasmic dynein is known to generate forces on microtubules in axons to power their movement via Stop-and-Go transport, but whether these forces influence bulk translocation of long microtubules embedded in the cytoskeletal meshwork has not yet been tested. Here, we use function-blocking antibodies targeted to the dynein intermediate chain and the pharmacological dynein inhibitor Ciliobrevin D to ask if dynein forces contribute to *en bloc* cytoskeleton translocation. By tracking docked mitochondria as fiduciary markers for bulk cytoskeleton movements, we find that translocation is reduced after dynein disruption. We then directly measure net force generation after dynein disruption and find a dramatic increase in axonal tension. Together these data indicate dynein generates forces that push the cytoskeletal meshwork forward *en masse* during axonal elongation.

4.2 Introduction

Axonal elongation is the process by which neurons send out long cellular projections that will eventually form synapses with prescribed targets. Proper extension and navigation through a complex array of tissue is guided by extracellular signaling molecules, many of which converge on the cytoskeleton (Dickson, 2002). Traditionally, the axonal cytoskeleton and the growth cone were considered to be stationary during elongation and that new axon was formed by the addition of new material at the growth cone, either through cytoskeleton polymerization or the deposition of material by motor-driven transport (Dent and Gertler, 2003; Goldberg and Burmeister, 1986; Lowery and Van Vactor, 2009). Recently, however, there have been numerous reports of cytoskeletal translocation in multiple model systems such as *Aplysia* growth cones (Lee and Suter, 2008), cultured chick sensory (Lamoureux et al., 2010; Miller and Sheetz, 2006), *Xenopus* neurons (Chang et al., 1998; Reinsch et al., 1991) and *Drosophila* motoneurons (Roossien et al., 2013). From this, a new model for axonal elongation has emerged, termed Stretch and Intercalation (SAI) (Suter and Miller, 2011), in which forces cause the microtubule rich central domain (C-domain) of the growth cone to advance in bulk. This is paired with stretching of the axon, which is followed by intercalated mass addition along the axon to prevent thinning (Lamoureux et al., 2010). In terms of the cytoskeleton, stretching presumably occurs because filaments are sliding apart either through pulling or pushing forces generated by molecular motors (Lu et al., 2013; Roossien et al., 2013; Suter and Miller, 2011). It is worth noting that because adhesions along the axon dissipate forces generated in the growth cone (O'Toole et al., 2008), these *en masse* movements of the cytoskeleton occur only in the distal axon and were thereby overlooked when observations were made near the cell body (Lim et al., 1990; Okabe and Hirokawa, 1990).

The question of what powers bulk translocation of the cytoskeletal meshwork has not been fully answered, but microtubule-based motors such as cytoplasmic dynein are logical candidates. Dynein is essential for proper growth and maintenance of the axon. Identified roles for dynein in growing axons include driving retrograde transport of membrane organelles (Schnapp and Reese, 1989) and establishment of the initial microtubule bundle during axon initiation (Ahmad et al., 1998; Dehmelt et al., 2006). Dynein forces in the growth cone are thought to be required for microtubules to resist retrograde actin flow (Myers et al., 2006; Vallee et al., 2009) and along the axon they resist actomyosin-based retraction and power Stop-and-Go transport of short microtubules (Ahmad et al., 1998; Ahmad et al., 2006; He et al., 2005). While it has been noted that these forces are likely to also impinge upon the entire array of long microtubules in the axon (Baas et al., 2006), whether they contribute to *en masse* cytoskeleton movement is unknown.

Here we used function-blocking antibodies toward dynein and acute pharmacological disruption using the recently published dynein inhibitor Ciliobrevin D (CilD) to study the role of dynein in axonal elongation. We found that both treatments resulted in a decrease in axonal elongation. By using docked mitochondria as fiduciary markers for the axonal cytoskeletal meshwork before and after CilD treatment, we also found that dynein activity drives forward translocation of the cytoskeletal meshwork during elongation. To determine if dynein contributes to axonal elongation by pulling or pushing material forward, we measured net force generation in axons and then added CilD to disrupt dynein. In response, we found an increase in neuronal tension. Together these studies indicate that dynein pushes microtubules embedded in the cytoskeletal meshwork forward in bulk during axonal elongation.

4.3 Results

4.3.1 Disruption of dynein activity reduces axonal elongation.

Previous studies of dynein function in axons have reported a decrease in elongation following dynein disruption (Ahmad et al., 2006; Ahmad et al., 2000; Grabham et al., 2007; Myers et al., 2006). Microinjection of function-blocking antibodies targeted to the N-terminal 63 amino acids of the 74 kDa dynein intermediate chain (αDIC) has become a gold standard for perturbing dynein function. In non-neuronal cells it has been used to study MTOC positioning (Palazzo et al., 2001), directed cell migration (Dujardin et al., 2003), and spindle formation and positioning during mitosis (Faulkner et al., 2000; O'Connell and Wang, 2000). In neurons, αDIC has been used to probe dynein function in retrograde axonal transport in rat hippocampal neurons (Yi et al., 2011) and in laminin-induced neurite elongation of chick sensory neurons (Grabham et al., 2007). We therefore wanted to first test if disruption of dynein function via microinjection of function-blocking antibodies slows axonal elongation under our culture conditions (i.e. neurons grown on plastic dishes coated with poly-ornithine). In our experiments, both αDIC and control antibodies (nonspecific mouse IgG proteins) were mixed at 10 mg/ml with 0.1 μg/ml FITC-dextran, allowing for visualization of fluid flow and screening for injected neurons. Injections were carried out in neuronal cell bodies approximately 18-20 h after plating. Two hours later, neurons were screened for successful injection based on the presence of fluorescent marker (Fig. 4.1A-B) and morphologically normal rounded cell bodies. Next, two minute phase time lapse movies at 10 s intervals were captured to visualize filopodia dynamics in the growth cone (Fig. 4.1C). We reasoned that because filopodial dynamics are due to actin protrusion at the leading edge of the growth cone (Jay, 2000; Mallavarapu and Mitchison, 1999) and not from dynein activity per se this would be a useful means to assess neuronal health. We found that the average

number of initiation events did not significantly differ between uninjected, IgG-injected, and αDIC-injected neurons (Fig. 4.1D). These control experiments indicate that microinjection does not significantly impair growth cone dynamics.

As a positive control to verify that injected αDIC antibodies decrease dynein function, we analyzed dynein dependent fast mitochondrial transport (Saxton and Hollenbeck, 2012) (Pilling et al., 2006). Mitochondria were labeled with Mitotracker immediately following microinjection and allowed to recover for two hours. Flux was then measured by counting the number of mitochondria that passed the midway point in the axon. We found no significant difference in mitochondrial flux in the retrograde direction between non-injected neurons and those injected with control IgG (Fig. 4.1E). Axons injected with αDIC, on the other hand, had average retrograde flux of 1.15 +/- 1.39 mito/hr (ave. +/- 95% CI), significantly lower than both non-injected axons and those injected with IgG (Fig. 4.1E; 5.60 +/- 1.87 and 8.31 +/- 2.11, respectively). This is in agreement with the previous analysis of retrograde axonal transport of other membrane organelles after αDIC injection (Yi et al., 2011). We also found, as previously reported (Yi et al., 2011), anterograde flux to be reduced in neurons injected with IgG. When we compared anterograde flux in IgG-injected neurons to αDIC-injected neurons, we found a further significant decrease (Fig. 4.1E). While this may seem surprising, it has been reported in other systems where dynein was disrupted (Martin et al., 1999). Together these experiments verify that microinjection of αDIC significantly reduces dynein activity.

To test if dynein contributes to neuronal growth, we measured the rate of axonal elongation of neurons injected with either IgG or αDIC. We found growth cones advanced at a rate of 18.4 +/- 9.2 μm/hr (ave. +/- 95% CI; n = 17 axons) after IgG injection, whereas growth cones injected with αDIC grew at a slow rate of 1.6 +/- 5.7 (ave. +/- 95% CI; n = 17 axons, p <

0.01). The reduction in the rate of axonal elongation is consistent with previous studies (Ahmad et al., 2006; Ahmad et al., 2000; Grabham et al., 2007; Myers et al., 2006) and indicates that dynein is essential for axonal elongation in chick sensory neurons grown under standard culture conditions.

4.3.2 Acute disruption of dynein with the pharmacological inhibitor Ciliobrevin D causes retraction of the axonal cytoskeleton.

Cilobrevins are a recently discovered class of small molecule dynein inhibitors (Firestone et al., 2012). They compete with ATP at its binding site in the dynein motor, thus they increase the time dynein spends attached to the microtubule in the post-power stroke conformation (Kikkawa, 2013). Their use offers advantages over previous approaches (i.e. RNAi, microinjection and genetic KO) in that they can be acutely and systematically applied. Of these inhibitors, the D form of Ciliobrevin (CilD) was shown to most effectively reduce dynein function as measured in microtubule gliding and vesicular transport assays (Firestone et al., 2012). Our first step in using CilD was to find a concentration that blocked elongation to an extent similar to that seen following microinjection of αDIC. We found that at 60 μM, elongation began to slow, at 100 μM growth cones became stationary, and at 150 μM and above retraction occurred (Fig 4.2A). To verify CilD disrupts dynein function, we measured fast mitochondrial transport as above at 60 and 100 μM and found effects similar to those seen with microinjection of αDIC. Retrograde transport was reduced to 66 and 22% of DMSO controls at 60 and 100 μM, respectively (Fig. 4.2B). Anterograde flux was not affected at 60 μM, but was decreased with 100 μM CilD (Fig. 4.2B). The similarity in results between 100 μM CilD and αDIC microinjection suggests this concentration is appropriate for impairing dynein function.

Dynein contributes to the Stop-and-Go transport of short microtubules and it has been speculated that it may generate forces that act on the array of long microtubules (Baas et al., 2006). We have previously shown that chick sensory neurons grow by axonal stretching and bulk forward movement of the cytoskeletal meshwork (Lamoureux et al., 2010; Miller and Sheetz, 2006). To test if dynein contributes to this process, we tracked the movement of docked mitochondria (see Methods) before and after addition of 100 μM CilD. In total, 32 elongating axons were imaged at 1 min intervals for 20 min prior to and 60 min after CilD addition in both phase and fluorescent channels. As seen in the phase images, CilD causes advancing growth cones to retract briefly, after which they become stationary (Fig. 4.2C). As shown in Fig. 4.2D, mitochondria in the distal axon and growth cone are advancing during the pre-treatment observation (red arrows), but the mitochondria begin retracting toward the cell body in the presence of the dynein inhibitor (orange arrows). This can also be seen in the mitochondria kymograph in Fig. 4.2H. By overlaying the fluorescent and phase image series, it appears that mitochondria in the growth cone are pulled backward out of the growth cone when dynein is acutely disrupted (Fig. 4.2E). To control for the possibility that our imaging conditions were causing retraction or impairing drug function, we measured the rate of axonal elongation of these individual growth cones in phase images before and after CilD addition. We found that 100 μM CilD significantly decreased the rate of elongation from 16.1 +/- 5.4 μm/hr to 2.8 +/- 0.9 μm/hr (Fig. 4.2F; ave. +/- 95% CI, $p < 0.01$ paired, two-tailed t-test). This is in agreement with the data in Fig. 4.2A, suggesting our imaging conditions were not causing retraction or impairing drug function. To quantify mitochondrial motion, velocities were measured before and after CilD treatment, sorted based on their position from the growth cone, placed in 25 μm bins and averaged (Fig. 4.2G). We found CilD causes a rapid and significant change from bulk forward

advance of the cytoskeletal meshwork (red bars, before drug) to bulk retraction (orange bars, 100 μM CilD). Together, these results suggest dynein positively regulates bulk forward movement of the axonal cytoskeleton during axonal elongation.

4.3.3 Local disruption of dynein in the growth cone and distal axon causes retraction independently of fast axonal transport.

In prior studies investigating the role of kinesin and dynein in axonal elongation, a caveat has been that it is difficult to separate the effects their disruption has on the delivery of new material to the growth cone. To this end, we focally applied CilD to the growth cone and distal 30 μm of the axon for 20 min using micropipettes in a flow chamber. In Fig. 4.3A, a phase time series shows visualization of drug application during the 20 min period of treatment with 150 μM CilD as red overlay on the phase images in the left column. We used this concentration to ensure a robust growth cone response and to account for rapid diffusion. The right column in Fig. 3A shows the growth cone advancing during the 20 min pre-treatment observation, then retracting during direct CilD application at the growth cone. Control growth cones treated with DMSO, on the other hand, continued to advance during fluid application (Fig. 4.3B). We tracked the position of individual growth cones at 1 min intervals and normalized them by adjusting initial position to 0 μm. When plotted together, DMSO treated growth cones continue to advance while those treated with CilD retract (Fig. 4.3C). The thick dark lines on the graph in Fig. 4.3C represent the average position at each time interval, showing dynein disruption in the growth cone and distal axon is sufficient for growth cone retraction. We calculated the average growth cone velocity based on final change in position at the end of the experiment and found it to be 17.4 +/- 7.0 μm/hr (ave +/- 95% CI; n = 18) in control growth cones and -22.1 +/- 6.9 μm/hr (n =

20; $p < 0.01$) in CilD treated growth cones. Therefore, dynein functions to drive axonal elongation in the distal portion of the axon independently of fast axonal transport along the length of the axon.

4.3.4 Dynein decreases translocation in the absence of non-muscle myosin II activity.

Dynein activity is required to resist non-muscle myosin II (NMII) induced retraction force (Ahmad et al., 2000), but how these two motors cooperate in bulk translocation of the cytoskeleton is unknown. We therefore combined CilD treatment with NMII disruption using blebbistatin (Straight et al., 2003). In these experiments, mitochondria were tracked in 28 axons for 15 min prior to drug addition (Fig. 4.4, blue arrows and bars), 45 min after 50 μM blebbistatin addition (Fig. 4.4, yellow arrows and bars), and then for a final 45 min in both blebbistatin and 100 μM CilD (Fig. 4.4, orange arrows and bars). Interestingly, we found NMII disruption caused an increase in bulk translocation of the growth cone from 21.9 +/- 7.4 to 31.2 +/- 5.2 μm/hr (ave. +/- 95% CI; Fig. 4.4). Subsequent inhibition of dynein resulted in a reduction in elongation to 13.1 +/- 3.2 μm/hr, significantly lower in CilD compared to both pre-treatment and in 50 μM blebbistatin alone ($\alpha = 0.01$, post-hoc Tukey's test). Average mitochondria velocities along the length of the axon remained significantly lower than pre-treatment velocities and although they consistently decreased compared to those in 50 μM blebbistatin, statistical significance was not reached. These experiments suggest that dynein generates forces that drive bulk translocation of the growth cone in opposition to NMII activity. In addition, that residual translocation occurs in the absence of both motors raises the possibility that other motors in addition to dynein and NMII modulate bulk translocation of the cytoskeletal meshwork.

4.3.5 Dynein disruption causes a dramatic increase in axonal tension.

There are two broad explanations for how dynein causes forward translocation of the cytoskeletal meshwork. It could be pulling microtubules forward as seen in non-neuronal cells during spindle pole positioning (Carminati and Stearns, 1997) and fibroblast migration (Dujardin et al., 2003) or it could be pushing on microtubules as observed in Stop-and Go transport (Ahmad et al., 2006; He et al., 2005) and in microtubule translocation near the cell cortex of non-neuronal cells (Mazel et al., 2013). In the first case, disruption of dynein would be predicted to decrease neuronal tension. In the second, it would increase. To test these predictions, we used force-calibrated towing needles in a rest tension assay to measure changes in net axonal force generation before and after 100 μM CilD addition (for a more detailed description of this technique, see Methods and (Lamoureux et al., 2011)). An individual force profile is shown in Fig. 4.5A. In red are the initial force measurements before CilD addition at 30 min, after which the measurements are plotted in blue. The arrows on the graph indicate the time span represented by a series of phase images in Fig 4.5B. When CilD is added, the growth cone pulls harder on the towing needle as indicated by the increase in axonal tension (Fig. 4.5A-B). Each of the 17 axons assayed responded the same. Force measurements for each axon were averaged during a 30 min period before CilD addition and a 30 min period after a new steady-state tension was established. On average, tension increased from 37.6 +/- 10.7 to 79.8 +/- 10.9 μdyne (Fig. 4.5C; ave. +/- 95% CI, $p < 0.01$, pairwise, two-tailed t-test). This supports the second model above, that net dynein force causes anterograde cytoskeleton translocation by pushing microtubules forward.

4.4 Discussion

Observations of bulk cytoskeletal translocation during axonal elongation (Chang et al., 1998; Lee and Suter, 2008; Miller and Sheetz, 2006; Reinsch et al., 1991) raise the question of what powers it. In the current study, we used the new pharmacological inhibitor Ciliobrevin D (Firestone et al., 2012) to disrupt dynein function and asked how this affects *en masse* movements of the cytoskeleton by tracking the movement of docked mitochondria. We found that dynein activity is required for bulk translocation of the growth cone and forward translocation of mitochondria along the axon (Fig. 4.2). From this we infer that dynein is powering *en masse* advance of the cytoskeletal meshwork, including microtubules (Suter and Miller, 2011).

While it is well accepted that dynein generates cellular forces (King, 2000; Paschal et al., 1987), the net forces generated by dynein in neurons have never been measured. Using a towing assay, we found disruption of dynein with CilD lead to a dramatic increase in neuronal tension (Fig. 4.5). Combining the observations of bulk movement with the force measurements strongly indicates dynein pushes the cytoskeletal meshwork forward during elongation.

The balance between dynein and NMII activity controls whether axons elongate or retract (Ahmad et al., 2000). Our data here suggest that these two motors work in opposition to control bulk transport: NMII inhibits and dynein promotes (Fig. 4.4). Because there is currently a limited understanding of how this works, as a starting point we have modeled several speculative possibilities (Fig. 4.6). (1) The first is NMII activity in the T-zone (Rochlin et al., 1995) inhibits bulk advance of microtubules by driving retrograde flow in the P-domain (Brown and Bridgman, 2003; Hur et al., 2011; Lin et al., 1996; Medeiros et al., 2006; Stiess and Bradke, 2011; Vallee et al., 2009). (2) Alternatively, axonal NMII (Bridgman and Dailey, 1989; Rochlin et al., 1995)

could generate tension (Bernal et al., 2007; Gallo, 2004; Joshi et al., 1985) that prevents axonal stretching and thus elongation. Dynein in turn (3) could drive microtubule advance by binding actin in the T-zone. This would be similar to how dynein positions the spindle pole in mitotic cells (Carminati and Stearns, 1997) and pulls microtubules forward during directed fibroblast migration (Dujardin et al., 2003). (4) Alternatively, by binding the plus-ends of microtubules along the axon (Kholmanskikh et al., 2006; Vaughan et al., 1999), dynein could cause neighboring microtubules to telescope apart (Reinsch et al., 1991). Finally, dynein could use cortical actin along the axon as an anchor to move microtubules, as occurs in non-neuronal cells (Mazel et al., 2013) and Stop-and-Go transport (Baas et al., 2006). We note that these models are not mutually exclusive or exhaustive, but simply represent an attempt to assemble a comprehensive molecular explanation for bulk transport and growth cone advance.

In addition to the activities of NMII and dynein, prior studies and our results here indicate that other protein motors are involved in axonal elongation and cytoskeleton translocation. In particular, we observe that when NMII and dynein are simultaneously disrupted, neurons continue to elongate via bulk translocation of the cytoskeletal meshwork. One interpretation of the data is that CilD at 100 μM leaves residual dynein activity that powers elongation. Thus there is a possibility that dynein is the sole motor that drives bulk advance of the cytoskeletal meshwork. Yet we think this is unlikely. Members of the myosin superfamily (i.e. I, II, V and X) have been implicated in neuronal growth (Suter, 2011). Perhaps they contribute to growth by modulating bulk transport. Furthermore, during the initial neurite outgrowth in *Drosophila* neurons, Kinesin-1 powers microtubule sliding into the nascent axon from the cell body (Lu et al., 2013). It is untested, but it seems reasonable, that it could be moving microtubules along the axon during later stages of axonal elongation as well.

A comprehensive picture of dynein function in neurons is beginning to emerge that includes driving retrograde transport of membrane organelles (Pilling et al., 2006; Schnapp and Reese, 1989; Yi et al., 2011) and anterograde transport of microtubules via Stop-and-Go transport (Ahmad et al., 1998; Ahmad et al., 2006), generating forces on microtubules in the growth cone to resist the rearward sweeping motion of retrograde actin flow (Grabham et al., 2007; Myers et al., 2006; Vallee et al., 2009) and resisting NMII-based retraction forces along the axon (Ahmad et al., 2000). Our work here indicates that an additional important function of this multi-faceted motor is to push microtubules embedded in the cytoskeletal meshwork forward during axonal elongation.

4.5 Materials and methods

4.5.1 Cell culture

Neurons from chick dorsal root ganglia were isolated and cultured as described previously in L-15 media supplemented with 0.6% glucose, 1 mM glutamine, 100 U/ml penicillin, 136 μg/ml streptomycin sulfate, 10% fetal calf serum, 50 ng/ml 7S nerve growth factor (Harlan Bioproducts, Indianapolis, IN) and N9 growth supplement (Lamoureux et al., 2010). Polystyrene culture dishes (Corning; Tewksbury, MA, USA) were treated with 0.01% poly-ornithine for 30 min then rinsed three times with sterile dH_2O.

4.5.2 Drug treatments

Stock (-)-blebbistatin (Sigma; St. Louis, MO, USA) was made at 50 mM in DMSO. Prior to addition to the culture dish, stock blebbistatin was pre-warmed and diluted 660 fold in supplemented L-15 media, sonicated for 5 min, then kept warm at 37°C for at least 30 min. Final dilutions of 1:6 were done directly into culture dish during image acquisition for a final blebbistatin concentration of 50 μM. Initial Ciliobrevin D (Millipore; Billerica, MA, USA) stock solution was made to 60 mM in DMSO. Handling of CilD was identical to blebbistatin, with final dilutions always at 1:6 for all concentrations used. For focal application, CilD was diluted to 150 μM in PBS containing 1 mg/ml TexasRed-dextran (10 kDa) (Invitrogen; Carlsbad, CA, USA), sonicated for 10 min, then stored at 37°C until use. Solutions were back loaded into TW100F-4 glass micropipettes (World Precision Instruments; Sarasota, FL, USA) pulled on a Sutter Instruments P-97 Flaming / Brown puller. To maximize focal application at the growth cone, the micropipette tips were positioned within 10-20 μm of the growth cone within a 10 ml flow chamber set to a flow rate of 0.42 ml/min. This resulted in drug application that was highest

at the growth cone and tapered away over the adjoining 20 to 30 μm of the axon. Pressure was manually applied to the micropipette using a 10 ml syringe connected through Tygon tubing. Manual pressure, in combination with monitoring the fluid as it comes out of the pipette by fluorescence, was used instead of a Picospritzer because it allows for tighter control of fluid flow out of the pipette. Phase images were captured every 10 s, and fluorescent images were captured every 1 min using 100 ms exposures.

4.5.3 Microinjection

Antibodies targeted to the 74.1 dynein intermediate chain (Millipore; Billerica, MA, USA) were concentrated to 10 mg/ml in sterile injection buffer (100 mM HEPES, 140 mM KCl) mixed with 1 μg/ml FITC-dextran (134 kDa) (Sigma; St. Louis, MO, USA) using Millipore Amicon Ultra 0.5 mL 50K centricon devices (Millipore; Billerica, MA, USA) spun at 10,000 x g at 4°C for 10 min. The molecular weight of dextran was chosen as to be similar to the molecular weight of IgG antibodies. Non-specific mouse IgG antibodies (Sigma; St. Louis, MO, USA) were used as control as in previous studies (Grabham et al., 2007; Yi et al., 2011), but at 10 mg/ml. Microinjection was carried out in chick sensory neuronal cultures approximately 18 h after plating. Antibodies were back loaded into the same micropipettes as above. Flow was started by manually pushing approximately 2 cc of air into a 10 ml syringe connected to the needle holder with tygon tubing. This was sufficient to supply steady flow of fluid for 30-45 min. After injection into neuronal cell bodies, dishes were recovered for 2 hours then successfully injected neurons were screened by the presence of fluorescent dextran in the cell. Following screening for injection, growth cones were monitored for filopodial initiation dynamics by capturing phase images every 10 s for 2 min total. Injected neurons were chosen for further

imaging based on the steady initiation of filopodia over the 2 min observation and for having normally rounded cell bodies.

4.5.4 Mitochondrial imaging

Chick sensory neurons were labelled with 0.1 μM MitoTracker Red CMXRos (Invitrogen; Carlsbad, CA, USA) in L-15 for 5 min at room temperature and recovered in fresh L-15 for 1 h at 37°C. For imaging, culture dishes were held in a ringcubator (Heidemann et al., 2003) set to 38°C on a Leica DM IRB inverted microscope and observed with a N Plan L 40x/0.55 corrPh2 with an djustable collar infinity/0-2/c objective. Cells were illuminated with a 100 W Xenon lamp attenuated 98% with neutral density filters through a TexasRed 49008 ET cube (Chroma; Rockingham, VT, USA) for visualization of MitoTracker. Transmitted light exposure was controlled with a VMM-D3 controller and CS25 shutter (Vincent Associates; Rochester, NY, USA). Fluorescent light exposure was controlled with a Lambda 10-C (Sutter Instruments; Novato, CA, USA). Acquisitions were controlled using micro-manager software (US National Institutes of Health) (Edelstein et al., 2010). Exposure times for mitochondria images were set to 100 ms, except for the combined blebbistatin and CilD treatments, which required 250 ms exposures. For fast transport imaging, fluorescent images were captured at 10 s intervals while phase images were captured every 5 min. For all other mitochondrial time lapse acquisitions, fluorescent images were captured every 30 s and phase images captured every 1 min.

4.5.5 Tension assay

Cultures were prepared and maintained for imaging as described above. For a detailed description on the preparation and calibration of towing needles, as well as the micromanipulation of growth cones see (Lamoureux et al., 2011). In brief, micropipettes were coated with 0.01% poly-ornithine (Sigma, St. Louis, MO, USA) for 30 min, followed by a 1 mg/ml Concanavalin A solution for 30 min. The growth cone was then attached to the coated needle and lifted off the substrate to allow firm attachment to the needle. After attachment, the growth cone is brought down near the dish to achieve a better plane of focus and the time lapse imaging is begun with 20 second intervals at 40x magnification. A half hour stabilizing and baseline period is observed before the 100 μM ciliobrevin addition. CilD was prepared as above and added to the dish manually with a long pasteur pipette. The reference needle position is maintained unaltered through the experiment so all tension changes are attributable the cellular response.

APPENDIX

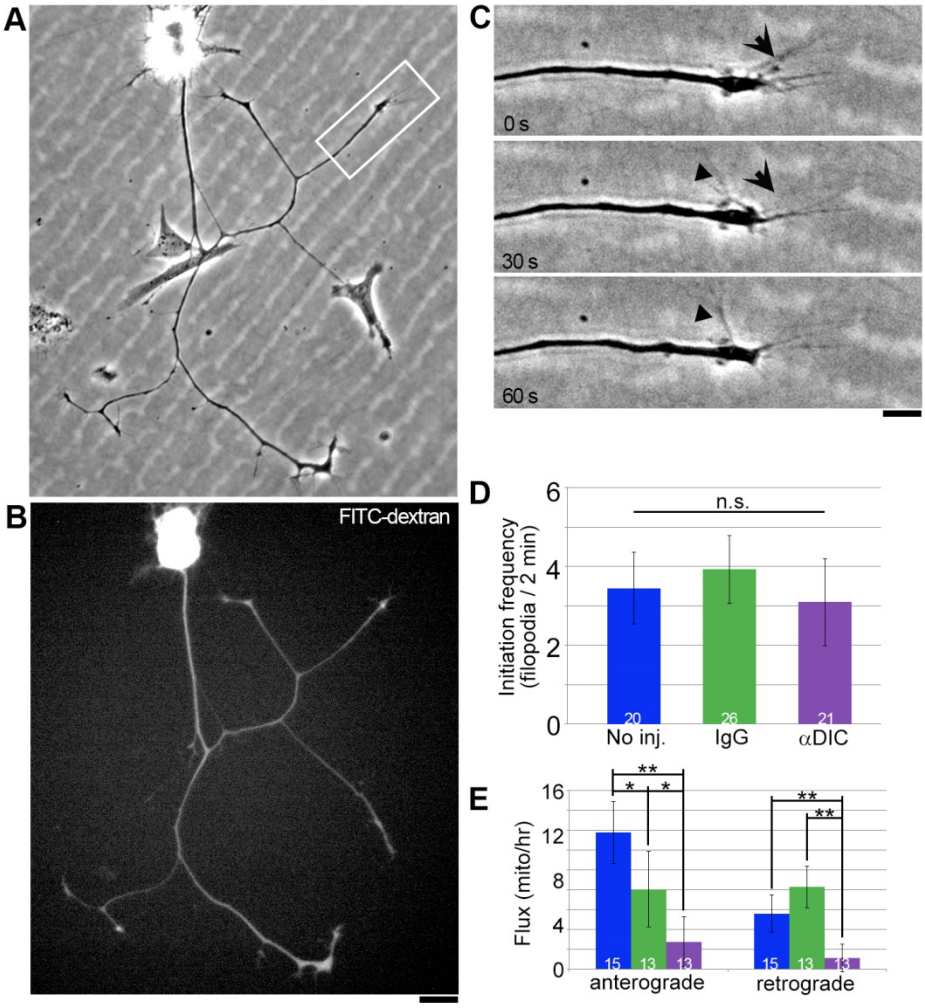

Figure 4.1 Microinjection of 74.1 dynein intermediate chain antibody impairs dynein function in chick sensory neurons. Neurons were microinjected with function-blocking antibodies toward dynein intermediate chain (αDIC) or nonspecific mouse IgG control antibodies mixed with FITC-dextran. (**A**) A neuron injected with αDIC two hours after injection shows normal cell body and neurite morphology. (**B**) Successful injection is confirmed by the presence of FITC-dextran throughout the entire neuron. Scale bar = 25 μm. (**C**) Phase images of the boxed growth cone in (A) at higher magnification show the initiation (triangles) and retraction (arrowheads) of filopodia after microinjection. Scale bar = 5 μm. (**D**) Average filopodial initiation over a 2 min period was similar between non-injected, IgG injected, and αDIC injected neurons. (**E**) Mitochondrial flux in both the anterograde and retrograde direction, measured by counting the number of mitochondria that passed the mid-way point of the axon is reduced with αDIC injection compared to IgG controls. * significance at $\alpha = 0.05$, ** $\alpha = 0.01$ by post-hoc Tukey's test. All error bars in figure represent 95% CI. Values at the bottom of the bars are number of axons used for each group.

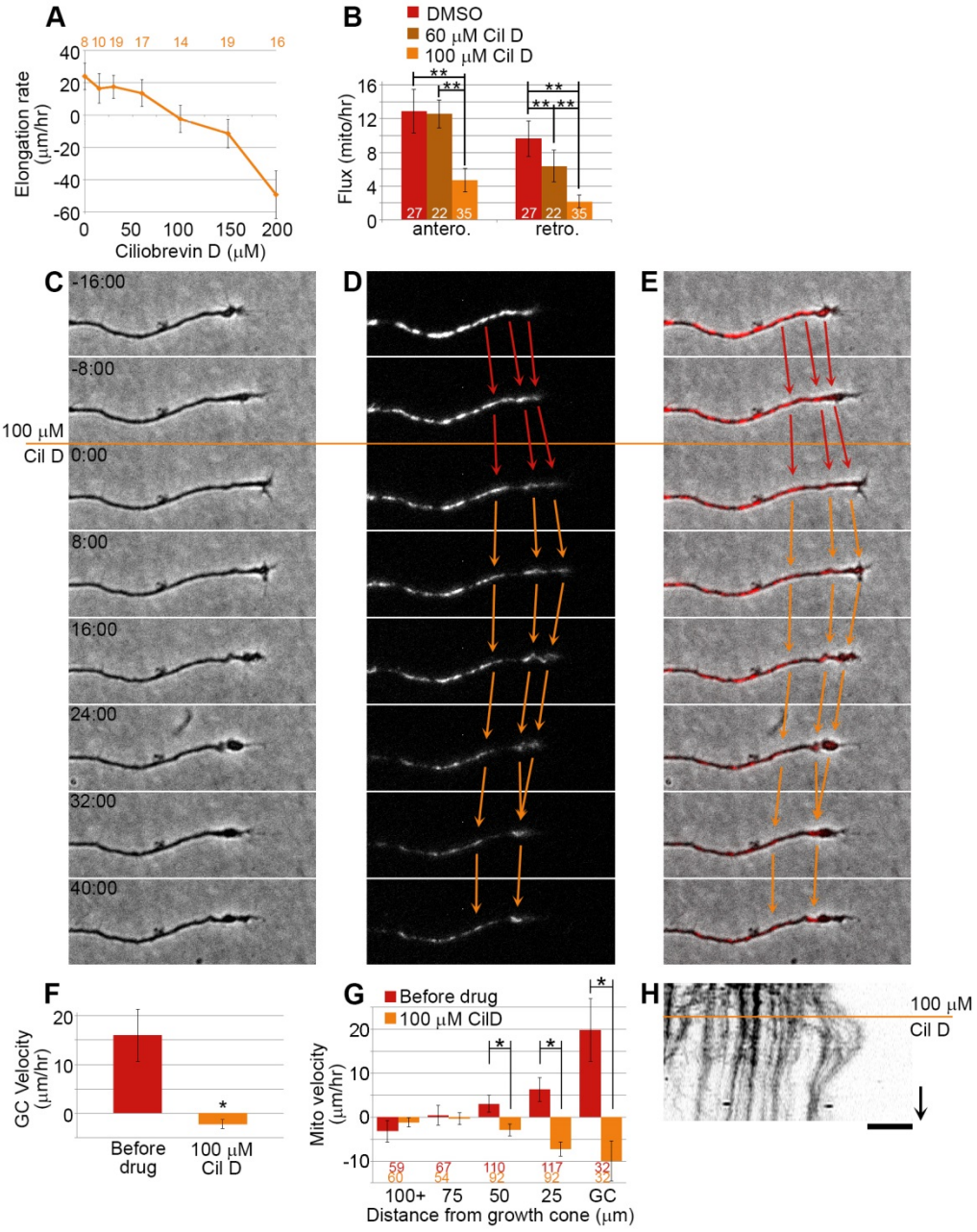

Figure 4.2 Acute pharmacological disruption of dynein with Ciliobrevin D slows axonal elongation and induces retraction of the axonal cytoskeleton. (**A**) Disruption of dynein with CilD reduces the rate of elongation in a dose-dependent manner. Orange numbers at the top, are the number of axons in each group; the concentration of 0 is the DMSO control. (**B**) Disruption of dynein reduces fast mitochondrial flux in a dose dependent manner. Numbers in white at the base of the bars are the numbers of axons used in each group. (**C**) Acute disruption of dynein initially induces retraction as seen in phase images. Afterwards the growth cones are stationary. The orange line is t = 0:00 for the bath application of 100 μM CilD. (**D**) Acute disruption of dynein induces retraction of docked mitochondria. (**E**) Overlaying the fluorescent and phase images (D-E) indicated that docked mitochondria continue to move rearward, even when the

Figure 4.2 (cont'd)

growth cone is stationary. (**F**) Rate of elongation using phase images in (C) shows fluorescent light does not impair CilD function or cause axonal retraction. (**H**) The color-inverted kymograph shows the shift from axonal stretching during elongation to bulk retraction and contraction along the axon following CilD treatment: time arrow = 15 min, scale bar = 20 μm. (**G**) Quantitative analysis demonstrates dynein disruption induces contraction and bulk retraction in the axon. Color-coded numbers at the bottom of the graph in (G) represent the number of mitochondria in each bin, where the growth cone bin (GC) comprises the most distal mitochondrion per axon. All error bars represent 95% CI. *$p < 0.01$ by unpaired, two-tailed t-test; ** $\alpha < 0.01$ by post-hoc Tukey's test.

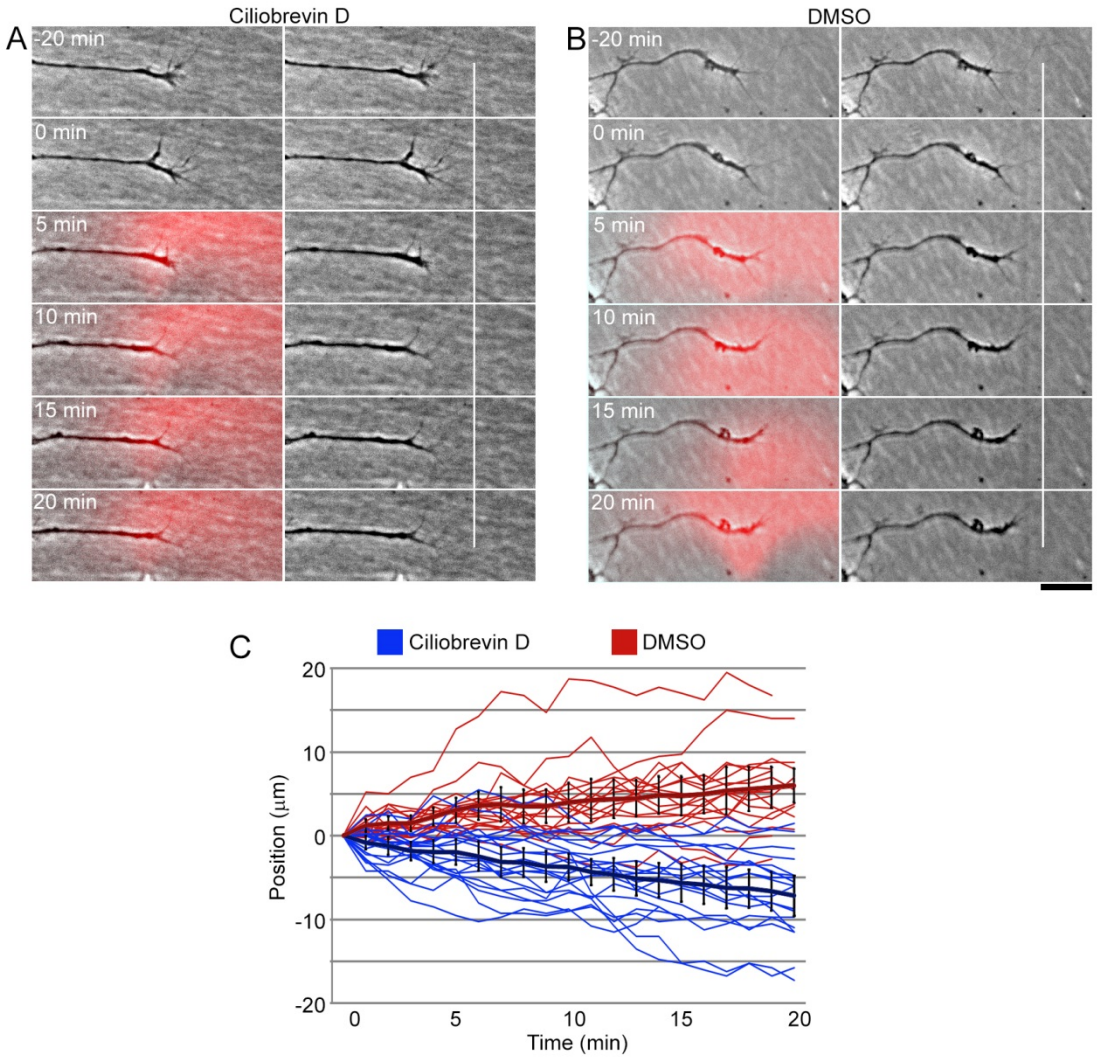

Figure 4.3 Focal disruption of dynein in the growth cone and distal axon causes retraction. (**A**) Focal application of CilD, to disrupt dynein the growth cone and distal axon, induced axonal retraction. The extent of drug application is shown by the red overlay in the phase images. (**B**) Focal application of DMSO, as a control, had no effect on axonal elongation. The arrows show the movement of the leading edge. (**C**) Individual growth cone movements were normalized for initial position and plotted during 20 min treatment of CilD (blue lines) or DMSO (red lines). Thick, dark bars are average growth cone position at each 1 min interval. Control growth cones grew at rate of 17.4 +/- 7.0 μm/hr (ave. +/- 95% CI). Focal disruption of dynein induced retraction at an average rate of -22.1 +/- 6.9 μm/hr (ave. +/- 95% CI). Scale bar = 20 μm. Error bars are 95% CI.

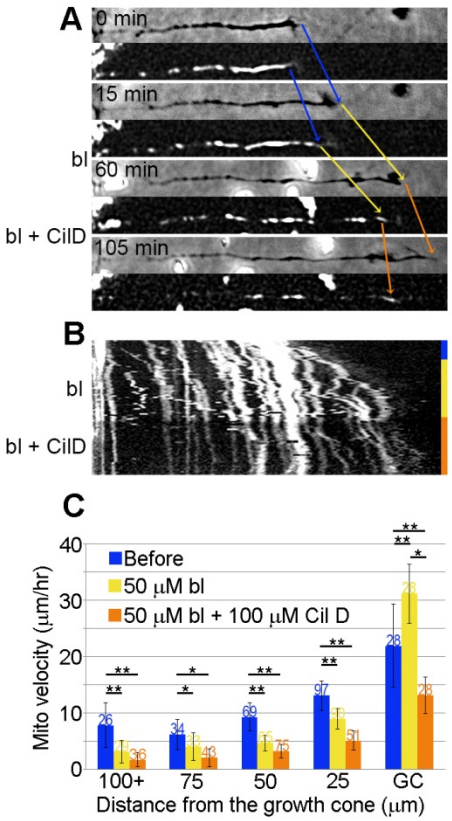

Figure 4.4 An antagonistic relationship between myosin II and dynein controls bulk growth cone advance. Neurons were treated with 50 μM blebbistatin to disrupt myosin II function for 45 min, after which 100 μM CilD was added. (**A**) Paired phase and fluorescent mitochondria images show blebbistatin increases growth cone advance (compare blue arrows to yellow arrows), while subsequent CilD addition reduces it (orange arrows versus yellow arrows). (**B**) Kymograph of docked mitochondria in the axon shown in (A). (**C**) Quantitative analysis of docked mitochondria illustrates blebbistatin causes an increase in bulk growth cone translocation and a decrease along the axon. Addition of CilD causes a subsequent reduction at all points in the axon compared to pre-treatment levels. Numbers above each bar represent number of mitochondria in each bin, where GC is the most distal mitochondria in each growth cone. Error bars show 95% CI, * significance at $\alpha = 0.05$, ** significance at $\alpha = 0.01$ by post-hoc Tukey's test.

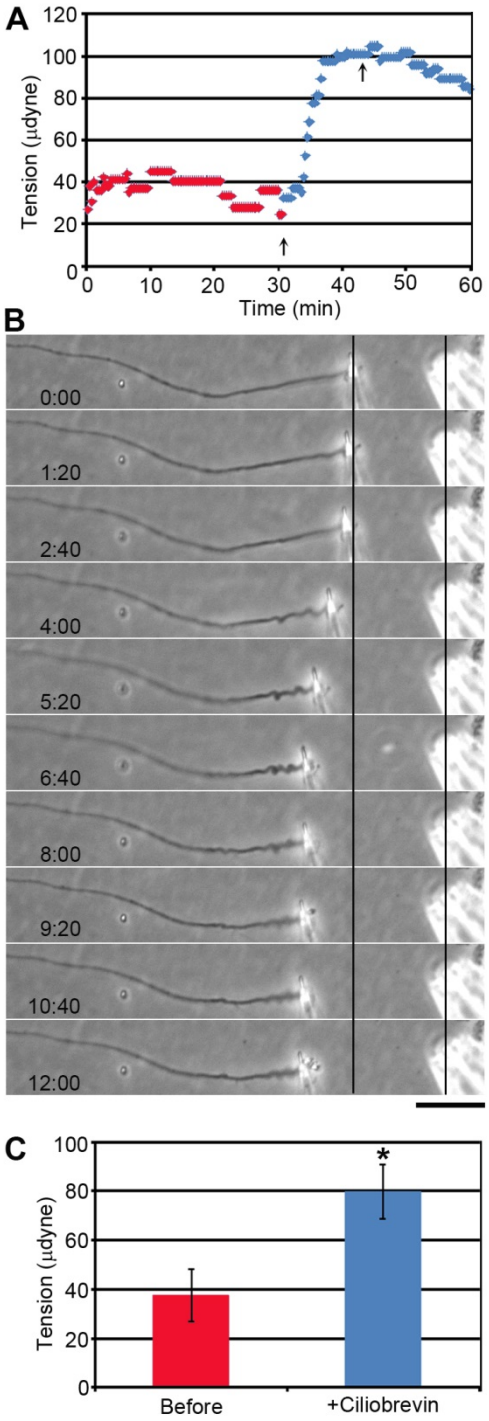

Figure 4.5 Dynein disruption with Ciliobrevin D increases axonal tension. Force-calibrated towing needles attached to growth cones are used to measure changes in forces after dynein disruption. (**A**) An individual force profile shows tension increases when 100 µM CilD is added at 30 min. In red are the force measurements taken before CilD and blue are the measurements after. (**B**) The increase in tension is seen as pulling on the needle in a series of phase images, corresponding to the time demarcated by arrows in (A). t = 0:00 represents time of CilD addition.

Figure 4.5 (cont'd)

Vertical lines have been added to the series to show initial position of the two needles at the time of CilD addition. (**C**) The average tension measurements before and after CilD addition. Error bars represent 95% CI. *$p < 0.01$ by paired, two-tailed t-test. Scale bar = 25 μm.

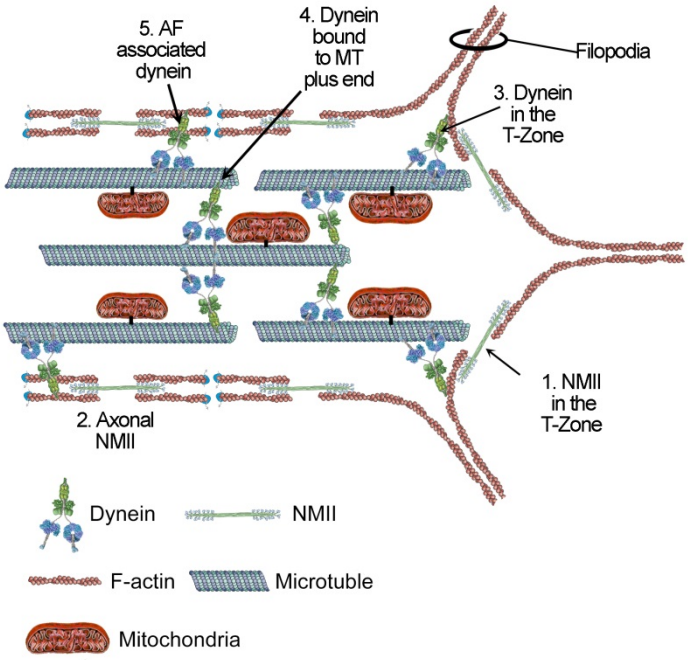

Figure 4.6 Sub-cellular model for dynein and NMII motor function in the axon and growth cone. This model proposes the following intracellular interactions between actin, NMII, microtubules, and dynein: (1) NMII in the T-zone drives retrograde actin flow and turnover. (2) NMII in the cell cortex along the axon generates contractile forces that oppose growth cone advance. (3) Dynein bound to actin in the T-zone moves microtubules forward. (4) Dynein bound to two neighboring microtubules generates forces that cause them to telescope apart. (5) Dynein uses cortical actin along the axon as an anchor to generate forces on long microtubules powering their advance.

REFERENCES

REFERENCES

Ahmad, F.J., C.J. Echeverri, R.B. Vallee, and P.W. Baas. 1998. Cytoplasmic dynein and dynactin are required for the transport of microtubules into the axon. *The Journal of cell biology*. 140:391-401.

Ahmad, F.J., Y. He, K.A. Myers, T.P. Hasaka, F. Francis, M.M. Black, and P.W. Baas. 2006. Effects of dynactin disruption and dynein depletion on axonal microtubules. *Traffic (Copenhagen, Denmark)*. 7:524-537.

Ahmad, F.J., J. Hughey, T. Wittmann, A. Hyman, M. Greaser, and P.W. Baas. 2000. Motor proteins regulate force interactions between microtubules and microfilaments in the axon. *Nature cell biology*. 2:276-280.

Baas, P.W., C. Vidya Nadar, and K.A. Myers. 2006. Axonal transport of microtubules: the long and short of it. *Traffic (Copenhagen, Denmark)*. 7:490-498.

Bernal, R., P.A. Pullarkat, and F. Melo. 2007. Mechanical properties of axons. *Physical review letters*. 99:018301.

Bridgman, P.C., and M.E. Dailey. 1989. The organization of myosin and actin in rapid frozen nerve growth cones. *The Journal of cell biology*. 108:95-109.

Brown, M.E., and P.C. Bridgman. 2003. Retrograde flow rate is increased in growth cones from myosin IIB knockout mice. *Journal of cell science*. 116:1087-1094.

Carminati, J.L., and T. Stearns. 1997. Microtubules orient the mitotic spindle in yeast through dynein-dependent interactions with the cell cortex. *The Journal of cell biology*. 138:629-641.

Chang, S., V.I. Rodionov, G.G. Borisy, and S.V. Popov. 1998. Transport and turnover of microtubules in frog neurons depend on the pattern of axonal growth. *The Journal of neuroscience : the official journal of the Society for Neuroscience*. 18:821-829.

Dehmelt, L., P. Nalbant, W. Steffen, and S. Halpain. 2006. A microtubule-based, dynein-dependent force induces local cell protrusions: Implications for neurite initiation. *Brain Cell Biol*. 35:39-56.

Dent, E.W., and F.B. Gertler. 2003. Cytoskeletal dynamics and transport in growth cone motility and axon guidance. *Neuron*. 40:209-227.

Dickson, B.J. 2002. Molecular mechanisms of axon guidance. *Science (New York, N.Y.* 298:1959-1964.

Dujardin, D.L., L.E. Barnhart, S.A. Stehman, E.R. Gomes, G.G. Gundersen, and R.B. Vallee. 2003. A role for cytoplasmic dynein and LIS1 in directed cell movement. *The Journal of cell biology*. 163:1205-1211.

Edelstein, A., N. Amodaj, K. Hoover, R. Vale, and N. Stuurman. 2010. Computer control of microscopes using microManager. *Curr Protoc Mol Biol*. Chapter 14:Unit14 20.

Faulkner, N.E., D.L. Dujardin, C.Y. Tai, K.T. Vaughan, C.B. O'Connell, Y. Wang, and R.B. Vallee. 2000. A role for the lissencephaly gene LIS1 in mitosis and cytoplasmic dynein function. *Nature cell biology*. 2:784-791.

Firestone, A.J., J.S. Weinger, M. Maldonado, K. Barlan, L.D. Langston, M. O'Donnell, V.I. Gelfand, T.M. Kapoor, and J.K. Chen. 2012. Small-molecule inhibitors of the AAA+ ATPase motor cytoplasmic dynein. *Nature*. 484:125-129.

Gallo, G. 2004. Myosin II activity is required for severing-induced axon retraction in vitro. *Experimental neurology*. 189:112-121.

Goldberg, D.J., and D.W. Burmeister. 1986. Stages in axon formation: observations of growth of Aplysia axons in culture using video-enhanced contrast-differential interference contrast microscopy. *The Journal of cell biology*. 103:1921-1931.

Grabham, P.W., G.E. Seale, M. Bennecib, D.J. Goldberg, and R.B. Vallee. 2007. Cytoplasmic dynein and LIS1 are required for microtubule advance during growth cone remodeling and fast axonal outgrowth. *The Journal of neuroscience : the official journal of the Society for Neuroscience*. 27:5823-5834.

He, Y., F. Francis, K.A. Myers, W. Yu, M.M. Black, and P.W. Baas. 2005. Role of cytoplasmic dynein in the axonal transport of microtubules and neurofilaments. *The Journal of cell biology*. 168:697-703.

Heidemann, S.R., P. Lamoureux, K. Ngo, M. Reynolds, and R.E. Buxbaum. 2003. Open-dish incubator for live cell imaging with an inverted microscope. *BioTechniques*. 35:708-714, 716.

Hur, E.M., I.H. Yang, D.H. Kim, J. Byun, Saijilafu, W.L. Xu, P.R. Nicovich, R. Cheong, A. Levchenko, N. Thakor, and F.Q. Zhou. 2011. Engineering neuronal growth cones to promote axon regeneration over inhibitory molecules. *Proceedings of the National Academy of Sciences of the United States of America*. 108:5057-5062.

Jay, D.G. 2000. The clutch hypothesis revisited: ascribing the roles of actin-associated proteins in filopodial protrusion in the nerve growth cone. *Journal of neurobiology*. 44:114-125.

Joshi, H.C., D. Chu, R.E. Buxbaum, and S.R. Heidemann. 1985. Tension and compression in the cytoskeleton of PC 12 neurites. *The Journal of cell biology*. 101:697-705.

Kholmanskikh, S.S., H.B. Koeller, A. Wynshaw-Boris, T. Gomez, P.C. Letourneau, and M.E. Ross. 2006. Calcium-dependent interaction of Lis1 with IQGAP1 and Cdc42 promotes neuronal motility. *Nature neuroscience*. 9:50-57.

Kikkawa, M. 2013. Big steps toward understanding dynein. *The Journal of cell biology*. 202:15-23.

King, S.M. 2000. The dynein microtubule motor. *Biochim Biophys Acta*. 1496:60-75.

Lamoureux, P., S. Heidemann, and K.E. Miller. 2011. Mechanical manipulation of neurons to control axonal development. *J Vis Exp*.

Lamoureux, P., S.R. Heidemann, N.R. Martzke, and K.E. Miller. 2010. Growth and elongation within and along the axon. *Developmental neurobiology*. 70:135-149.

Lee, A.C., and D.M. Suter. 2008. Quantitative analysis of microtubule dynamics during adhesion-mediated growth cone guidance. *Developmental neurobiology*. 68:1363-1377.

Lim, S.S., K.J. Edson, P.C. Letourneau, and G.G. Borisy. 1990. A test of microtubule translocation during neurite elongation. *The Journal of cell biology*. 111:123-130.

Lin, C.H., E.M. Espreafico, M.S. Mooseker, and P. Forscher. 1996. Myosin drives retrograde F-actin flow in neuronal growth cones. *Neuron*. 16:769-782.

Lowery, L.A., and D. Van Vactor. 2009. The trip of the tip: understanding the growth cone machinery. *Nat Rev Mol Cell Biol*. 10:332-343.

Lu, W., P. Fox, M. Lakonishok, M.W. Davidson, and V.I. Gelfand. 2013. Initial Neurite Outgrowth in Drosophila Neurons Is Driven by Kinesin-Powered Microtubule Sliding. *Curr Biol*.

Mallavarapu, A., and T. Mitchison. 1999. Regulated actin cytoskeleton assembly at filopodium tips controls their extension and retraction. *The Journal of cell biology*. 146:1097-1106.

Martin, M., S.J. Iyadurai, A. Gassman, J.G. Gindhart, Jr., T.S. Hays, and W.M. Saxton. 1999. Cytoplasmic dynein, the dynactin complex, and kinesin are interdependent and essential for fast axonal transport. *Mol Biol Cell*. 10:3717-3728.

Mazel, T., A. Biesemann, M. Krejczy, J. Nowald, O. Muller, and L. Dehmelt. 2013. Direct observation of microtubule pushing by cortical dynein in living cells. *Mol Biol Cell*.

Medeiros, N.A., D.T. Burnette, and P. Forscher. 2006. Myosin II functions in actin-bundle turnover in neuronal growth cones. *Nature cell biology*. 8:215-226.

Miller, K.E., and M.P. Sheetz. 2006. Direct evidence for coherent low velocity axonal transport of mitochondria. *The Journal of cell biology*. 173:373-381.

Myers, K.A., I. Tint, C.V. Nadar, Y. He, M.M. Black, and P.W. Baas. 2006. Antagonistic forces generated by cytoplasmic dynein and myosin-II during growth cone turning and axonal retraction. *Traffic (Copenhagen, Denmark)*. 7:1333-1351.

O'Connell, C.B., and Y.L. Wang. 2000. Mammalian spindle orientation and position respond to changes in cell shape in a dynein-dependent fashion. *Mol Biol Cell*. 11:1765-1774.

O'Toole, M., P. Lamoureux, and K.E. Miller. 2008. A physical model of axonal elongation: force, viscosity, and adhesions govern the mode of outgrowth. *Biophysical journal*. 94:2610-2620.

Okabe, S., and N. Hirokawa. 1990. Turnover of fluorescently labelled tubulin and actin in the axon. *Nature*. 343:479-482.

Palazzo, A.F., H.L. Joseph, Y.J. Chen, D.L. Dujardin, A.S. Alberts, K.K. Pfister, R.B. Vallee, and G.G. Gundersen. 2001. Cdc42, dynein, and dynactin regulate MTOC reorientation independent of Rho-regulated microtubule stabilization. *Current biology : CB*. 11:1536-1541.

Paschal, B.M., H.S. Shpetner, and R.B. Vallee. 1987. MAP 1C is a microtubule-activated ATPase which translocates microtubules in vitro and has dynein-like properties. *The Journal of cell biology*. 105:1273-1282.

Pilling, A.D., D. Horiuchi, C.M. Lively, and W.M. Saxton. 2006. Kinesin-1 and Dynein are the primary motors for fast transport of mitochondria in Drosophila motor axons. *Mol Biol Cell*. 17:2057-2068.

Reinsch, S.S., T.J. Mitchison, and M. Kirschner. 1991. Microtubule polymer assembly and transport during axonal elongation. *The Journal of cell biology*. 115:365-379.

Rochlin, M.W., K. Itoh, R.S. Adelstein, and P.C. Bridgman. 1995. Localization of myosin II A and B isoforms in cultured neurons. *Journal of cell science*. 108 (Pt 12):3661-3670.

Roossien, D.H., P. Lamoureux, D. Van Vactor, and K.E. Miller. 2013. Drosophila growth cones advance by forward translocation of the neuronal cytoskeletal meshwork in vivo. *PLoS One*. 8:e80136.

Saxton, W.M., and P.J. Hollenbeck. 2012. The axonal transport of mitochondria. *Journal of cell science*. 125:2095-2104.

Schnapp, B.J., and T.S. Reese. 1989. Dynein is the motor for retrograde axonal transport of organelles. *Proceedings of the National Academy of Sciences of the United States of America*. 86:1548-1552.

Stiess, M., and F. Bradke. 2011. Neuronal polarization: the cytoskeleton leads the way. *Developmental neurobiology*. 71:430-444.

Straight, A.F., A. Cheung, J. Limouze, I. Chen, N.J. Westwood, J.R. Sellers, and T.J. Mitchison. 2003. Dissecting temporal and spatial control of cytokinesis with a myosin II Inhibitor. *Science (New York, N.Y.* 299:1743-1747.

Suter, D.M. 2011. Functions of Myosin Motor Proteins in the Nervous System. *In* Neurobiology of Actin. Springer. 45-72.

Suter, D.M., and K.E. Miller. 2011. The emerging role of forces in axonal elongation. *Progress in neurobiology*. 94:91-101.

Vallee, R.B., G.E. Seale, and J.W. Tsai. 2009. Emerging roles for myosin II and cytoplasmic dynein in migrating neurons and growth cones. *Trends Cell Biol*. 19:347-355.

Vaughan, K.T., S.H. Tynan, N.E. Faulkner, C.J. Echeverri, and R.B. Vallee. 1999. Colocalization of cytoplasmic dynein with dynactin and CLIP-170 at microtubule distal ends. *Journal of cell science*. 112 (Pt 10):1437-1447.

Yi, J.Y., K.M. Ori-McKenney, R.J. McKenney, M. Vershinin, S.P. Gross, and R.B. Vallee. 2011. High-resolution imaging reveals indirect coordination of opposite motors and a role for LIS1 in high-load axonal transport. *The Journal of cell biology*. 195:193-201.

CHAPTER 5:

Summary and Future Directions

5.1 Summary of results

The goals of this research were to characterize how axonal elongation occurs *in vivo* and to investigate candidate molecular motors proposed to regulate elongation. Because the results were discussed in detail in their respective chapters, below is a summary of key results found for each specific aim of this dissertation. The broader impacts and future directions will be discussed in the following section.

Aim 1) How do axons elongate *in vivo*?

- Cytoskeleton translocation during axonal elongation is a conserved process between vertebrates and invertebrates.
- The addition of extracellular matrix proteins to the substrate increases axonal stretching
- *Drosophila a*xons grow by forward translocation of the cytoskeleton *in vivo*.

Aim 2) How does non-muscle myosin II influence cytoskeletal meshwork translocation?

- Global NMII disruption increases axonal stretching and decreases net tension
- NMII disruption increases stretching by decreasing viscosity and adhesion strength
- Focal NMII disruption in the growth cone causes retraction
- NMII along the axon restrains growth cone advance by preventing stretching, in opposition to NMII in the growth cone.

Aim 3) Does cytoplasmic dynein generate forces required for cytoskeletal meshwork translocation?

- Dynein disruption slows elongation by decreasing bulk translocation of the cytoskeletal meshwork.
- Dynein generates pushing forces on microtubules embedded in the cytoskeletal meshwork to cause bulk translocation.

5.2 Future directions

We provide here the first molecular mechanism for how forces generated in the axon regulate bulk translocation of the growth cone and cytoskeletal meshwork. Forces generated by NMII in the growth cone act to pull material forward, while dynein along the axon pushes microtubules forward. These are both opposed by NMII activity along the length of the axon, which increases axonal viscosity and maintains adhesion. While the data give novel insights into the role of molecular motors in axonal elongation, they raise several intriguing questions: What other motors generate forces that move the cytoskeleton? What are the signaling pathways initiated by extracellular guidance cues that alter the activity of dynein and NMII to regulate the rate of elongation? How do motors power cytoskeleton translocation *in vivo*?

One intriguing observation is that residual cytoskeletal meshwork translocation and axonal stretching occurs when both NMII and dynein are acutely inhibited. This suggests that there are other force generating mechanisms involved in bulk transport. Logical candidates to test are members of the kinesin superfamily, such as kinesin-1. During initial outgrowth of primary *Drosophila* neurons, kinesin-1 generates forces that cause microtubules to slide into the nascent axon (Lu et al., 2013). It is therefore likely that these forces continue to drive microtubule telescoping or bulk advance along the axon in a manner similar to dynein. Genetic and pharmacological inhibition of the various motors while examining bulk growth cone and cytoskeleton movements will be important experiments to perform.

There is also evidence that motors could be acting as a brake on microtubules to prevent axonal elongation. Disruption of both plus end directed kinesin-5 and kinesin-12 increases the rate of axonal elongation (Liu et al., 2010; Myers and Baas, 2007). Although this has been tested in the context of Stop-and-Go transport, it is possible that, like dynein, these motors also

generate forces that impinge upon long microtubules embedded in the cytoskeletal meshwork. In this case, however, they would be preventing microtubule telescoping. One intriguing hypothesis to consider is that it is that neurons are sensitive to the amount and direction of net force and utilizes a wide variety of motors to elicit a desired net force outcome required for elongation and / or retraction.

The opposing function of NMII in the growth cone and along the axon suggests that these two functional pools of NMII are regulated differently. It is likely that ROCK activates NMII along the axon by inhibiting MLCP, whereas the pool of NMII that drives bulk translocation of the growth cone relies on a MLCP variant that is insensitive to ROCK phosphorylation (Amano et al., 1996; Kimura et al., 1996; Vereshchagina et al., 2004; Zhang et al., 2003). Our data suggest that ROCK activity along the axon therefore decreases axonal stretching and growth cone advance. This is interesting in that ROCK inhibition has recently shown potential to be a useful strategy to augment axonal regeneration following injury (Arakawa et al., 2003; Borisoff et al., 2003; Tonges et al., 2011). However, how ROCK inhibition modulates bulk growth cone translocation and stretching during regeneration has not yet been considered.

There is also evidence suggesting the different pools of NMII activity correspond to different NMII isoforms. For example, NMIIB is located in the T-zone and drives retrograde flow, whereas NMIIA is located in the C-domain and axon shaft and only powers retrograde flow when NMIIB is knocked out (Bridgman et al., 2001). It is therefore tempting to speculate a mechanism in which NMIIA is located in the C-domain and along the axon, where it is under the control of MLCK and ROCK, to generate forces that oppose growth cone advance and axonal stretching, whereas NMIIB is located in the T-zone and is under the control of MLCK to drive

retrograde flow. Developing pharmacological agents that can selectively disrupt the different isoforms of NMII will be of interest in the future to tease apart the contributions each makes to axonal elongation.

We also report the first evidence that axons grow by bulk translocation of the growth cone *in vivo*. Growth *in vitro* closely mimics *in vivo* growth when endogenous extracellular matrix proteins are added to the culture substrate. While this is not surprising, this is the first direct comparison of outgrowth on different substrates to that seen *in vivo* and underscores the profound relationship between extracellular environment and the biophysics of axonal elongation. While the use of endogenous extracellular proteins can aid in creating permissive tissue culture environments, whether this accurately recapitulates the *in vivo* environment is always in question. As such, time-lapse imaging of live *Drosophila* embryos as shown here provides a powerful tool to compare *in vitro* and *in vivo* phenotypes.

There are other distinct advantages of using *Drosophila* as a model system. One is that filet preparation of embryos can be used for manipulation of internal tissue. This maintains an *in situ* environment for axon growth that closely mimics the *in vivo* environment, but gives access to the body cavity. The tissue can be directly manipulated and has been used previously to characterize axonal tension *in situ* (Ahmed et al., 2012; Siechen et al., 2009). Combining this with genetic mutations will give insight as to how motors generate axonal forces *in vivo*. By exposing the body cavity, cytoskeleton and motor disrupting drugs can also be added directly to the tissue, allowing for acute motor and cytoskeleton disruption. These methods will be critical going forward to study axonal biophysics *in situ*.

While there are multiple rodent models for nerve injury and regeneration, these models are less amenable to time-lapse *in vivo* imaging. This is yet another area in which *Drosophila*

will prove to be a useful model system (Fang and Bonini, 2012). Using larvae, nerves can be physically crushed (Xiong et al., 2010) or ablated with lasers (Stone et al., 2010) and regenerating axons can be imaged shortly afterwards. Complete axotomy can be accomplished by cutting the edge of the wing in the adult fly, resulting in a more long-term regeneration process (Fang et al., 2012). Both of these approaches are done in tissue that is fairly transparent, thereby facilitating *in vivo* imaging. By expressing fluorescent markers to track the intracellular movement of the cytoskeleton in these injury models, we can make comparisons between bulk transport during development and regenerative growth.

A major goal in neuronal cell biology is to develop effective therapies to repair nerve damage after spinal cord and peripheral nerve injury. Following injury, the surrounding scar tissue secretes signals that prevent axonal regeneration (Schwab et al., 1993; Silver and Miller, 2004; Yiu and He, 2006). Most current strategies focus on blocking the effects of these inhibitory molecules (Case and Tessier-Lavigne, 2005; Filbin, 2003; Silver and Miller, 2004; Yiu and He, 2006). Unfortunately, these have proven to be marginal at best (Lu et al., 2012). As there is a lag between initial injury and formation of the inhibitory scar, increasing the rate of axonal elongation following injury can improve regeneration (Chen et al., 2007). Our work here suggests that decreasing NMII activity along the axon or increasing dynein activity can increase the rate of elongation. In broader terms, modulating the activity of motor proteins and axonal stretching is a promising avenue for developing strategies to augment axonal regeneration following nerve damage.

REFERENCES

REFERENCES

Ahmed, W.W., T.C. Li, S.S. Rubakhin, A. Chiba, J.V. Sweedler, and T.A. Saif. 2012. Mechanical tension modulates local and global vesicle dynamics in neurons. *Cell Mol Bioeng*. 5:155-164.

Amano, M., M. Ito, K. Kimura, Y. Fukata, K. Chihara, T. Nakano, Y. Matsuura, and K. Kaibuchi. 1996. Phosphorylation and activation of myosin by Rho-associated kinase (Rho-kinase). *The Journal of biological chemistry*. 271:20246-20249.

Arakawa, Y., H. Bito, T. Furuyashiki, T. Tsuji, S. Takemoto-Kimura, K. Kimura, K. Nozaki, N. Hashimoto, and S. Narumiya. 2003. Control of axon elongation via an SDF-1alpha/Rho/mDia pathway in cultured cerebellar granule neurons. *The Journal of cell biology*. 161:381-391.

Borisoff, J.F., C.C. Chan, G.W. Hiebert, L. Oschipok, G.S. Robertson, R. Zamboni, J.D. Steeves, and W. Tetzlaff. 2003. Suppression of Rho-kinase activity promotes axonal growth on inhibitory CNS substrates. *Mol Cell Neurosci*. 22:405-416.

Bridgman, P.C., S. Dave, C.F. Asnes, A.N. Tullio, and R.S. Adelstein. 2001. Myosin IIB is required for growth cone motility. *J Neurosci*. 21:6159-6169.

Case, L.C., and M. Tessier-Lavigne. 2005. Regeneration of the adult central nervous system. *Current biology : CB*. 15:R749-753.

Chen, Z.L., W.M. Yu, and S. Strickland. 2007. Peripheral regeneration. *Annu Rev Neurosci*. 30:209-233.

Fang, Y., and N.M. Bonini. 2012. Axon degeneration and regeneration: insights from Drosophila models of nerve injury. *Annual review of cell and developmental biology*. 28:575-597.

Fang, Y., L. Soares, X. Teng, M. Geary, and N.M. Bonini. 2012. A novel Drosophila model of nerve injury reveals an essential role of Nmnat in maintaining axonal integrity. *Current biology : CB*. 22:590-595.

Filbin, M.T. 2003. Myelin-associated inhibitors of axonal regeneration in the adult mammalian CNS. *Nature reviews*. 4:703-713.

Kimura, K., M. Ito, M. Amano, K. Chihara, Y. Fukata, M. Nakafuku, B. Yamamori, J. Feng, T. Nakano, K. Okawa, A. Iwamatsu, and K. Kaibuchi. 1996. Regulation of myosin phosphatase by Rho and Rho-associated kinase (Rho-kinase). *Science (New York, N.Y.* 273:245-248.

Liu, M., V.C. Nadar, F. Kozielski, M. Kozlowska, W. Yu, and P.W. Baas. 2010. Kinesin-12, a mitotic microtubule-associated motor protein, impacts axonal growth, navigation, and branching. *J Neurosci*. 30:14896-14906.

Lu, P., A. Blesch, L. Graham, Y. Wang, R. Samara, K. Banos, V. Haringer, L. Havton, N. Weishaupt, D. Bennett, K. Fouad, and M.H. Tuszynski. 2012. Motor axonal regeneration after partial and complete spinal cord transection. *J Neurosci*. 32:8208-8218.

Lu, W., P. Fox, M. Lakonishok, M.W. Davidson, and V.I. Gelfand. 2013. Initial Neurite Outgrowth in Drosophila Neurons Is Driven by Kinesin-Powered Microtubule Sliding. *Curr Biol*.

Myers, K.A., and P.W. Baas. 2007. Kinesin-5 regulates the growth of the axon by acting as a brake on its microtubule array. *The Journal of cell biology*. 178:1081-1091.

Schwab, M.E., J.P. Kapfhammer, and C.E. Bandtlow. 1993. Inhibitors of neurite growth. *Annu Rev Neurosci*. 16:565-595.

Siechen, S., S. Yang, A. Chiba, and T. Saif. 2009. Mechanical tension contributes to clustering of neurotransmitter vesicles at presynaptic terminals. *Proceedings of the National Academy of Sciences of the United States of America*. 106:12611-12616.

Silver, J., and J.H. Miller. 2004. Regeneration beyond the glial scar. *Nature reviews. Neuroscience*. 5:146-156.

Stone, M.C., M.M. Nguyen, J. Tao, D.L. Allender, and M.M. Rolls. 2010. Global up-regulation of microtubule dynamics and polarity reversal during regeneration of an axon from a dendrite. *Mol Biol Cell*. 21:767-777.

Tonges, L., J.C. Koch, M. Bahr, and P. Lingor. 2011. ROCKing Regeneration: Rho Kinase Inhibition as Molecular Target for Neurorestoration. *Frontiers in molecular neuroscience*. 4:39.

Vereshchagina, N., D. Bennett, B. Szoor, J. Kirchner, S. Gross, E. Vissi, H. White-Cooper, and L. Alphey. 2004. The essential role of PP1beta in Drosophila is to regulate nonmuscle myosin. *Mol Biol Cell*. 15:4395-4405.

Xiong, X., X. Wang, R. Ewanek, P. Bhat, A. Diantonio, and C.A. Collins. 2010. Protein turnover of the Wallenda/DLK kinase regulates a retrograde response to axonal injury. *The Journal of cell biology*. 191:211-223.

Yiu, G., and Z. He. 2006. Glial inhibition of CNS axon regeneration. *Nature reviews. Neuroscience*. 7:617-627.

Zhang, X.F., A.W. Schaefer, D.T. Burnette, V.T. Schoonderwoert, and P. Forscher. 2003. Rho-dependent contractile responses in the neuronal growth cone are independent of classical peripheral retrograde actin flow. *Neuron*. 40:931-944.